



MID-AMERICA TRANSPORTATION CENTER

Report # MATC-UNL: 004-31

Final Report
WBS:25-1121-0005-004-31

UNIVERSITY OF
Nebraska
Lincoln

THE UNIVERSITY
OF IOWA

THE UNIVERSITY OF
KU KANSAS

MISSOURI
S&T

LINCOLN
UNIVERSITY
MISSOURI



UNIVERSITY OF
Nebraska
Omaha

University of Nebraska
Medical Center

KU MEDICAL
CENTER
The University of Kansas

Protecting Critical Infrastructure Against Impact from Commercial Vehicles, Phase I

Daniel G. Linzell, Ph.D., P.E., F.ASCE.

Associate Dean for Graduate and International Programs
Department of Civil Engineering
University of Nebraska-Lincoln

Yong-Rak Kim, Ph.D.

Professor

Chen Fang

Graduate Research Assistant

Gabriel M. Nsengiyumva

Graduate Research Assistant

UNIVERSITY OF
Nebraska
Lincoln

2019

A Cooperative Research Project sponsored by
U.S. Department of Transportation- Office of the Assistant
Secretary for Research and Technology

MATC

The contents of this report reflect the views of the authors, who are responsible for the facts and the accuracy of the information presented herein. This document is disseminated in the interest of information exchange. The report is funded, partially or entirely, by a grant from the U.S. Department of Transportation's University Transportation Centers Program. However, the U.S. Government assumes no liability for the contents or use thereof.

Protecting Critical Civil Infrastructure Against Impact from Commercial Vehicles

Phase I Final Report

Daniel G. Linzell, Ph.D., P.E., F.ASCE.
Associate Dean for Graduate and International Programs
Department of Civil Engineering
University of Nebraska-Lincoln

Chen Fang
Graduate Research Assistant
Department of Civil Engineering
University of Nebraska-Lincoln

Yong-Rak Kim, Ph.D.
Professor
Department of Civil Engineering
University of Nebraska-Lincoln

Gabriel M. Nsengiyumva
Graduate Research Assistant
Department of Civil Engineering
University of Nebraska-Lincoln

A Report on Research Sponsored by

Mid-America Transportation Center

University of Nebraska–Lincoln

July 2019

TECHNICAL REPORT DOCUMENTATION PAGE

1. Report No. 25-1121-0005-004-31	2. Government Accession No.	3. Recipient's Catalog No.	
4. Title and Subtitle Protecting Critical Civil Infrastructure Against Impact from Commercial Vehicles - Phase I	5. Report Date July 2019		6. Performing Organization Code
	7. Author(s) Daniel G. Linzell https://orcid.org/0000-0002-7158-1776 , Yong-Rak Kim https://orcid.org/0000-0002-5421-750X , Chen Fang, Gabriel Nsengiyumva		
9. Performing Organization Name and Address Mid-America Transportation Center 2200 Vine St. PO Box 830851 Lincoln, NE68503-0851	10. Work Unit No.		8. Performing Organization Report No. 25-1121-0005-004-31
	11. Contract or Grant No. 69A3551747107		
12. Sponsoring Agency Name and Address U.S. Department of Transportation 1200 New Jersey Avenue, SE Washington, DC 20590	13. Type of Report and Period Covered January 1, 2018 ~ June 30, 2019		
	14. Sponsoring Agency Code MATC TRB No. 91994-20		
15. Supplementary Notes Conducted in cooperation with the U.S. Department of Transportation, Federal Highway Administration.			
16. Abstract Bridge pier columns are critical load carrying elements and are often positioned in a fashion where it is neither possible nor economically feasible to place protective devices around them. Pier columns could be under-designed for commercial vehicle impacts and additional events that could occur, such as blast. The project is focusing on improving pier column resiliency and robustness in the event of an accidental or purposeful vehicle impact coupled with an additional event, e.g., an air blast, and a fire. To achieve this goal, a literature search was performed that focused on the studies that investigate the behavior of reinforced concrete (RC) structures under vehicle impact and blast, current design specifications related to the bridge piers subjected to these demands, and general reinforced concrete bridge element design and detailing criteria. Based on the literature review, a multi-column, highway, bridge pier and its supporting foundation was used as the prototypical supporting unit for the analytically focused project. Initial studies used a 3D, LS-DYNA numerical model of a single, circular, reinforced concrete column from the piers along with that column's supporting spread footing and piles. Surrounding soil and air volumes were also modeled using LS-DYNA. Impact was supplied from a Ford F800 Single-Unit truck. Air blasts of varying magnitude were represented using an Arbitrary Lagrangian-Eulerian approach. The model was validated against published RC structural element impact and blast tests and predicted response well. As a result, the validated modeling approach was recommended for future studies in association with the project. After a literature review, experimental efforts were undertaken to characterize adhesion of the retrofitting polymer to concrete also with impact and blast properties for resistance of the retrofitted specimens. Adhesion testing as accomplished by a modified single edge notched beam (SEND) with a cement-polyurea (PU)-glue-cement sandwiched layers in the middle. Adhesion test results indicated a strong interface bonding between cement and PU which further improved by treatment of the cement surface to increase the roughness. Impact testing was performed using a drop-tower, where the results showed that PU coating increased damping behavior of the concrete specimen by permitting the impact load to be distributed on a larger area and for a longer time. Blast testing will be carried out using TNT explosives on reinforced concrete slabs which will require assistance from the Nebraska State Patrol for the testing.			
17. Key Words Bridge; Reinforced Concrete; Column; Collision; Blast; Vehicle		18. Distribution Statement Data and reports will be limited to members of the program until publications and presentations are submitted.	
19. Security Classif. (of this report) Unclassified	20. Security Classif. (of this page) Unclassified	21. No. of Pages 103	22. Price

Table of Contents

Acknowledgments.....	viii
Disclaimer	ix
Abstract	x
Chapter 1 Introduction and Background.....	1
1.1 Background.....	1
1.2 Problem Statement.....	3
1.3 Objective.....	4
1.4 Scope.....	4
Chapter 2 Literature Review.....	6
2.1 Introduction.....	6
2.2 Response of RC Bridge Elements under Vehicle Impact, Blast, Fire	6
2.2.1 Material properties under impact and blast.....	6
2.2.2 Response of RC bridge elements under vehicle impact.....	8
2.2.3 Response of RC bridge elements to blast	16
2.2.4 Response of RC bridge elements under fire	25
2.3 Development and Implementation of Innovative Materials and Bridge Support to Resist Multiple Hazards.....	28
2.3.1 Examples of bridges subjected to multiple hazards.....	29
2.3.2 Studies of innovative retrofit materials.....	30
2.3.3 Studies of innovative designs.....	37
2.3.4 Studies on experimental testing to get material properties	44
2.3.4.1 Blast studies	44
2.3.4.2 Impact studies	49
2.3.4.3 Bond Studies	50
2.4 Improving Soil Response under Impact and Blast.....	52
2.5 Reliability-based Indices and Equations for RC Bridge Elements	57
2.6 Conclusions.....	62
Chapter 3 Finite Element Model Development	63
3.1 Introduction.....	63
3.2 Prototype Pier Column.....	63
3.3 Impact and Blast Modeling.....	66
3.3.1 Vehicle model	66
3.3.2 Simulation of blast load	66
3.4 Material Models	67
3.4.1 Concrete	67
3.4.2 Steel.....	69
3.4.3 Soil.....	69
3.4.4 Explosive and air.....	70
3.5 Model Coupling and Boundary Conditions	72
3.6 Conclusions.....	74
Chapter 4 Experiments for Material Properties	75
4.1 Retrofitting Materials Selection:.....	75
4.2 Sample Preparation and Set-up.....	76

4.2.1 Adhesion test.....	76
4.2.2 Impact testing.....	78
4.2.3 Blast testing.....	80
4.3 Test results and discussions	82
4.3.1 Impact testing.....	82
4.3.2 Adhesion testing.....	84
Chapter 5 Validation Study.....	88
5.1 Introduction.....	88
5.2 RC beams under impact load	88
5.3 RC column under blast load.....	91
5.4 Conclusions.....	94
Chapter 6 Conclusions	95
6.1 Summary	95
6.2 Ongoing Research.....	95
References	97

List of Figures

Figure 1.1 I-65 vehicle collision and explosion [1].....	1
Figure 1.2 Pier column damage, protective barrier in place (2)	2
Figure 2.1 Pier column damages with crash barrier (10).....	7
Figure 2.2 Relationship between steel strength and strain rate [9].....	8
Figure 2.3 I-37 pier collision (6).....	9
Figure 2.4 I-35 pier collision (6).....	10
Figure 2.5 I-80 pier collision (16).....	11
Figure 2.6 Shock wave parameters for TNT explosions (9).....	17
Figure 2.7 Idealized pressure-time history of an explosive in free air (29).....	18
Figure 2.8 Pressure-time history for Mach reflection and regular reflection (31).....	19
Figure 2.9 Effect of angle of incidence on the reflected pressure coefficient (31).....	20
Figure 2.10 Blast-loading categories (31).....	21
Figure 2.11 Pressure design ranges (9).....	22
Figure 2.12 I-580 bridge fire (46).....	26
Figure 2.13 I-85 bridge fire (47).....	27
Figure 2.14 Highway bridge vehicle explosion and fire (52).....	30
Figure 2.15 Standard furnace test on RC column (61)	33
Figure 2.16 Corrugated aluminum sandwich structure (67).....	35
Figure 2.17 Multi-column pier system with concrete-filled steel tube columns (41).....	39
Figure 2.18 Multi-double skin composite panel column bent and column (83).....	40
Figure 2.19 Double skin composite bridge deck (83).....	41
Figure 2.20 Multi-double skin composite bridge wall pier (83).....	42
Figure 2.21 Concrete-filled double skinned tube (84).....	43
Figure 2.22 Multi-concrete-filled double skinned tube column pier (83, 84)	43
Figure 2.23 Steel plate shear wall box bridge pier (85).....	44
Figure 2.24 Blast test setup and sensor locations(86).....	45
Figure 2.25 Blast testing: (a) Slab instrumentation and (b) LVDT connection to the underside of a test specimen (88).	46
Figure 2.26 Blast testing: (a) procedure of concrete specimen fabrication and (b) test set-up (89).	47
Figure 2.27 Experimental setup for blast tests (91).	49
Figure 2.28 Impact test instrument used in (92)	50
Figure 2.29 Three-point bending test for CFRP-Concrete interface: (a) details of test specimen and (b) test set-up (93).	51
Figure 2.30 Adhesion testing used by Khedmati, Alanazi et al. (94).....	52
Figure 2.31 Effect strain rate on soil shear strength (95).....	53
Figure 2.32 Modified Mohr-Coulomb model (96)	54
Figure 2.33 Proposed viscoplastic cap model and experimental soil pressure and impulse comparisons (98).....	55
Figure 2.34 Comparison of predicted and measured soil ejected heights, improved viscoplastic cap model (99)	56
Figure 2.35 Fragility estimates for a RC column (102).....	58
Figure 2.36 RC column fragility contours, performance level P3 (20, 21).....	59

Figure 2.37 Reliability curves for RC columns under blast (103).....	60
Figure 2.38 Fragility curves for bridge under blast (104).....	61
Figure 2.39 RC column collapse probability curves (105).....	62
Figure 3.1 Prototype pier and column	64
Figure 3.2 Finite element model of column and foundation.....	65
Figure 3.3 FHWA soil model failure surface (96).....	70
Figure 3.4 Representative column finite element model	74
Figure 4.1 Polyurea spraying at a local supplier (VersaFlex®).....	76
Figure 4.2 PU-concrete adhesion test: (a) sample configuration and (b) sample preparation process.	77
Figure 4.3 Impact testing of PU coated concrete specimens test: (a) sample configuration and (b) sample preparation process.	79
Figure 4.4 Blast experiment set-up: (a) experimental set-up, (b) rebars design top view and (b) rebars design side view.	81
Figure 4.5 Impact test results: (a) acceleration vs. time at impact, (b) cracks in uncoated specimen (control) and (c) coated specimens after two impact testings.....	83
Figure 4.6 Load vs. time results from adhesion testing: (a) for untreated surface and (b) for treated surface.	85
Figure 4.7 Failure surfaces: (a) cement-cement, (b) PU-glue and (c) cement-PU interface.	87
Figure 5.1 Drop-hammer impact test setup and numerical model (mm) (122)	89
Figure 5.2 Comparison between experimental and simulated damage for: (a) $h_d = 600$ mm; (b) $h_d = 1200$ mm (122)	90
Figure 5.3 RC beam experimental and modeled impact force time histories (122)	91
Figure 5.4 RC beam experimental and modeled midspan displacement time histories (122).....	91
Figure 5.5 Experimental configuration and FE model (mm).....	92
Figure 5.6 Damage patterns comparisons	93
Figure 5.7 Mid-height displacement time histories	94

List of Tables

Table 2.1 Tests on the FRP strengthened RC beams (56)	32
Table 3.1 Material properties of concrete and steel reinforcement	68
Table 3.2 Soil material parameters	70
Table 3.3 TNT material and EOS parameters.....	71
Table 3.4 Air material and EOS parameters	72
Table 4.1 Specimen Information and Failure Characteristics of Adhesion Test Specimens.....	84

Acknowledgments

This work was completed utilizing the Holland Computing Center of the University of Nebraska, which receives support from the Nebraska Research Initiative. The authors would like to gratefully acknowledge computational support provided by the University of Nebraska's Holland Computing Center.

Disclaimer

The contents of this report reflect the views of the authors, who are responsible for the facts and the accuracy of the information presented herein. This document is disseminated in the interest of information exchange. The report is funded, partially or entirely, by a grant from the U.S. Department of Transportation's University Transportation Centers Program. However, the U.S. Government assumes no liability for the contents or use thereof.

Abstract

Bridge pier columns are critical load carrying elements and are often positioned in a fashion where it is neither possible nor economically feasible to place protective devices around them. Pier columns could be under-designed for commercial vehicle impacts and additional events that could occur, such as blast. The project is focusing on improving pier column resiliency and robustness in the event of an accidental or purposeful vehicle impact coupled with an additional event, e.g., an air blast, and a fire. To achieve this goal, a literature search was performed that focused on the studies that investigate the behavior of reinforced concrete (RC) structures under vehicle impact and blast, current design specifications related to the bridge piers subjected to these demands, and general reinforced concrete bridge element design and detailing criteria. Based on the literature review, a multi-column, highway, bridge pier and its supporting foundation was used as the prototypical supporting unit for the analytically focused project. Initial studies used a 3D, LS-DYNA numerical model of a single, circular, reinforced concrete column from the piers along with that column's supporting spread footing and piles. Surrounding soil and air volumes were also modeled using LS-DYNA. Impact was supplied from a Ford F800 Single-Unit truck. Air blasts of varying magnitude were represented using an Arbitrary Lagrangian-Eulerian approach. The model was validated against published RC structural element impact and blast tests and predicted response well. As a result, the validated modeling approach was recommended for future studies in association with the project. After a literature review, experimental efforts were undertaken to characterize adhesion of the retrofitting polymer to concrete also with impact and blast properties for resistance of the retrofitted specimens. Adhesion testing was accomplished by a modified single edge notched beam (SNEB) with a cement-polyurea (PU)-glue-cement sandwiched layers in the middle. Adhesion test results indicated a strong interface bonding between cement and PU which

further improved by treatment of the cement surface to increase the roughness. Impact testing was performed using a drop-tower, which the results showed that PU coating increased damping behavior of the concrete specimen by permitting the impact load to be distributed on a larger area and for a longer time. Blast testing will be carried out using TNT explosives on reinforced concrete slabs which will require assistance from the Nebraska State Patrol for the testing.

Chapter 1 Introduction and Background

1.1 Background

Bridge piers consisting of reinforced concrete (RC) columns are common substructure units. When piers are located close to travel lanes, they can be highly vulnerable to impact loads due to an accidental or purposeful vehicle collision and significant damage or complete failure could result. When the impact is coupled with an air blast, further deterioration could occur, possibly resulting in the collapse of the pier and possibly multiple spans and the entire bridge. Current American Association of State Highway and Transportation Officials (AASHTO's) bridge design codes do not explicitly account for vehicle collision coupled with an air blast.

Numerous examples of collisions coupled with air blasts exist. For example, in Nashville, Tennessee, a reinforced concrete bridge over I-65 was impacted by a tanker truck and a subsequent explosion occurred, in 2014 (1). As shown in figure 1.1, the bridge pier and girders it supported suffered significant damage, resulting in an unsafe condition.



Figure 1.1 I-65 vehicle collision and explosion [1]

Protective devices including crash barriers, fencing, and bollards, are often utilized to protect bridges from vehicle collision and coupled air blasts, be they intentional or unintentional, by preventing direct impact and increasing explosion physical standoff distance. Bridge piers are often located in a fashion where it is neither possible nor economically feasible to place the protective devices around them. As shown in figure 1.2, if protective devices are not feasibly positioned their effectiveness can be severely compromised (2). Additional steps could be taken to strengthen the supporting pier columns and caps in-situ via enhanced structural detailing and hardening techniques.

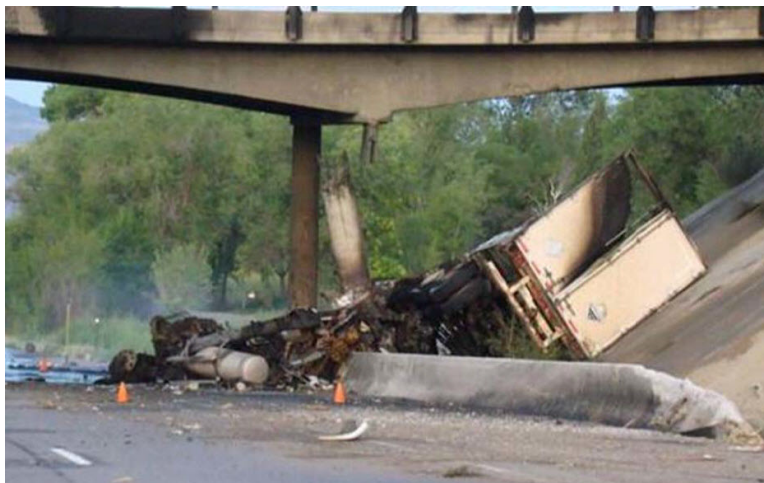


Figure 1.2 Pier column damage, protective barrier in place (2)

AASHTO's Load and Resistance Factor Design (LRFD) Specification and accompanying state Department of Transportation (DOT) bridge design guides and specifications are the primary design codes for highway bridge design in the U.S. (3). The 8th edition of the LRFD mandates representing vehicle collision design loads with an equivalent static force (ESF) of 600 kips (2670 kN) at a distance of 5 ft. (1.5 m) above for piers 20 ft. (9.1 m) from the roadway edge (3). Recent research indicates that this standard AASHTO-LRFD impact design load may be

non-conservative for heavy trucks at high velocities (4-7). In addition, multi-hazards involving a vehicle impact and an additional event, such as a blast or fire, are not explicitly considered in the LRFD code. Hence, additional research that determined appropriate impact bridge pier columns design loads for various hazardous events would be beneficial along with work that addressed improving their resistance to these extreme events.

1.2 Problem Statement

This research will aim to accomplish the following:

- (1) Add to the limited studies that have been published examining bridge pier column under collision and blast loads in an attempt to parametrize structural response and damage;
- (2) Improve bridge column resistance to collisions from vehicles traveling high speeds coupled with air blast and possibly fire;
- (3) Investigate column response, damage levels, and beneficial or detrimental detailing during a coupled collision and explosion event that may provide useful information for both retrofitting existing and constructing new columns;
- (4) Address the inaccurate representation of demands placed on bridge columns subjected to vehicle impact, air blast, and possibly fire;
- (5) Perform laboratory experimental testing for impact and blast resistance of polymer-coated concrete specimens;
- (6) Perform adhesion characterization of the retrofitting polymeric coating with concrete and surface treatment to improve the adhesion.

1.3 Objective

The overall purpose of the research study is to improve the resiliency and robustness of bridge pier columns in the event of intentional or accidental vehicle collision coupled with a possible explosion. Research studies completed to date have investigated the behavior of bridge and bridge components under either vehicle collision or blast, including experimental tests and numerical simulations on bridge and bridge components, but have not examined bridge columns under combined collision and blast loads. To obtain accurate materials properties for finite element modeling, experimental testing will evaluate adhesion of retrofit polymer coating to concrete specimens and characterize contribution of the coating to the impact and blast resilience of concrete.

1.4 Scope

These objectives will be addressed by:

- 1) Performing a detailed literature review of: studies that investigated the response of reinforced concrete bridge column subjected to the vehicle impact and blast; current U.S. design specification as it relates to these demands; relevant, general RC structural element U.S. specification criteria; and potential retrofit techniques for improving bridge column and substructure unit performance under impact and blast;
- 2) Developing finite element models of single and multiple RC bridge columns that are validated using the experimental results from the literature;
- 3) Completing numerical simulations of validated column models subjected to simulated truck impacts and air blast;
- 4) Developing an equation that calculates an equivalent static design force;

- 5) Performing parametric studies that investigate the effects of significant design and demand parameters on pier column response;
- 6) Assessing column residual capacity and developing a predictive equation;
- 7) Evaluate the effectiveness of various retrofitting techniques to improve the resistance of bridge columns to impact and blast;
- 8) Performing literature review for experimental testing of impact, blast and adhesion testing;
- 9) Investigating the appropriate polymeric coating material based on practicality and availability;
- 10) Evaluating appropriate method of polymer coating and surface treatment;
- 11) Conducting preliminary testing to determine appropriate parameters for impact, adhesion and blast testing; and
- 12) Performing tests using the determined testing parameters, analyzing and interpreting the results.

Chapter 2 Literature Review

2.1 Introduction

In many locations, it is neither possible nor economically feasible to place shielding (e.g., crash barriers) around exposed bridge columns. Some recent research has shown that the standard AASHTO-LRFD design impact load is non-conservative for heavy vehicles and high speeds, which indicates that current bridge columns are under-designed for commercial vehicle impacts (6, 7). In addition, bridges exposed to intentional or unintentional blasts and, possibly, fires that occur in association with the impact event are at risk of significant damage and possibly failure. The purpose of this research is to improve the resiliency and robustness of bridge pier columns in the event of an accidental or purposeful vehicle impact coupled with another event e.g. an explosion, possible fire. This goal will be accomplished by contributing to the state of the art associated with bridge pier column design and response of structural systems and components acted on by vehicle impact and explosion events, with an emphasis on bridge piers. To achieve this goal, a literature search was performed that focused on: studies that examined the behavior and analysis of materials and structures subjected to the vehicle impact and blast, with emphasis on research related to reinforced concrete (RC) and its constituent materials; current design specifications as they relate to bridge piers, with a focus on pier columns; and reliability-based indices for RC structural elements.

2.2 Response of RC Bridge Elements under Vehicle Impact, Blast, Fire

2.2.1 Material properties under impact and blast

The dynamic response of reinforced concrete structural elements depends heavily on loading rate (8). Since concrete cracks generally develop slowly, a high loading rate from impact and blast could inhibit their development. Under a high rate load, the concrete strength increases

due to inertial confinement provided by structural components as it cannot deform as fast as the components deform (9). Additional confinement is generated by the surrounding concrete. Concrete experiences a significant increase in strength as what is termed the “strain-rate threshold” is reached. Fig. 2.1 details the relationship between concrete strength and strain rate and shows that the strain-rate threshold in tension is approximately 2.5 s^{-1} , with the compression strain-rate threshold equaling 30 s^{-1} (10).

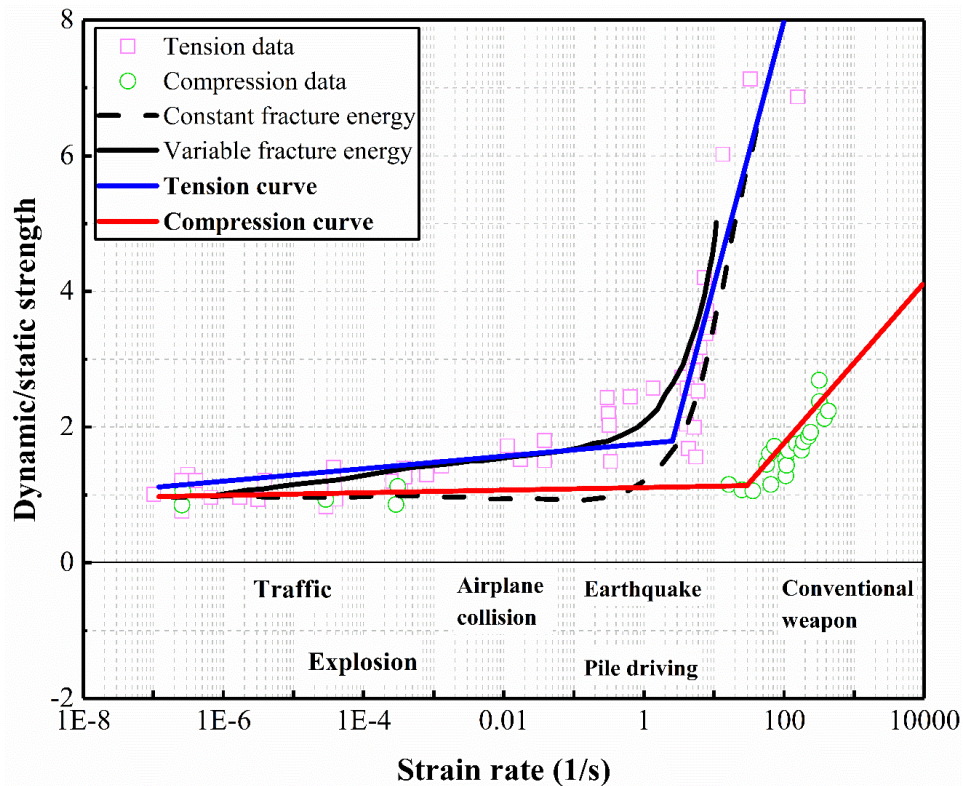


Figure 2.1 Pier column damages with crash barrier (10)

Properties of steel reinforcing bars embedded in the concrete are also affected by high loading rates (11). Yield and ultimate strengths of this ductile material experience a significant increase due to strain-rate effects. The elastic modulus of the steel does not change with the

increase in strain rate; however, a significant reduction of the ductility occurs to the steel at a high strain rate, which is referred to as “high-velocity brittleness”. Fig. 2.2 shows the relationship between the strength of the steel and the strain rate (11).

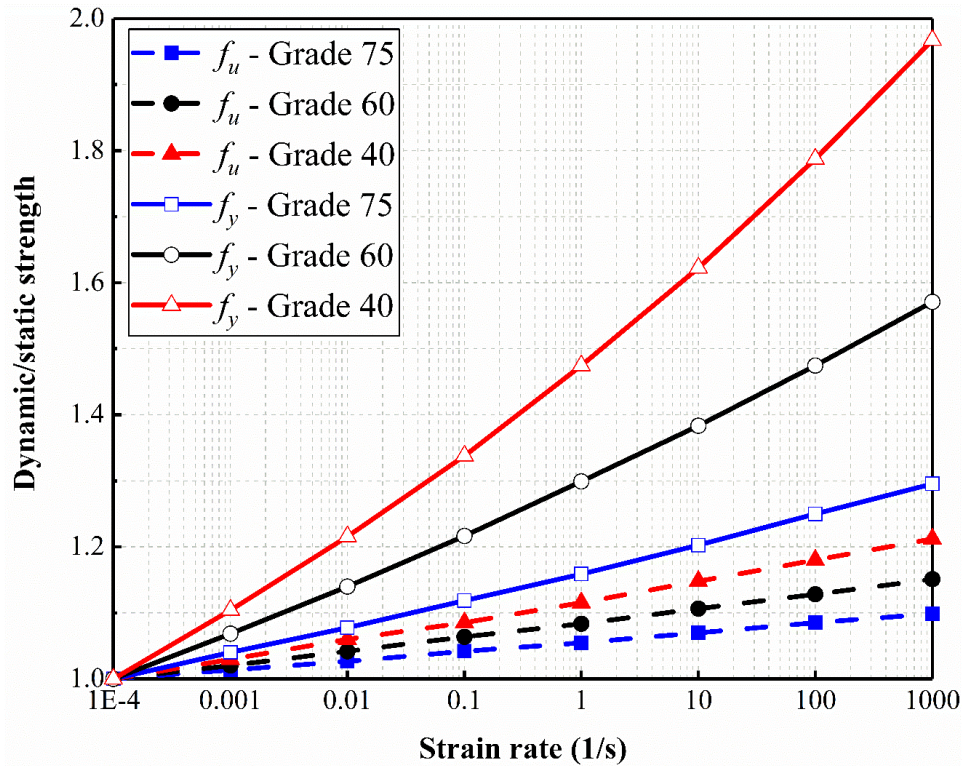


Figure 2.2 Relationship between steel strength and strain rate [9]

2.2.2 Response of RC bridge elements under vehicle impact

2.2.2.1. Examples of vehicle collisions with bridge elements

A large vehicle collision with a bridge is treated as a rare event when designing supporting columns; however, multiple cases of these types of collisions have happened, resulting in unsafe situations or complete collapse. Some representative events are summarized below. This information was taken from the studies performed by Buth et al. (6, 7), Wehbe et al. (12), Maghiar et al. (13), and other researchers (14, 15).

In Corpus Christi, Texas, a reinforced concrete bridge pier over I-37 was impacted by a tanker truck in 2004 (6). The truck collided with the easternmost column in a three-column pier at a speed of 55 mph (88.5 km/h) and subsequently the truck overturned, as shown in Fig. 1.3. The 2.5-ft (0.75-m) diameter column failed due to complete spalling of the concrete cover at the top and the bottom of the column and subsequent fracture or buckling of reinforced steel. As shown in fig. 2.3, bridge collapse did not occur.



Figure 2.3 I-37 pier collision (6)

In Red Oak, Texas, a tractor-trailer truck collided with a reinforced concrete bridge pier over I-35 in 2005 (6). The truck collided with a 2.5-ft (0.75-m) diameter column in a three-column pier at a speed of 60 mph (96.6 km/h). Failure of the RC column occurred due to shear at the top and bucking of the reinforcement. As shown in fig. 2.4, the bridge did not collapse.



(a) Truck collision with RC column



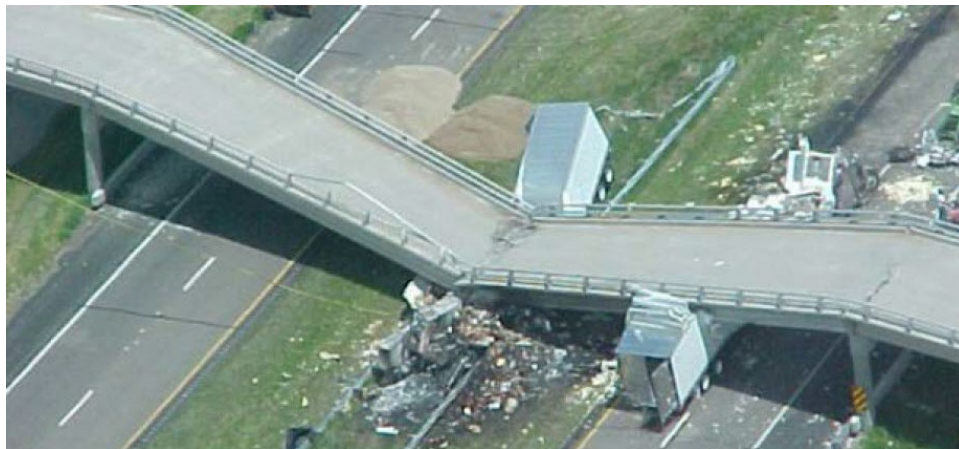
(b) Column failure mode

Figure 2.4 I-35 pier collision (6)

In Big Springs, Nebraska, a reinforced concrete overpass bridge was impacted by a semitrailer truck in 2003 (12, 16). As shown in fig. 2.5, bridge collapse occurred and a second truck travelling in the opposite direction was impacted by the collapsed bridge component. One person died and traffic was severely disrupted. The impact speed and bridge geometries were not provided in the literature.



(a) Truck collision with RC column



(b) Bridge collapse

Figure 2.5 I-80 pier collision (16)

As exhibited by representative cases summarized herein, impact and subsequent damage caused does not always lead to structural collapse but can certainly lead to costly repairs and extended bridge and roadway closures. These closures most certainly adversely affect social and economic activities for those traveling along the roadway(s) and living in close proximity to the bridge.

2.2.2.2. Research studies on vehicle collisions with bridges and bridge components

According to research conducted by Wardhana and Hadipriono (20) that examined causes of bridge failures in the United States between 1989 to 2000, the 503 bridge failures that were analyzed were mainly caused by hydraulic items (e.g. scour), collisions, overloads, deterioration, fires, and earthquakes. Vehicle collision was the cause of 59 failures, 10% of the total and the third highest failure category.

Bridges in the United States are designed and built following the AASHTO's-LRFD Bridge Design Specification (3) along with State DOT bridge design guides and specification that largely utilize information supplied from the LRFD. Including a vehicle collision load in the design process was proposed and considered in the 1st Edition of the Specification published in 1994 (17). The specification introduced an equivalent static force of 400 kips (1,780 kN) to design the bridge columns with this equivalent force applied in any, critical, horizontal 4 ft (1.2 m) above the ground. The equivalent static force was determined from a series of full-scale, 80,000-lb (36,300 kg) tractor-trailer 50-mph (80.5-km/h) barrier collisions (17), with the barriers designed to sustain a Test Level 3 (TL-3) impact according to Manual for Assessing Safety Hardware (18). Given that more studies on vehicle collision with the bridge systems were completed since initial publication, vehicle collision design loads were updated for the 6th Edition of the Specification (19), with the equivalent static horizontal load increased to 600 kips (2,670 kN) at 5 feet (1.5 m) above the ground. The impact direction was stated to be “zero to 15 degrees with the edge of the pavement.” The updated equivalent static load was based on research performed by Buth et. al (6, 7) that included completing a full-scale collision of an 80,000-lb (36,300 kg) tractor-trailer into a bridge pier consisting of a 3-ft (0.91-m) diameter

simulated rigid steel bridge column and a brace supporting frame at a speed of 50 mph (80.5-km/h).

Sharma et al. (20, 21) investigated the responses of reinforced concrete bridge columns under vehicle collisions using the LS-DYNA finite element and multiphysics structural analysis program and evaluated column performance. The research developed a framework for performance-based design and analysis of bridge columns subjected to vehicle impact. Performance levels were defined for a representative bridge column: fully operational with no damage; operational with damage; and complete collapse. Probabilistic models were then proposed to estimate bridge column shear capacity and demand under vehicle collisions. These performance levels were calibrated against impact demand and resistance factors to obtain desired levels of performance when completing a design.

El-Tawil et al. (22) developed finite element models of vehicle collisions with bridge piers using LS-DYNA to study their performance under impact and to evaluate the feasibility of the proposed models to estimate the response of bridge piers against impacting load. Two vehicle models produced by the National Crash Analysis Center (23), a Chevy C-2500 pickup truck and a Ford F800 single-unit truck, impacted pier models having different geometric characteristics. A parametric study was conducted to evaluate modeling techniques and analyze effects of various key parameters, which includes barrier flexibility, coefficient of friction, and damping ratio, on the impact load. Results indicated that the design collision load required in the 2002 LRFD Bridge Design Specification was lower than computed equivalent static loads from the analyses.

Agrawal et al. (24) conducted an analytical investigation of the response of reinforced concrete bridge piers subjected to vehicle collisions from a Ford F800 Single-Unit Truck (SUT) to parametrically examine dynamic forces between the vehicle and impacted piers. A LS-DYNA

finite element model of a three-span bridge was developed that included the superstructure, piers and pile foundations. Each pier was a three-column bent with each column being of rectangular cross section. Several parameters, including vehicle velocity, pier diameter, and impact incidence angle, were considered. Performance of bridge support columns was evaluated based on failure observed modes and with damage assessed using a damage ratio, which was defined as the ratio between peak dynamic impact force to pier shear capacity.

Gomez et al. also (25) investigated structural response of reinforced concrete bridge piers subjected to the vehicle collisions using LS-DYNA. A parametric study was performed to examine the effects of pier diameter, transverse reinforcement spacing, vehicle impact velocity, pile cap height, and number of columns on response of the bridge column to vehicle collision. The studied bridge piers consisted of a single reinforced concrete column, portions of the superstructure, and a simplified pile foundation system. It was shown that vehicle collisions with stiff piers led to high forces, low lateral displacements and high shear resistance. Pier diameter had critical influence on failure modes and force distribution of the bridge column.

Buth et al. also performed experimental and analytical studies of vehicle collisions with simulated bridge piers (6, 7). Two full-scale crash tests using an 80,000-lb (36.3 Mg) tractor-trailer were performed on 3-ft (0.91-m) diameter simulated rigid bridge piers. Finite element models were developed and validated against experimental results and were then used to conduct a parametric analysis on force demands on a bridge pier during a vehicle impact. Parameters included the type of truck, type of cargo, impact speed, and pier diameter. The research demonstrated that collision forces were much larger than 400 kips (1,780 kN), the impact load from the LRFD Design Specification. The research also developed a methodology for estimating the risk of a vehicle leaving the road and hitting a bridge pier.

Thilakarathna et al. (26) investigated vulnerability and performance of reinforced concrete columns under low to medium velocity vehicle impacts and developed potential mitigation techniques. Validated finite element models were used to parametrically predict impact response of reinforced concrete columns, with results being subsequently used to develop equations to predict critical impact force and impulse. It was shown that triangular impact pulses would best represent an actual collision. New guidelines for determination of contact area between colliding objects were developed. A new limit state was proposed to assess column resistance to impact loads.

Abdelkarim and ElGawady (4) parametrically evaluated reinforced concrete bridge pier performance under vehicle collision to develop a design equation. Examined parameters included the: concrete constitutive model; unconfined concrete compressive strength; strain rate; amount of longitudinal reinforcement; amount of shear (hoop) reinforcement; column span-to-depth ratio; column diameter; top boundary conditions; axial load level; vehicle velocity and mass; roadside distance between errant vehicle and an unshielded bridge column; and soil depth above the top of the column footing. The research used three approaches to determine and compare equivalent static forces (ESFs) for columns that were analyzed. The first approach focused on calculating an ESF that produced the same maximum displacement at the point of impact. The second used equations from the Eurocode (27) to calculate the ESF. The third defined the ESF as the Peak of the Twenty-five Milli Second moving Average (PTMSA). Resulting ESFs were compared against the 600-kip (2,670-kN) design collision force required in the LRFD Specification. It was demonstrated that the design force was sufficient for heavy vehicle and/or high-speed impact, but was too conservative for light vehicle and/or low speed impact. The

research developed an equation to calculate design impact force based on impact velocity and vehicle mass.

2.2.3 Response of RC bridge elements to blast

This section gives a brief overview of air blast physics and how those effects can be simulated. Studies examining the response of bridge structural elements to air blast are then summarized.

2.2.3.1 Blast load

The Hopkinson or Cube-root scaling law is an effective approach for approximating air blast shock waves generated by different combinations of explosive weights and standoff distances (28). The scaling law is used to economically expand applicability of experimental blast tests to different impulse levels. It is expressed as shown in equation 2.1.

$$Z = \frac{R}{\sqrt[3]{w_{TNT}}} \quad (2.1)$$

where Z is the scaled standoff distance or “scaled distance” ($\text{ft}/\text{lbs}^{1/3}$), R is the standoff distance (ft.), and w_{TNT} is the TNT-equivalent explosive weight (lbs).

Z is used to represent blast load intensity and provides a relationship between explosive weight and the standoff distance when defining a blast wave. The TNT-equivalent explosive weight relates output energies from different types of explosive to TNT and is determined by multiplying explosive weight by the ratio of that explosive’s yield to that of TNT, with the yield representing approximate energy release during the detonation of a metric ton of the explosive. Tests have shown that the scaling law is valid for Z greater than $0.4 \text{ ft}/\text{lbs}^{1/3}$ ($0.16 \text{ m}/\text{kg}^{1/3}$). The

figure is based on numerous experimental tests and theoretical work and can be utilized for both hemispherical and spherical blasts (9).

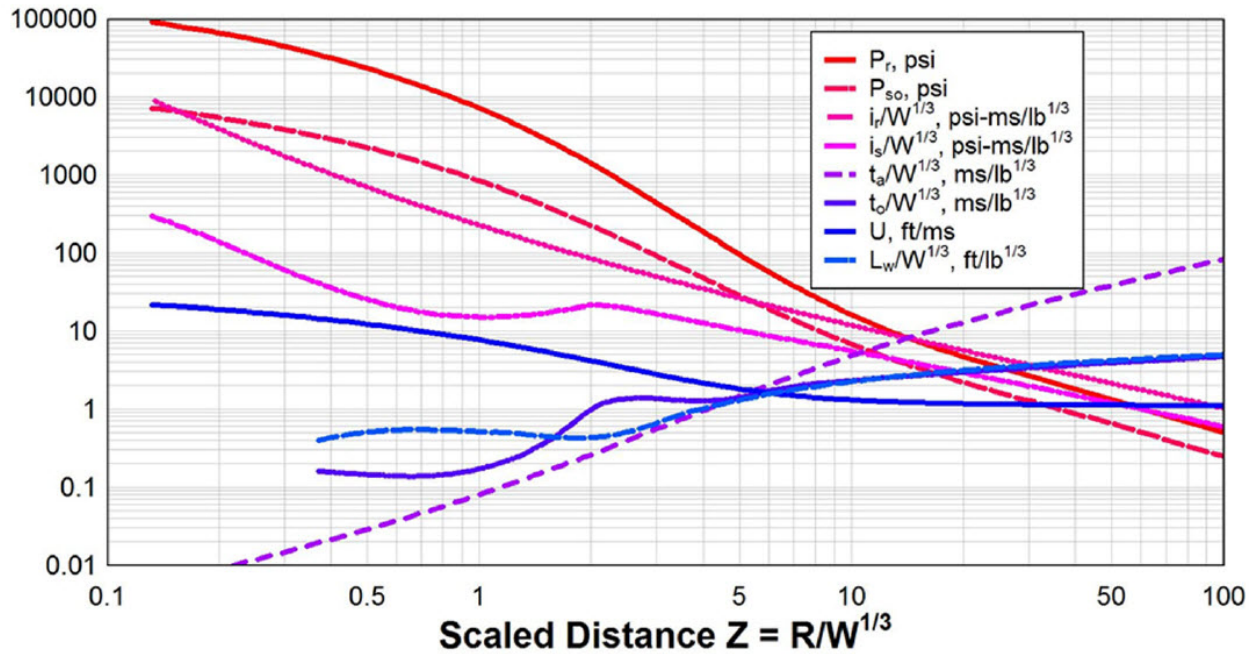


Figure 2.6 Shock wave parameters for TNT explosions (9)

The detonation of an explosive is due to a rapid chemical reaction that creates a shock wave from a sudden release of energy. The shock wave travels from the explosive material as highly compressed air at high speed and temperature and produces over and dynamic pressures, characteristics that can be idealized using a pressure-time history (9). The overpressure is the pressure produced by the explosive, much higher than the ambient pressure in an air volume, and the dynamic pressure is pressure experienced in that air volume after the shock waves pass. Fig. 2.7 shows an idealized pressure-time history of an explosion in free air. P_0 is the ambient pressure of the air and t_A is the arrival time of the shock wave. As shown in the figure, the shock wave consists of a positive phase and a negative phase. In the positive phase, the overpressure

“pushes” on the structure and is represented by P_{so} . The negative phase creates an overpressure that “pulls” on the structure and is denoted by P_{so-} .

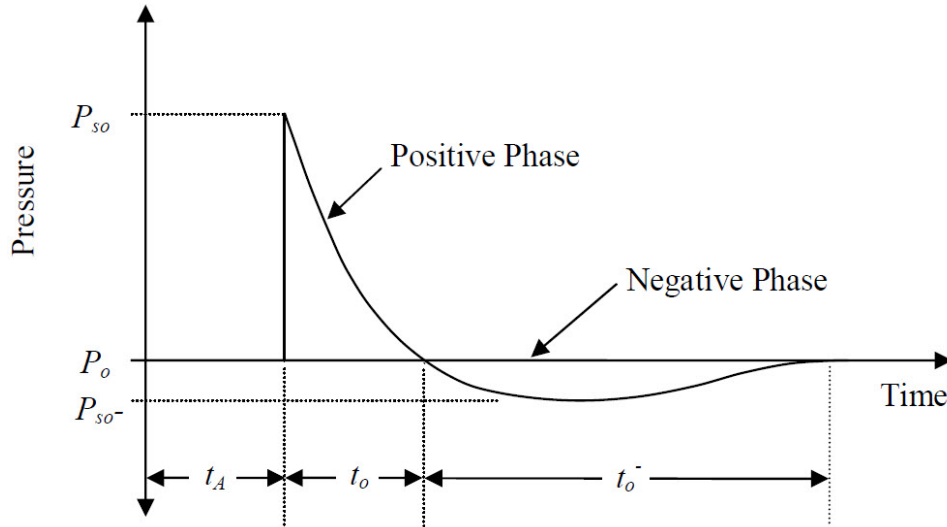


Figure 2.7 Idealized pressure-time history of an explosive in free air (29)

An explosion produces radiating shock waves with waves originating from the explosion termed incident waves. As the incident waves hit any surfaces of a structure, they are reflected off those surfaces and are defined as reflected waves. Reflected waves could merge with incident waves if explosive sources are close enough to reflecting surfaces. The overpressure would not reduce to the ambient pressure before the reflected and incident waves merge, an occurrence known as Mach reflection (30). Therefore, two independent overpressure peaks could occur in the resulting pressure-time curve. Fig. 2.8 (a) shows a pressure-time curve where the reflected wave merged with and incident wave and Fig. 2.8 (b) is a pressure-time curve when the waves do not merge (9).

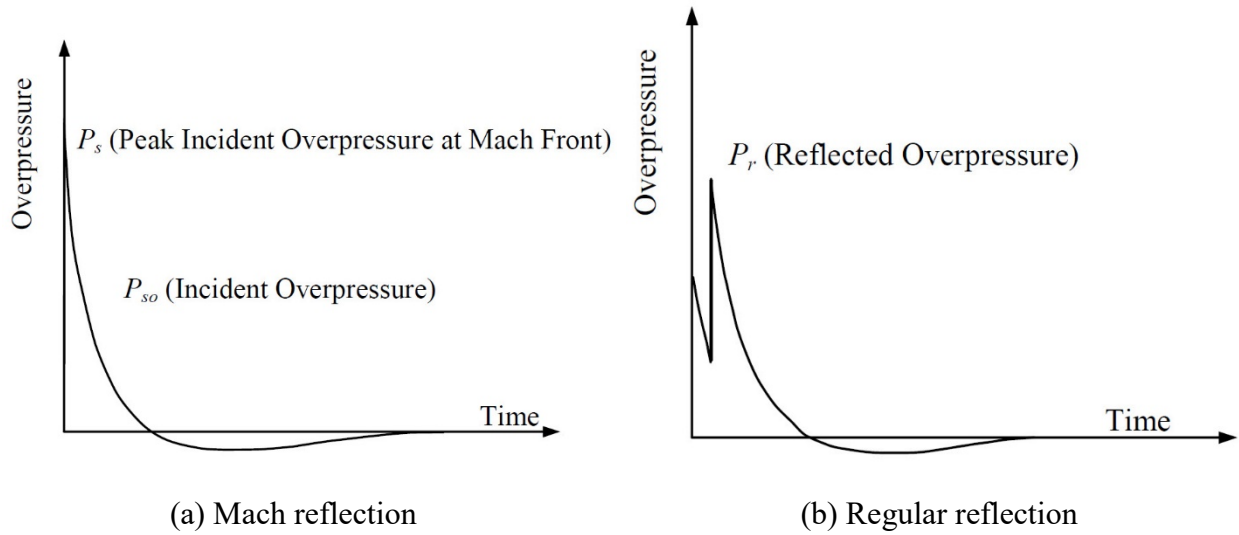


Figure 2.8 Pressure-time history for Mach reflection and regular reflection (31)

Reflected peak pressures depend on incident pressure and angle between the wave and the reflective surface. A relationship between incident angle and peak reflected pressure is provided by Department of Defense (31) as shown in fig. 2.9. C_{ra} is the peak reflected pressure coefficient which is defined as a ratio of peak reflected to peak incident pressure. Curves shown in the figure were developed based on semi-empirical data and analytical solutions of shock equations.

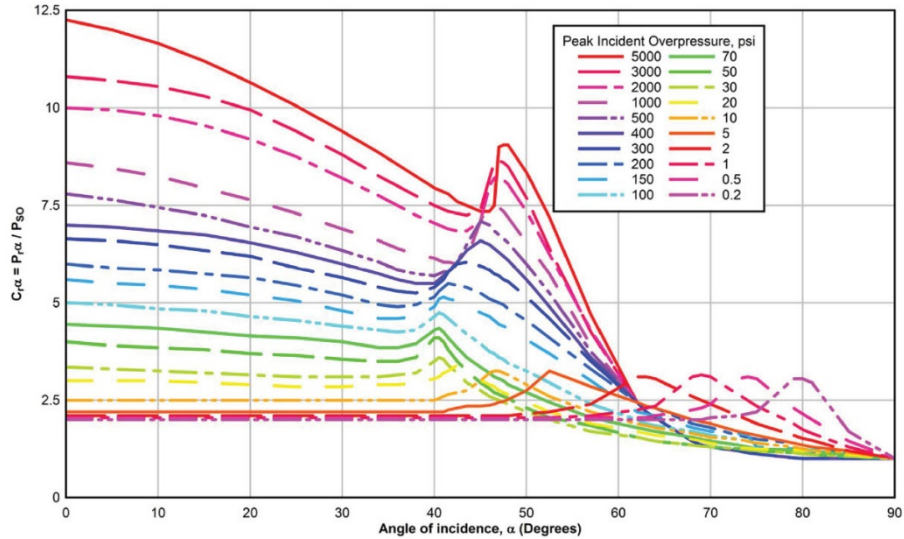
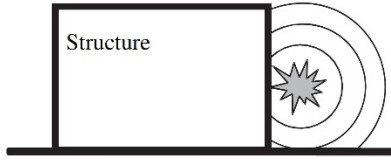
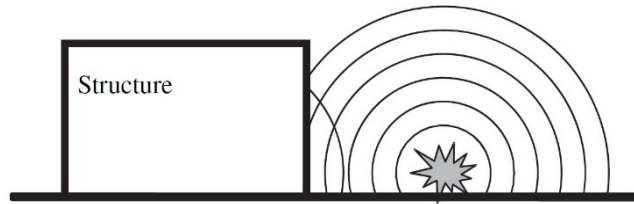


Figure 2.9 Effect of angle of incidence on the reflected pressure coefficient (31)

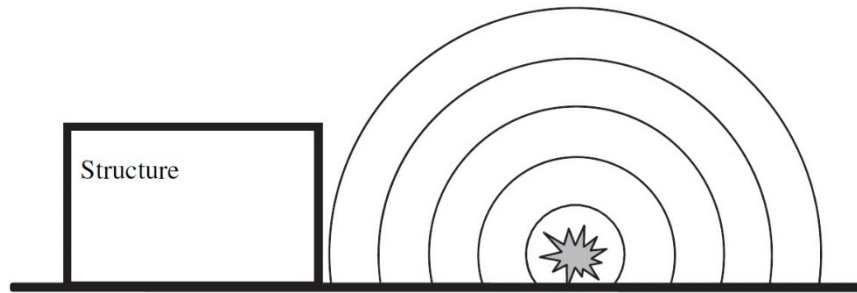
Three categories are commonly used to define blast-loads on structures (9, 31): (1) contact blasts; (2) close-in blasts; (3) and planar-wave blasts. Fig. 2.10 details these different categories. As shown in the figure, a contact blast produces a high-intensity, impulsive load on the structure. A close-in blast produces a non-uniform, spherical shock wave. Long standoff distances generate planar-wave blasts that can be represented using a uniform distributed load. Based on these loading categories, three design ranges could be provided as a function of structure response time and explosion duration (9): (1) impulsive load; (2) dynamic (or pressure-time) load; and (3) quasi-static (or pressure) load. Fig. 2.11 details these three ranges based on the time at which the structure experiences maximum deflection (t_m) and the duration of the positive phase (t_0). Since vehicle explosion produces a high-intensity shock wave at a close range, bridge design to resist vehicle explosion generally falls in the impulsive loading category.



(a) contact blast



(b) close-in blast



(c) planar-wave blast

Figure 2.10 Blast-loading categories (31)

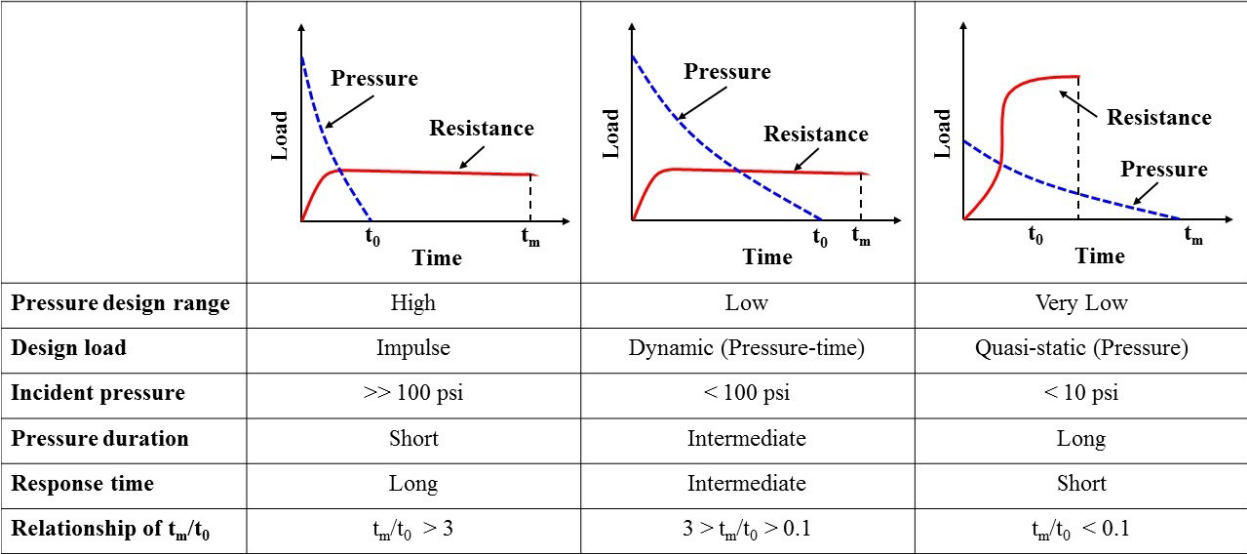


Figure 2.11 Pressure design ranges (9)

2.2.3.2 Research studies on blast effects on bridges and bridge components

In the public domain, designing bridges to resist air blast is a relatively immature research area and seismic design and detailing techniques have been suggested as possible design options (31, 32). It has also been suggested that several building, blast-resistant design guidelines could be utilized as references to design bridges, including: Structures to Resist the Effects of Accidental Explosions (9), Design of Blast-Resistant Buildings in Petrochemical Facilities (33), and Design and Analysis of Hardened Structures to Conventional Weapons Effects (34).

One of the more focused research efforts associated with bridge analysis and design for blast was completed in association with National Highway Research Program (NCHRP) Project 12-74 (31). The report largely focuses on substructure units and: provides an overview of the response of concrete bridge columns to blast loads; discusses means to develop analytical models of those columns; and presents a blast-resistant design framework. Presented procedures are intended for practicing engineers and, as such, were developed to be straightforward and easy to

incorporate into existing design criteria and processes. The developed general design and analytical procedure for blast-resistant bridge columns is defined as a function of scaled standoff, Z . Three design categories are defined with: design category A [$Z > 3 \text{ ft/lbs}^{1/3}$ ($Z > 1.19 \text{ m/kg}^{1/3}$)] requires no special considerations to resist potential threats; design category B [$1.5 \text{ ft/lbs}^{1/3} < Z \leq 3 \text{ ft/lbs}^{1/3}$ ($0.6 \text{ m/kg}^{1/3} < Z \leq 1.19 \text{ m/kg}^{1/3}$)] uses the seismic detailing approaches to harden pier columns and requires larger development (hook) lengths and designing and detailing for plastic hinging of the column; design category C [$Z < 1.5 \text{ ft/lbs}^{1/3}$ ($Z < 0.6 \text{ m/kg}^{1/3}$)] addresses the most severe threats and requires higher transverse reinforcement ratios and even larger development lengths. A single-degree-of-freedom dynamic response analysis is required for the design category C to ensure adequate ductility and rotation support.

Williamson and Winget completed a literature search that summarized effective methods to mitigate risks associated with terrorist attacks on critical bridges (32, 35). Risk management was aided via development of bridge protection categories based on their importance and type. A performance-based retrofit and design guideline was also proposed to harden the bridge and bridge components and reduce risks to an acceptable level. The standards were proposed based on bridge criticality and damage susceptibility under proposed design loads, with design loads and acceptable damage levels determined from threat and risk assessments.

Williams (29) conducted experimental and finite element analysis studies of the response of reinforced concrete bridge columns to blast loads. A series of tests of half-scale column specimens were performed to determine failure modes under various blast loads. Numerical models were developed using LS-DYNA and validated against test data. Results indicated that circle columns experienced lower net impulse than square columns for similar values of Z . The research identified the mechanics of damage development and failure modes for reinforced

concrete bridge columns and proposed a simplified method to predict blast effects on the columns.

Matthews (36) investigated response of a precast, prestressed reinforced concrete girder subjected to blast. A series of experimental tests of two full-scale girder specimens were conducted under different blast loads. A numerical model of a precast and prestressed girder was developed and validated against the tests. Four loading scenarios were considered: a blast located between two girders above and below the deck; and a blast centered on a girder above and below the deck. Two-hundred and fifty pounds of TNT was placed at a standoff distance of 4 ft (1.2 m) for the load cases above the deck and 500-lbs (226.8-kg) TNT was placed at a standoff distance of 10 ft (3.0 m) below the deck. Results showed highly localized damage was caused by 250-lbs (113.4-kg) of TNT above the deck and the deck failed for the 500-lbs (226.8-kg) TNT cases with small damage to the girders.

Yi et al. (37, 38) investigated the performance of a three-span, reinforced concrete highway bridge subjected to blast load using LS-DYNA. A new simulation approach, which was referred to as the hybrid blast load (HBL) method and considered reflection and diffraction, was utilized to generate loads. Numerical models were validated against experimental results (39) and results identified possible damage mechanisms. It was found that local damage to bridge components could lead to complete collapse. In addition, displacement at pier tops was greatly reduced when the ratio of ductility to strength reduction factor is larger than 6.

Fujikura et al. (40, 41) experimentally examined the performance of concrete-filled, steel tube bridge piers subjected to blast loads. A multiple-column pier was tested at 1/4-scale to demonstrate feasibility of the proposed system. The study indicated that the prototype pier system exhibited satisfactory resistance and ductility under blast loading.

Tang and Hao (42, 43) studied response of a cable-stayed bridge to air blast using LS-DYNA. A 978-ft (298-meter) high bridge was subjected to a simulated blast load from a 2,200-lb (1,000-kg) TNT explosion at a distance of 1.65-ft (0.5-m) from the bridge tower and 3.30-ft (1.0-m) above the deck. The study examined the damage mechanisms and failure modes. A progressive collapse analysis was also performed and the feasibility of FRP retrofit techniques examined. Results showed that the bridge deck was significantly damaged and that the minimum scaled distance at which complete collapse did not occur was $3.0 \text{ ft/lbs}^{1/3}$ ($1.20 \text{ m/kg}^{1/3}$) for the tower and $3.5 \text{ ft/lbs}^{1/3}$ ($1.33 \text{ m/kg}^{1/3}$) for the pier.

Tokal-Ahmed (44) investigated blast effects on the components of a two-span, simply-supported prestressed concrete girder bridge using a 3D analysis program Extreme Loading for Structures (ELS). An applied element model of bridge was developed and subjected to simulated blast loads with vulnerable components identified. Various protection measures were proposed and evaluated. It was demonstrated that similar levels of reinforcement should be provided at the top and bottom of the bridge deck when subjected to below-deck blast scenarios. Redundancy and continuity were also shown to be key factors to prevent progressive collapse.

2.2.4 Response of RC bridge elements under fire

Fire associated with a vehicle collision or impact, a blast or their combination has been shown to greatly alter material characteristics. As a result, their ability to maintain safe levels of operation is often compromised, with complete collapse being a possibility.

2.2.4.1 Cases of bridge fires

A survey completed by the New York Department of Transportation (N.Y.DOT) (45) examined prominent causes of bridge failures. The survey identified that, out of 1,746 bridge failures, 52 collapses were caused by fires.

A typical bridge fire incident is the collapse of the MacArthur Maze bridge in Oakland, California (46). In 2007, a tanker carrying 8,600 gallons (32.6 m³) of gasoline was overturned on an I-580 overpass, resulting in a severe fire. The bridge was constructed with six welded plate girders and a reinforced concrete deck. Two spans failed due to fracture of the plate girders as shown in fig. 2.12.



Figure 2.12 I-580 bridge fire (46)

Another recent example is fire-induced partial collapse of an elevated portion of I-85 in Atlanta, Georgia (47). In 2017, an overpass bridge suffered a severe fire. The fire started from ignition of materials stored under the bridge. As shown in the fig. 2.13, the fire led to a collapse of a 92-ft (28.0-m) long reinforced concrete span. Five bridge spans close to the collapsed section also needed to be removed.

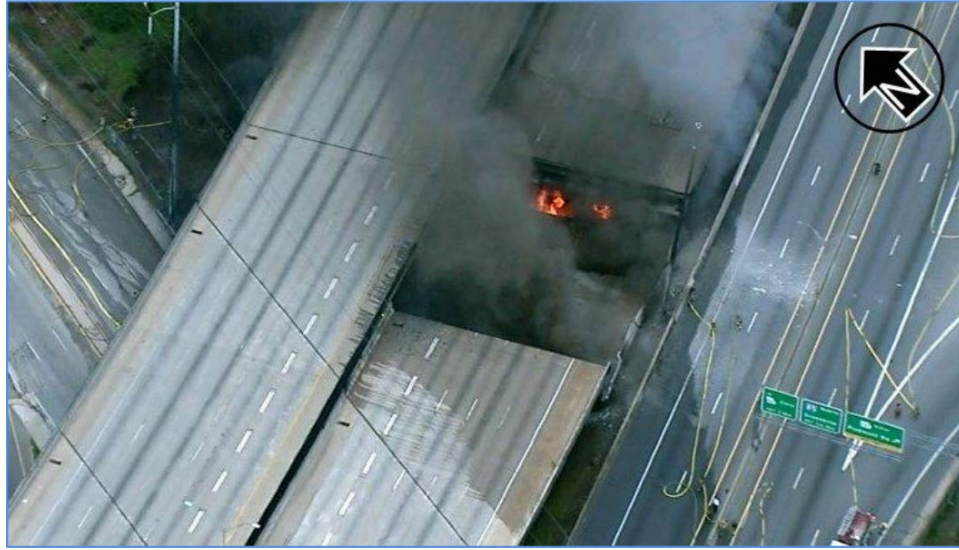


Figure 2.13 I-85 bridge fire (47)

2.2.4.2 Research studies of fire influence on RC bridge and bridge components performance

Mendes et al. (48) conducted research that examined the response of reinforced concrete bridge deck subjected to fire using a 2D numerical model. The research was completed in response to an event where a ship fire caused significant damage to a bridge deck. Three fire scenarios were considered and damage intensity examined. A parametric study was performed to examine effects of deck geometry, thermal radiation, fuel type, and radiation transfer on damage intensity. Results identified that the prestressing anchorage for the deck experienced serious damage 20-30 minutes after the fire started and failure of the anchorage caused progressive collapse

Nigro et al. (49) investigated thermo-mechanical performance of reinforced concrete bridge slabs strengthened with fiber reinforced polymers (FRP) under various fire events. Both 0.49-ft (0.15-m) thick and 0.66-ft (0.20-m) thick slabs were examined. Two possible fire situations were considered: asphalt overlay at a temperature of 180 °C; and a fire event acting

above the deck caused by an accident. Results showed that placing a concrete overlay above the FRP layer was recommended to prevent FRP fracture.

Nahid (50) studied response of bridge components to a vehicle fire using the Fire Dynamics Simulator fluid dynamics code embedded in ABAQUS. Localized fires were simulated using a non-uniform fire exposure model and a standard uniform furnace exposure model and performance was studied in bridges constructed using multiple steel plate girders and steel tubs. A parametric analysis was performed to determine factors that governed component failure. Results showed fire dynamics and the heat transfer to bridge components were controlled by girder geometry, with the single and double lane tub girder exhibiting better behavior under heavy fire exposure.

Payá-Zaforteza and Garlock (51) completed a finite element fire analysis of the performance of a 40-ft (12.2-m) long, singly supported, reinforced concrete bridge deck. The bridge consisted of five steel girders and a reinforced, non-composite concrete slab and the models were developed using LUSAS. The bridge deck was subjected to a simulated hydrocarbon design fire and parametric analyses were performed to examine effects of gravity load and axial restraint on the performance. Results identified that any potential interaction between the studied span and adjacent spans should be considered during a fire event.

2.3 Development and Implementation of Innovative Materials and Bridge Support to Resist Multiple Hazards

Highways can be subjected to one or more hazards, earthquakes, tsunamis, and, as is the focus of the present research, vehicle collisions, blasts, and fires. Bridge elements, such as piers, are designed and detailed to address some, but not all demands caused by these hazards and their

performance could be compromised as a result. A number of studies have been completed that focus on developing innovative materials and designs to address potential hazards.

2.3.1 Examples of bridges subjected to multiple hazards

Multiple hazards, which typically refer to a vehicle collision coupled with an explosion or/and a fire, are treated as rare events during a bridge design. However, several cases of these types of incidents have happened, imposing severe threats to bridges and bridge components. Two typical multiple-hazard events for highway bridges are summarized: a vehicle collision coupled with an explosion as described in chapter 1; and vehicle explosion followed by fire. This information has been reported by local and global news (1, 52).

The representative incident of vehicle collision followed by severe fire occurred in Bologna, Italy in 2018. A tanker truck exploded on a reinforced concrete highway bridge leading to a subsequent bridge fire (52). Bridge decks failed due to the complete spalling of concrete cover and buckling of the reinforcement embedded in the concrete. As shown in fig. 2.14, partial bridge collapse occurred due to the failure of bridge decks.



(a) Tanker explosion and fire

(b) Partial bridge collapse

Figure 2.14 Highway bridge vehicle explosion and fire (52)

2.3.2 *Studies of innovative retrofit materials*

Innovative materials, including fiber reinforced polymer (FRP) composites and ultra-high molecular weight polyethylene (UHMWP) concrete (53) and other materials, have been used to increase structural element resistance to various demands, including blast, impact and fires. A summary of relevant research is provided in the sections that follow.

2.3.2.1 Fiber reinforced polymer

Many types of fiber reinforced polymer (FRP) and polymer materials are available to strengthen bridges and bridge components. Proper use can increase the axial, flexural, and shear capacities and improve the stiffness and ductility of the bridge components under extreme conditions. Popular materials include carbon fiber reinforced polymer (CFRP) and glass fiber reinforced polymer (GFRP) and they are selected based on performance and cost. The FRP composites have been used to strengthen and retrofit beam, column, slab, and retaining wall (54).

For beams, columns, and decks, FRP composites are commonly bonded on their tensile face to improve flexural resistance. For compression members, FRP sheets are typically wrapped around the members to confine the concrete, thereby increasing axial capacity. For structural members subjected to large shear force, FRP stripes are often utilized to improve shear capacity.

Baylot et al. (55) studied the effectiveness of an FRP system for strengthening typical masonry walls subjected to blast loads using a series of tests of ¼-scale specimens. Two FRP application techniques were evaluated: 0.04-in. (1-mm) thick glass FRP bonded on the back surface of the wall; and a two-part sprayed-on FRP coating with thickness of 0.13 in. (3.2 mm) attached on the back face of the wall. A control specimen with 0.04-in. (1-mm) thick hot-dipped galvanized steel sheets overlapped at the top and bottom of the reaction structures was also studied. Results showed that all retrofitted walls collapsed; however, the FRP coating systems prevented fragments and debris from being ejected.

Ross et al. (56) conducted research that experimentally examined FRP effectiveness for strengthening reinforced concrete beams subjected to blast loads. Three reinforced concrete beams were strengthened using CFRP sheet bonded to the sides and bottom. The specimens were subjected to explosions using 244 lbs (110.6 kg) ANFO explosives located at the mid-span. Table 2.1 lists test information and results. Preliminary observations showed that FRP-strengthened specimens did not fail completely, while non-strengthened beams experienced a shear failure.

Table 2.1 Tests on the FRP strengthened RC beams (56)

Test	Standoff (m)	Retrofit	Impulse (MPa-ms)	Residual displacement (mm)	Comment
5	5.49	-	-	0	Multiple cracks
6	4.57	-	-	150	Multiple cracks & shear failure
7	5.34	-	1.52	0	Multiple cracks from beam top to beam
8	4.57	0.45 mm CFRP sides & bottom	-	-	Survive initial blast but rebounded with reflected pressure
9	4.57	0.45 mm CFRP sides & bottom	2.07	-	Side CFRP delaminated
10	4.57	0.45 mm CFRP wrapping	1.55	0	Side CFRP delaminated. Cracks at the top

Muszynski et al. (57) experimentally examined the performance of reinforced concrete walls retrofitted with CFRP and GFRP subjected to blast loading. Maximum displacements were reduced by approximately 30% for the GFRP retrofitted RC walls and 13% for the CFRP retrofitted RC walls when compared to a non-strengthened wall. The control walls experienced spalling, and spalling was not observed for the FRP-retrofitted walls.

Erki and Meier (58) completed impact tests on two 26.2-ft (8-m) long reinforced concrete retrofitted beams. Two RC beams were strengthened, one using CFRP and the second using a steel plate. Impact loads were generated by lifting and dropping the beams. The CFRP-strengthened beam was dropped from the heights of 1.64 ft. (0.5 m), 3.28 ft. (1.0 m), and 4.92 ft. (1.5 m). The CFRP-strengthened beam failed at the 4.92-ft (1.5-m) height dropping. The failure mode for the CFRP-strengthened beam was debonding of outside FRP and rupturing of intermediate laminate. The steel plate strengthened beam failed due to debonding of the

laminates. Results showed that the CFRP-strengthened beam performed better under impact loading, and the CFRP improved the impact resistance of RC beam to impact load.

Firno et al. (59, 60) investigated the behavior of CFRP strengthened concrete block using double lap shear tests at temperatures ranging between 20 °C and 120 °C. The effects of a mechanical anchorage on performance was investigated. Results indicated that bonding strength reduced with an increase in temperature, which led to an increase in axial strain distributions at the interface due to adhesive softening.

Bisby et al. (61, 62) experimentally studied the behavior of CFRP-strengthened circular reinforced concrete column covered with an intumescent epoxy coating at high temperatures using a furnace test. Two full-scaled column specimens were fabricated with a diameter of 16 in. (0.4 m) and a height of 12.5 ft (3.81 m), as shown in figure 2.15 (a). The CFRP strengthened columns demonstrated an increase in the axial strength of 26%, as shown in figure 2.15(b). The insulation system was effective to protect RC columns and maintain the overall capacity of RC columns during fire.

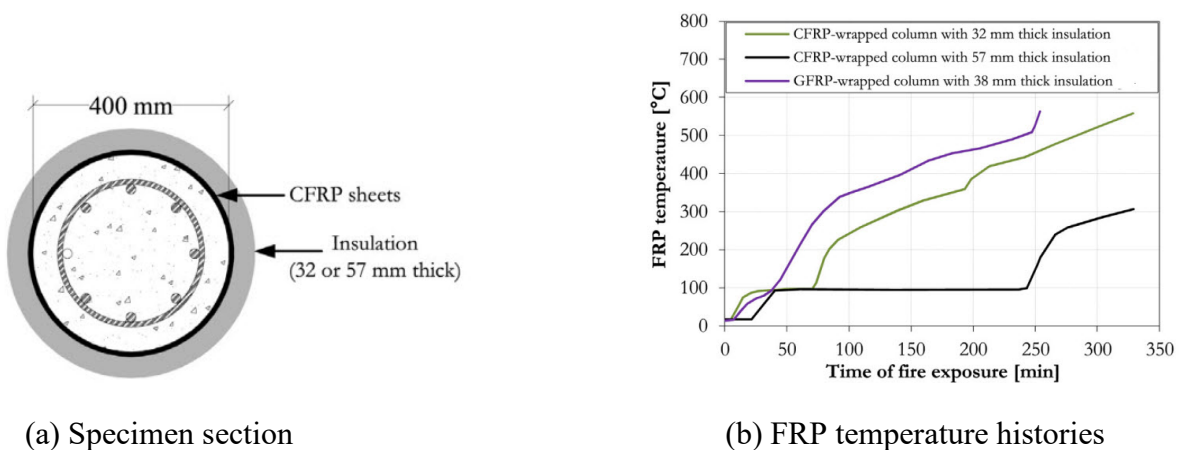


Figure 2.15 Standard furnace test on RC column (61)

2.3.2.2 Ultra-high molecular weight polyethylene (UHMWP)

Ultra-high molecular weight polyethylene (UHMWP) is a semicrystalline polyethylene with a high molecular mass (63). The high strength material has been used to make ropes, tear resistant fabrics, and ballistic impact protection systems (64, 65). While extensive studies have been completed examining its behavior over a wide range of demands, limited studies have been performed that examine the feasibility of a UHMWP as a retrofit technique for bridge and bridge components subjected to impact and blast.

Lässig et al. (66) studied the behavior of a UHMWP composite under shock conditions using an inverse planar plate impact test and the shock reverberation technique. Inverse planar plate tests were conducted using particle velocities between 380 mph (170 m/s) and 2013.2 mph (900 m/s). The shock reverberation technique helped determine the mechanical response of the UHMWP under high pressure. Results indicated UHMWP porosity or voids did not significantly influence behavior of the UHMWP composite at low shock pressures.

Zhang et al. (65) performed ballistic experimental research to investigate UHMWP flat panel response. The effects of fiber orientation and boundary constraints on material deformation and failure were evaluated using a back-face deformation experiment. Results showed that the boundary constraints did affect back-face deformation for hybrid panels and that expansion rate of the back-face deformation zone in the transverse direction reduced over time. Major delamination was shown at the cross-ply and non-cross-ply interface of the hybrid panels.

O' Masta et al. (67) experimentally studied the ballistic impact response of an UHMWP fiber reinforced polymer laminate encasing an aluminum-alumina hybrid panel. Figure 2.16 shows that two types of corrugated aluminum sandwich structures were tested and impacted by a spherical steel projectile. Results indicated that loading area on the inner surface of the rear

laminates were highest for a prism base impact and lowest for a prism apex impact. Ceramic fragmentation and nodal failures of the corrugated panel controlled redistribution of impact momentum. Large deflection for the full thickness laminate helped dissipate the kinetic energy in the core sandwich panel.

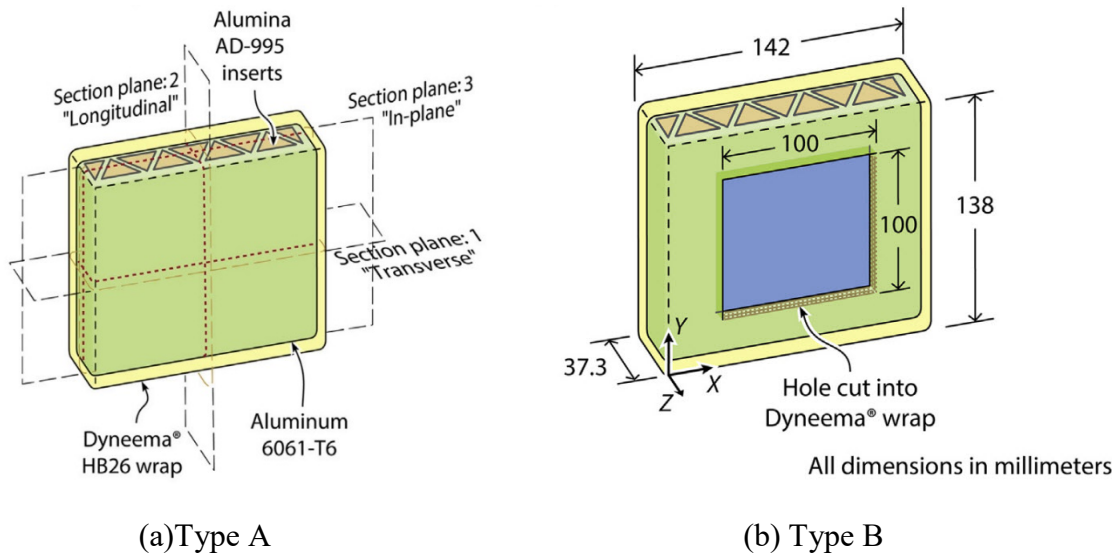


Figure 2.16 Corrugated aluminum sandwich structure (67)

Lee et al. (68) investigated high-energy impact behavior using drop-impact tests of hybrid composite plates strengthened with 3D-UHMWP composites. A thermographic procedure was implemented to inspect impact-loaded specimens. Results showed that UHMWP composite effectively reduce brittle fracture of the concrete and improve concrete resistance. Width of the mesh used to fabricate the UHMWP composite had significant influence on protection effectiveness.

2.3.2.3 Polyurea

Polyurea has been found to be an efficient retrofitting material against dynamic loads. It has been used to strengthen masonry and light weight steel structures subjected to dynamic loads

(55, 69). Polyurea material retrofitting leads to an increase in robustness and flexural strength of concrete (70). In addition, coating or spraying with polyurea has been shown to enhance temperature and humidity endurance for many types of structures (e.g., timber framed systems, pipelines, and tanks) (71, 72), accordingly improving their performance and survivability under dynamic loads. Limited studies have been conducted that evaluate the application of polyurea material on bridges and bridge components subjected to impact and blast.

Chen et al. (73, 74) completed experimental and numerical studies to examine the effectiveness of polyurea on the behavior of steel plates under impact loading. Pendulum impact tests were conducted to investigate the performance of polyurea coated steel plates, with corresponding finite element models developed for parametric studies. The study identified that no failures occurred to steel plates retrofitted using polyurea material under impact loading, and polyurea coating can be used as an energy-absorbing approach for steel structures.

Iqbal et al. (75) conducted an experimental investigation on the effect of polyurea coating on survivability of concrete subjected to blast. A shock tube facility was used to simulate blast loads and variation of polyurea coating thickness on survivability was examined. The research showed that the polyurea coating was feasible to improve concrete performance with enhanced capacity to resist higher peak pressures. Survivability of the polyurea coating concrete increased with an increase in the coating thickness.

Raman et al. (76, 77) experimentally and numerically investigated blast response of a RC slab retrofitted using polyurea. The $86 \times 47 \times 5.5$ in. ($2190 \times 1190 \times 140$ mm) test specimen was subjected to blast loads using 11023 lbs (5000 kg) TNT at a standoff of 131.2 ft. (40 m). Numerical models of the corresponding specimens were developed using LS-DYNA and validated against the tests. Experimental observations showed that retrofit RC panels experienced

small damage with concrete cracking on the top surface. Numerical simulations identified that polyurea coating beneficially affected displacement and deformation of RC panels when applied to the tension surface.

Fallon et al. (78) completed an experimental study that evaluated the application of a spray-on elastomer coating on concrete under impact loading for damage mitigation. Concrete specimens were subjected to impact from a gas gun at velocities between 100.5 mph (45 m/s) and 335.5 mph (150 m/s). Experimental results demonstrated that polyurea beneficially influenced concrete performance under impact loading with enhanced damage resistance.

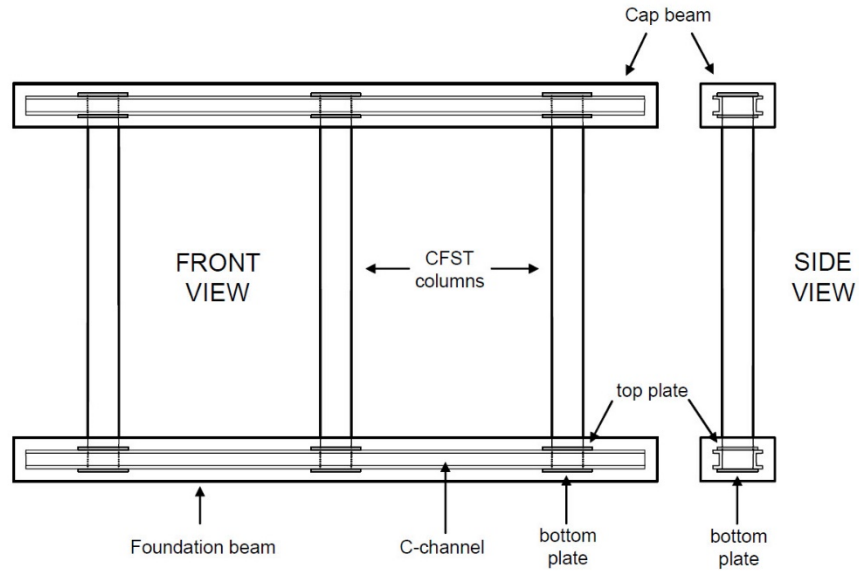
Carey et al. (79) performed experimental and numerical blast load investigations on the behavior of reduced-scale RC panels coated with polyurea materials. The research evaluated effectiveness of plain polyurea and discrete fiber-reinforced polyurea. Panels were $46.5 \times 46.5 \times 3.5$ in. ($1180 \times 1180 \times 90$ mm) and were subjected to a blast using 3.0 lbs (1.36 kg) C4 explosive at a 12 in. (305 mm) standoff distance. Numerical models were developed using LS-DYNA and validated against the experimental tests. Results showed that flexural failure occurred for all panels and that the polyurea coating helped mitigate concrete spalling damage at the top surface. Numerical results identified that the coating acted as a supplementary energy-dissipation material.

2.3.3 Studies of innovative designs

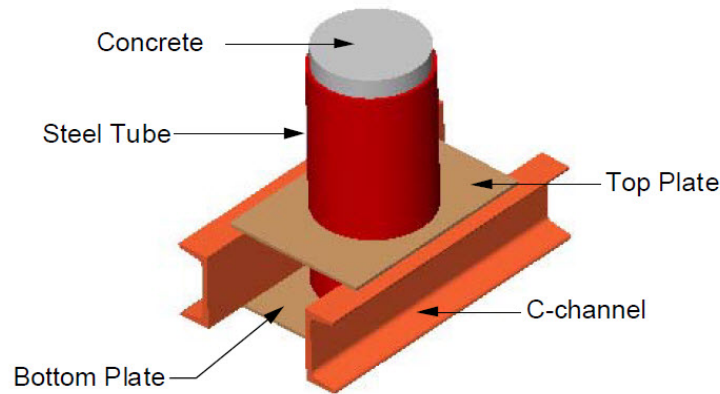
While guidelines to improve bridge component and system resistance against multiple hazards are not explicitly provided in the available codes and specifications (80), innovative designs have been implemented to improve performance under multiple hazards. Some of those design are summarized below.

2.3.3.1 Concrete-filled steel tube columns bridge piers

Concrete-filled steel tube columns have been studied for both building and bridge applications (81). A multi-column pier system using concrete-filled steel tubes (41) was developed and designed as shown in figure 2.17. The study showed that the concrete-filled steel tube column shows acceptable energy-dissipation and good seismic or blast load resistance. Concrete-embedded channels were connected to the column using steel plates to help ensure that the columns developed their full moment capacity.



(a) Pier system



(b) Column and foundation

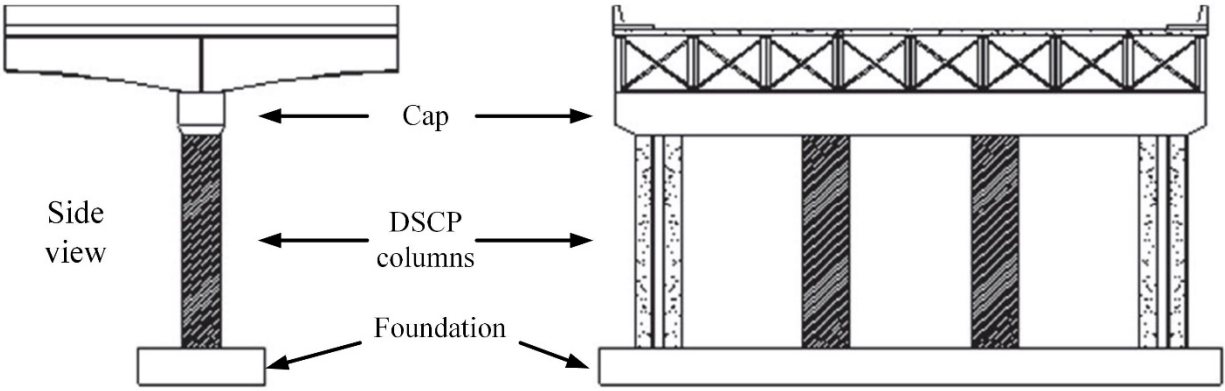
Figure 2.17 Multi-column pier system with concrete-filled steel tube columns (41)

2.3.2.2 Multi-double skin composite panels-column bent

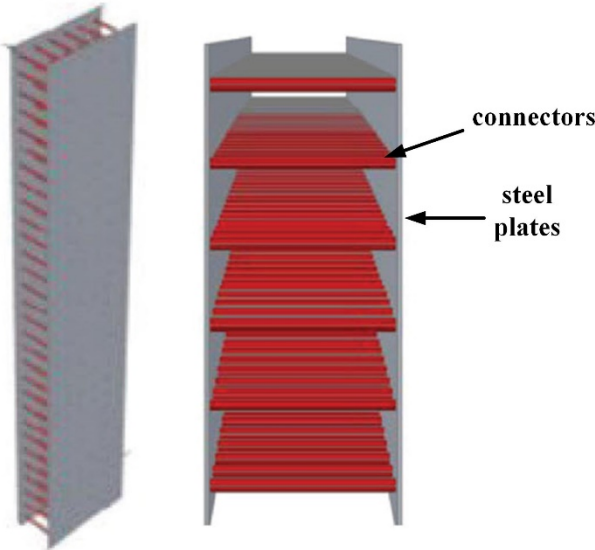
Double skin composite panels (DSCP) have been developed as a means to protect piers, deck slabs, and other structural elements from multiple hazards. They are constructed using two steel face plates with transverse bars connecting them with concrete placed between the plates (82).

A new composite pier system, the multi-double skin composite panels-column bent, was

developed as shown in figure 2.18 (83). An innovative bridge deck could also be developed using the DCSP as shown in figure 2.19 (83) and a hammerhead pier as shown in figure 2.20 (83).

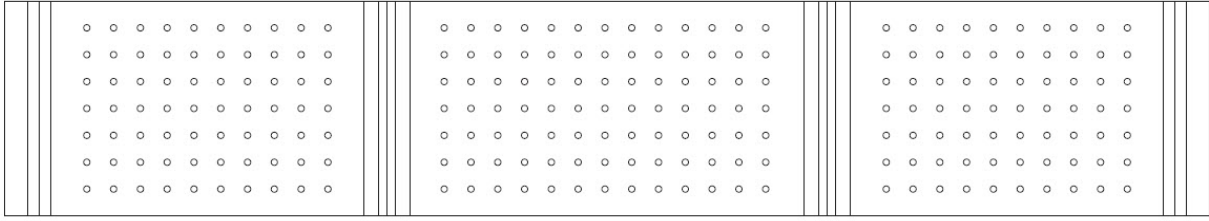


(a) Multi-double skin composite panels-column bent

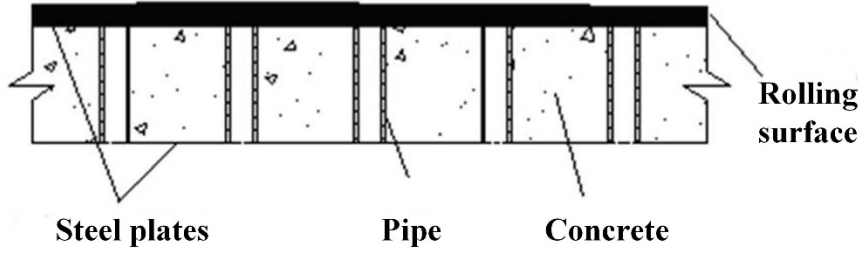


(b) DSCP column

Figure 2.18 Multi-double skin composite panel column bent and column (83)

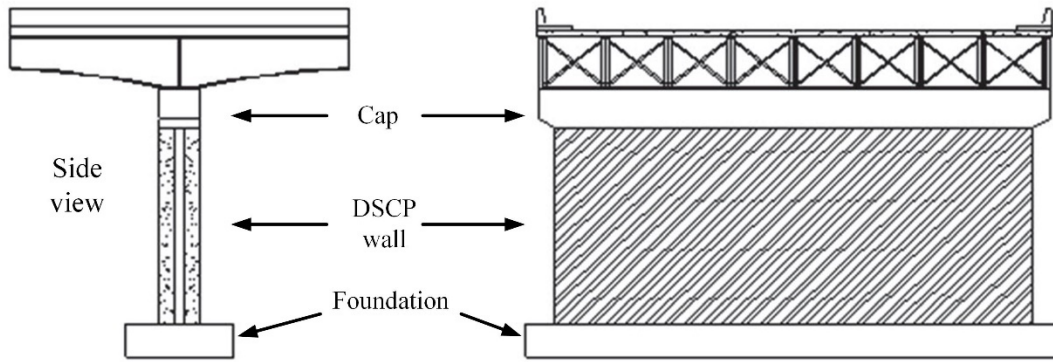


(a) Double skin composite panel bridge deck

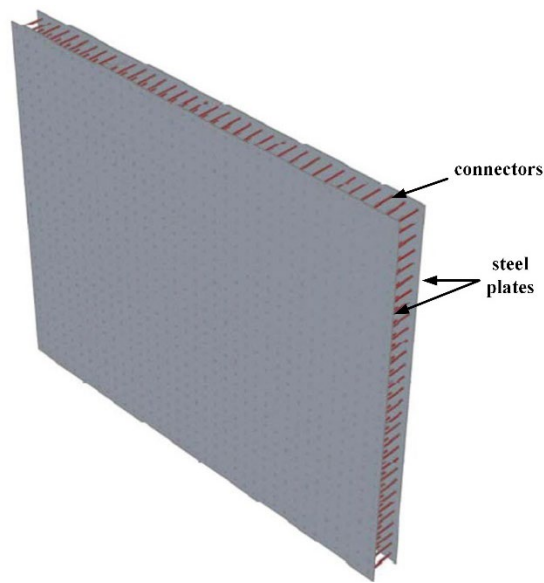


(b) Bridge deck

Figure 2.19 Double skin composite bridge deck (83)



(a) Multi-double skin composite panels hammerhead pier



(b) Double skin composite panel

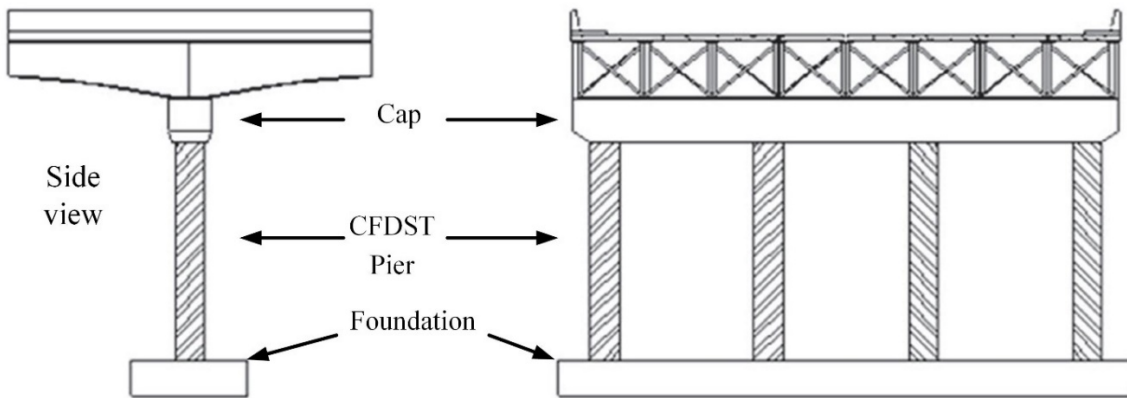
Figure 2.20 Multi-double skin composite bridge wall pier (83)

2.3.2.3 Concrete-filled double skinned tube pier columns

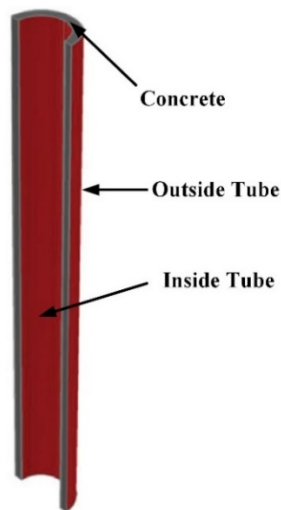
Concrete-filled double skinned tubes (CFDST) consist of two concentric steel tubes with concrete between them as shown in figure 2.21 (84). The use of this design as a bridge pier column, as shown in figure 2.22, has been explored by Fouché et al. under various hazards (84).



Figure 2.21 Concrete-filled double skinned tube (84)



(a) Multi-concrete-filled double skinned tube column pier



(b) Concrete-filled double skinned tube column

Figure 2.22 Multi-concrete-filled double skinned tube column pier (83, 84)

2.3.2.4 Steel plate shear wall pier

A steel plate shear wall (SPSWs) pier, as shown in figure 2.23, was proposed and implemented for a highway bridge by Keller and Bruneau (85). The concept was developed from the traditional SPSWs used in buildings and has demonstrated high ductility, good redundancy, and ease of repair. It consists of a four-sided, tubular boundary frame wrapped with steel plates and as shown to meet demands under multiple extreme hazards.

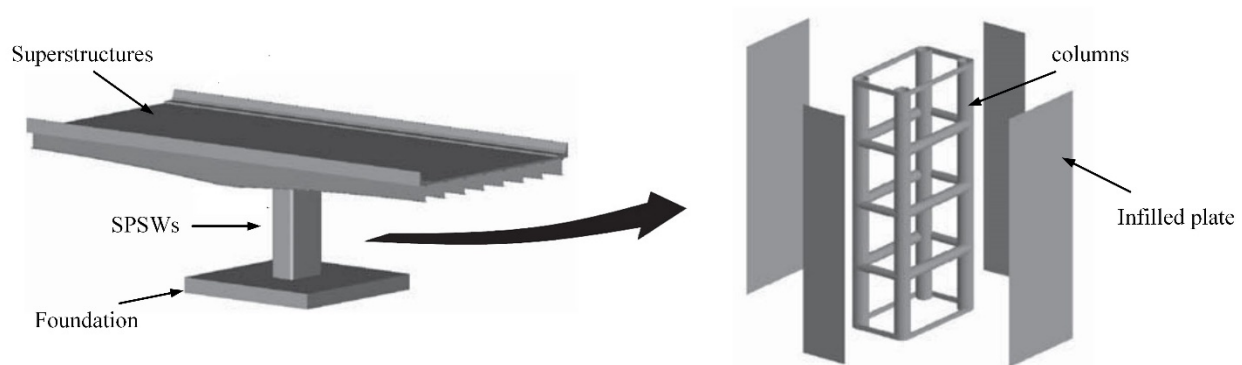


Figure 2.23 Steel plate shear wall box bridge pier (85)

2.3.4 Studies on experimental testing to get material properties

2.3.4.1 Blast studies

Tabatabaei, Volz et al. (86) studied the blast resistance properties of carbon fiber reinforced concrete (CFRC) using a 34 kg TNT equivalent explosive charge at a standoff distance of 1,675 mm from 1,830 mm wide, 1,830 mm long, 165 mm thick concrete panels (fig. 2.24). Test data were collected with two free-field incident pressure sensors and three pressure transducers. LS-DYNA using Material Model 159 successfully modeled the response of the concrete that was exposed to blast loading. Modeling parameters were automatically generated by LS-DYNA by targeting concrete compressive strength of 52 MPa. A similar study was

conducted by *Castedo, Segarra et al. (87)* on concrete slabs but the blast simulation used 111-Johnson_Holmquist_Concrete and 159-CSCM_concrete. In both studies, successful simulation of the blast response of concrete was evaluated based on the percentage of surface damage and cracking pattern.

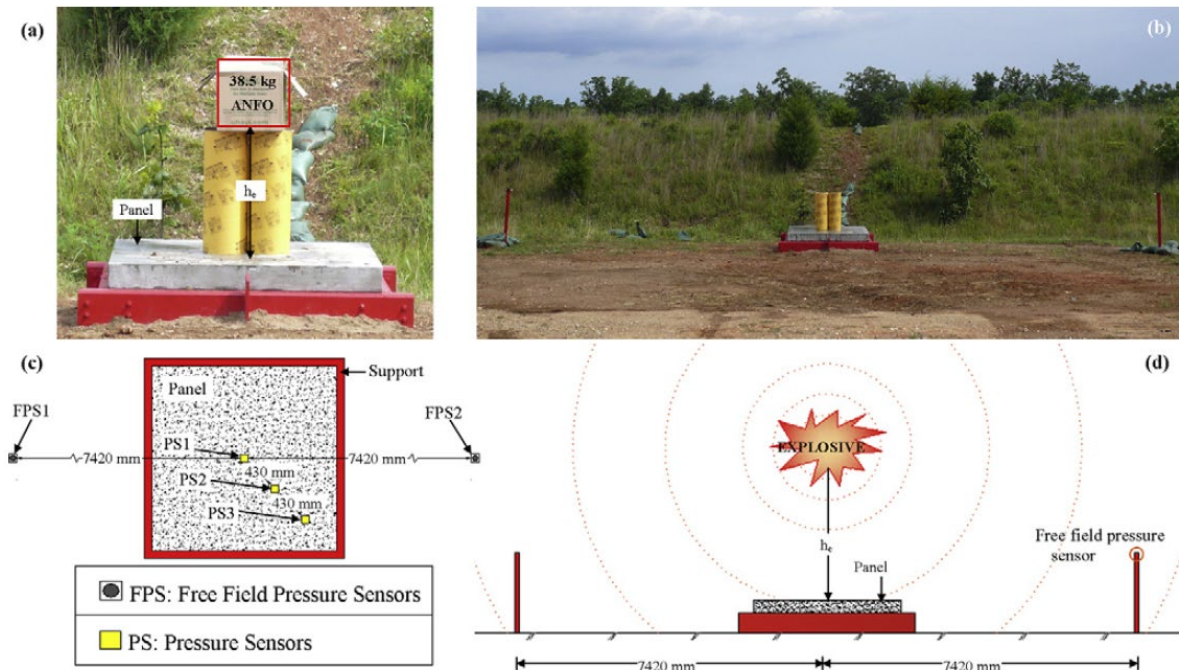


Figure 2.24 Blast test setup and sensor locations(86)

Wu, Oehlers et al. (88) studied blast resistance of externally bonded fiber-reinforced polymer (FRP)-retrofitted concrete slabs. FRP of several thicknesses and widths were tested at varying standoff distances ($0.75 \leq d \leq 3.0$ m) and explosive masses ($1007 \leq m \leq 20101$ g). As shown in figure 2.25, a high sampling rate LVDT of 2 MHz located in the center of the slab, two pressure transducers and a high-speed camera were used for data acquisition. The test results

showed that externally retrofitting FRP material to the compressive face of the normal reinforced concrete (NRC) slab improved blast resistance.

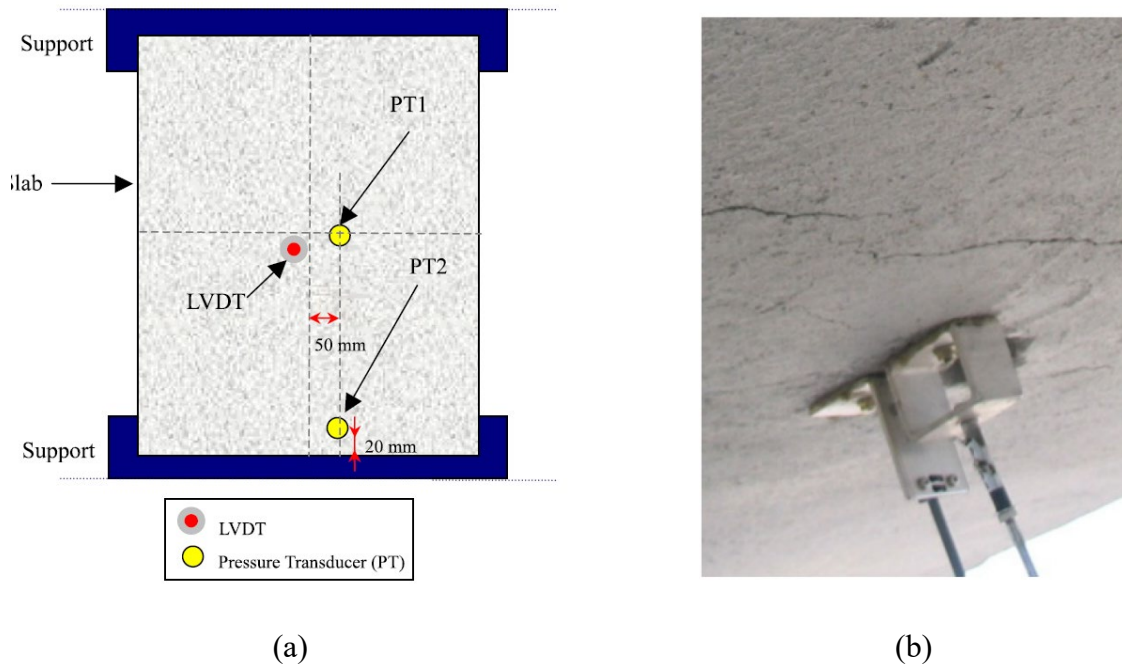


Figure 2.25 Blast testing: (a) Slab instrumentation and (b) LVDT connection to the underside of a test specimen (88).

Ha, Yi *et al.* (89) conducted a study that evaluated the effect of panel retrofitting on RC blast resistance. Carbon fiber reinforced polymer (CFRP), polyurea (PU) and a hybrid of CFRP-PU (CPU) were used as the retrofitting panels (fig. 2.26). Blast tests were performed on 1000 mm wide, 1000 mm long and 150 mm thick RC slabs using a 15.88 kg ANFO explosive at a standoff distance of 1.5 m. Data acquisition was achieved by LVDTs, strain gauges and a high-speed camera capable of 6000 frames per second (fps). Blast energy absorption was calculated based on the area under the pressure-displacement curve, which showed that CPU was the most prominent blast retrofitting material in comparison to CFRP and PU. It was observed that the

higher ductility of PU allowed 30% more energy absorption as compared to CFRP retrofitting material.

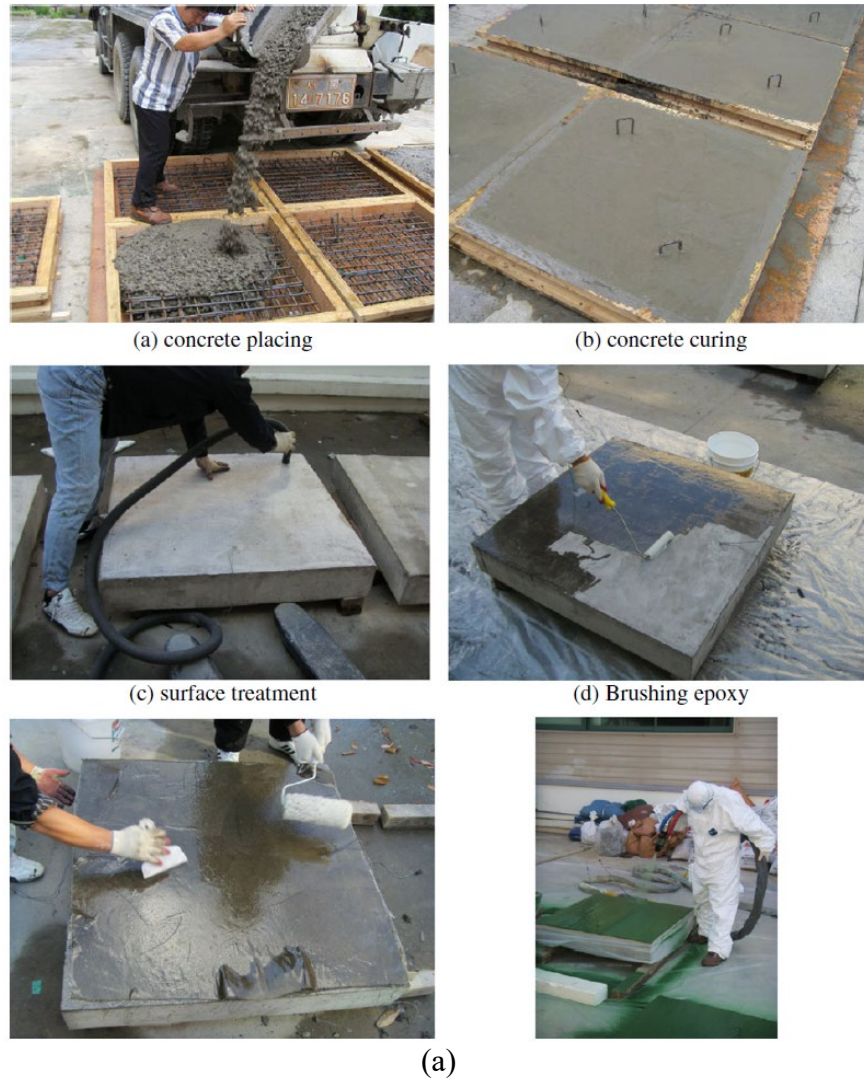
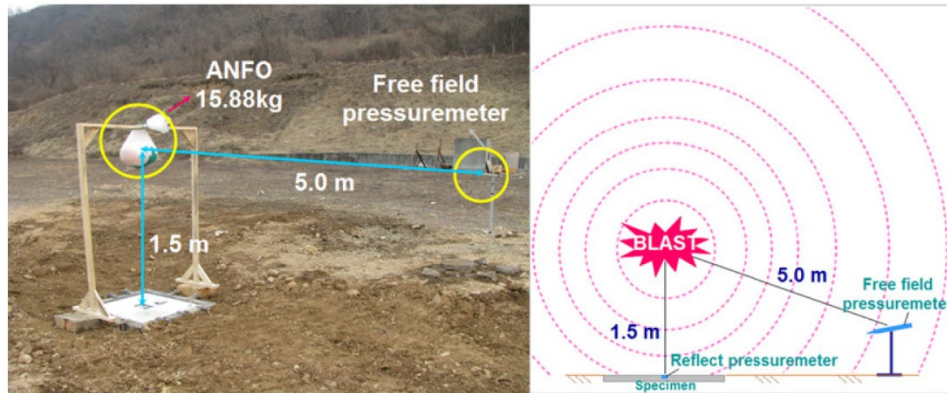


Figure 2.26 Blast testing: (a) procedure of concrete specimen fabrication and (b) test set-up (89).



(b)

Figure 2.26 cont. Blast testing: (a) procedure of concrete specimen fabrication and (b) test set-up (89).

Another study by *Kong, Qi et al. (90)* investigated the effectiveness of aramid fiber reinforced polymer (AFRP) on the blast resistance properties of RC. The results from a blast testing on the concrete slabs using 2.09 kg equivalent of TNT at a 0.6 m standoff distance were used to calibrate a numerical model that was then used for a parametric study (i.e., thickness and type of retrofit layer). The results showed that a thickness beyond four layers of AFRP did not result in increased blast performance of the retrofitted concrete. This study suggested the existence of a certain thickness of the FRP layer that can provide adequate blast resistance while being economical.

Maazoun, Belkassem et al. (91) performed blast testing on concrete slabs in a laboratory environment using 40 grams of C4 explosive and a tube to uniformly distribute the blast pressure, as shown in figure 2.27. A high-speed digital image correlation (DIC) and strain gauges were used for data acquisition. The tested slabs were retrofitted with a different number of strips of CFRP on the tension side of the slabs. The test set-up is shown in below:

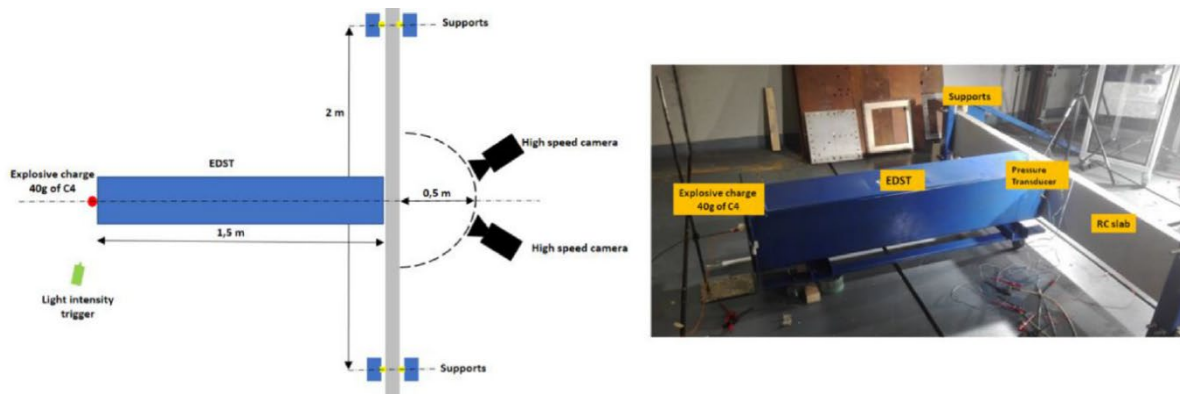


Figure 2.27 Experimental setup for blast tests (91).

The test results showed that an increased number of CFRP strips on the tension side increased the blast resistance of the concrete slabs while placement of CFRP on both compression and tension sides further improved the resistance.

2.3.4.2 Impact studies

Khalil, Abd-Elmohsen et al. (92) used a custom instrument shown in figure 2.28 to investigate the impact resilience of rubberized concrete. Specimens were 150 mm in diameter and 50 mm in height. Impact was achieved with a falling hammer of 44.7 N from a height of 457 mm. The number of hammer fallings (impacts) until crack appearance was recorded and

correlated to material properties. The results showed that increased rubber content improved impact resistance of the concrete but reduced the strength and elastic modulus.

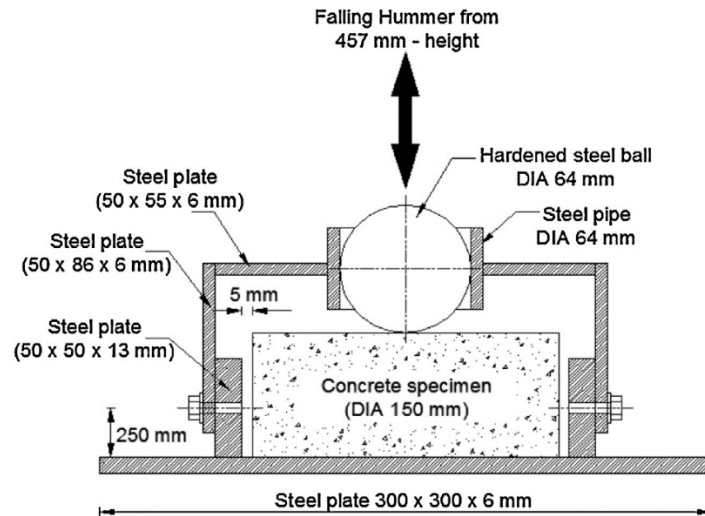
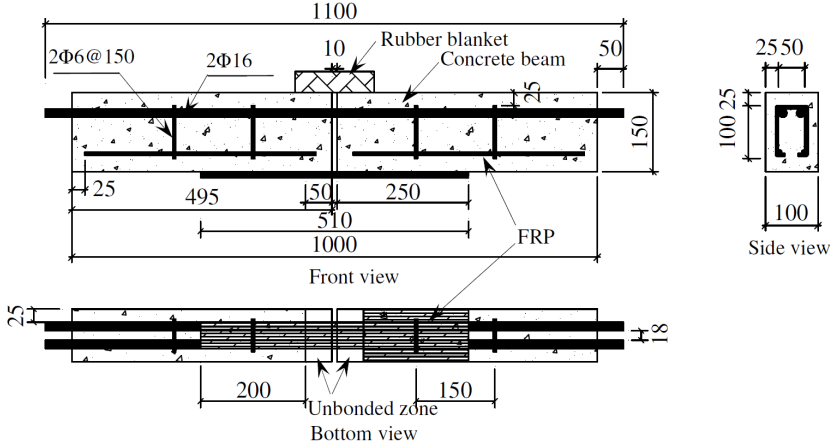


Figure 2.28 Impact test instrument used in (92)

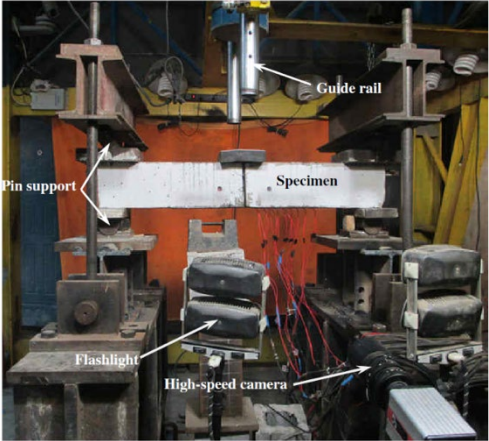
2.3.4.3 Bond Studies

Huo, Liu et al. (93) studied the behavior of the interface bonding between carbon fiber-reinforced polymer (CFRP) and concrete. Both static and dynamic testing were conducted on a three-point bending specimen, as shown in figure 2.29. To test bonding, two concrete prisms were connected in the compression side while the tension side (i.e., bottom) was connected by an externally bonded CFRP strip. This set-up ensured shear failure of the CFRP-concrete. For the dynamic testing, a drop hammer of 198 kg was dropped at varying heights ($h = 200, 400, \text{ and } 600 \text{ mm}$) onto specimens of varying thicknesses and widths of CFRP strips. For the static test, a hydraulic machine was used to apply a loading rate of 2 kN/min until failure. Data acquisition was achieved by a combination of high-speed cameras (capable of 1000 fps) and strain gauges with a sampling rate of 5-million per second per channel. Impact test results showed a rate

dependency of interface properties and an increased strain distribution gradient. The study proposed a bond-slip model for simulating the CFRP-concrete interface.



(a)



(b)

Figure 2.29 Three-point bending test for CFRP-Concrete interface: (a) details of test specimen and (b) test set-up (93).

Khedmati, Alanazi et al. (94) used a different method for identifying interface properties of aggregate-paste interphase in fly ash-based geopolymer mixtures. Unlike *Huo, Liu et al. (93)*,

as shown in figure 1.1, *Khedmati, Alanazi et al. (94)* used a single-edge notched beam specimen with an vertical interface in the middle that was parallel to the loading direction, which allowed the interface to fail (i.e., fracture) from tension. Using the test set-up, the study successfully characterized several interfaces by varying mixture compositions and aggregates types.

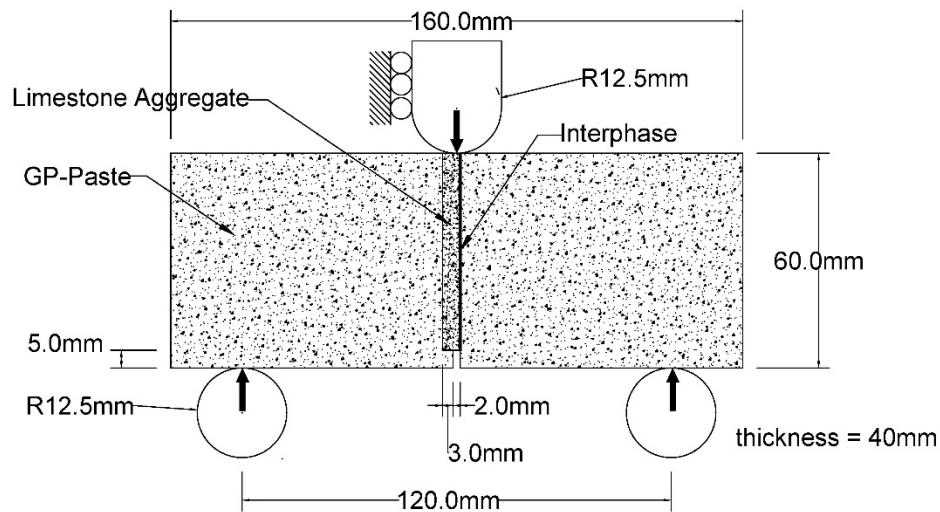


Figure 2.30 Adhesion testing used by *Khedmati, Alanazi et al. (94)*

The key difference between the interface adhesion testing method used by *Khedmati, Alanazi et al. (94)* and that by *Huo, Liu et al. (93)* is that *Khedmati, Alanazi et al. (94)* used smaller geometry without reinforcement and thus is easier to fabricate.

2.4 Improving Soil Response under Impact and Blast

Behavior of the surrounding soil and interaction between the soil and foundation system have significant effects on bridge response to impact and blast. Soil stiffness significantly increase with strain rate. High strain rate also enhances its strength. Studies indicate that strain rates above 2 s^{-1} increase dense and loose soil shear strengths by 30% (95). Figure 2.31 depicts the effect of strain rate on shear strength. The effect of high strain rate is more significant for

dense soils at high confining pressures. A substantial increase in strength also occurs in highly saturated soils due to a reduction in pore pressure.

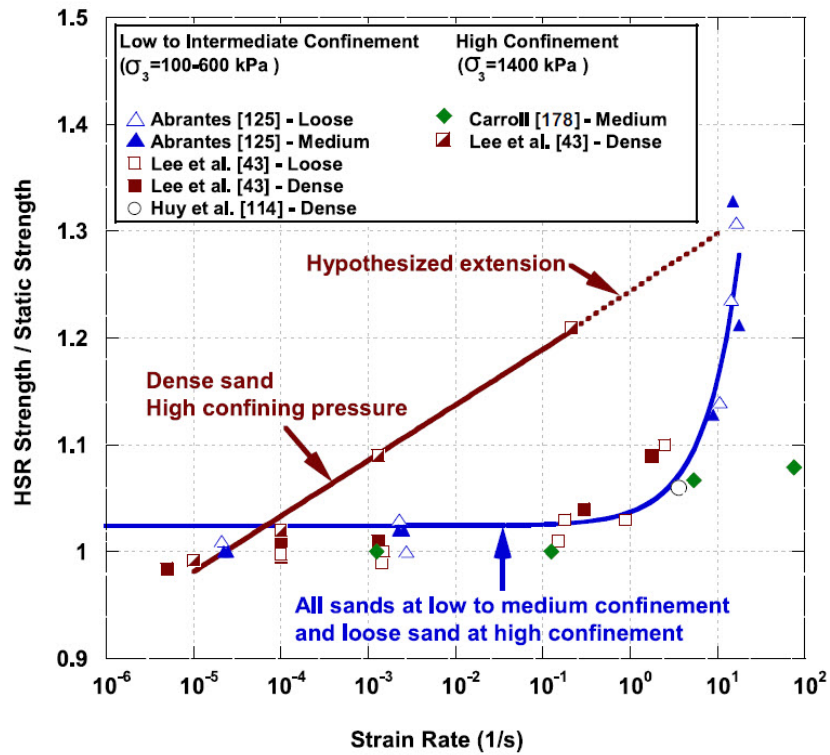


Figure 2.31 Effect strain rate on soil shear strength (95)

Design codes currently do not provide specific information about appropriate soil models to use for analysis and design of bridges and bridge components under impact and blast. However, some research has been conducted related to this topic.

Lewis et al. (96, 97) developed a soil material model for the roadside safety applications for LS-DYNA. It was based on a first order Mohr-Coulomb model to consider kinematic hardening, strain softening, and rate strengthening under impact. Figure 2.32 depicts the resulting, modified Mohr-Coulomb model. The study indicated that the proposed model was applicable for any type of soil when accurate material parameters were defined.

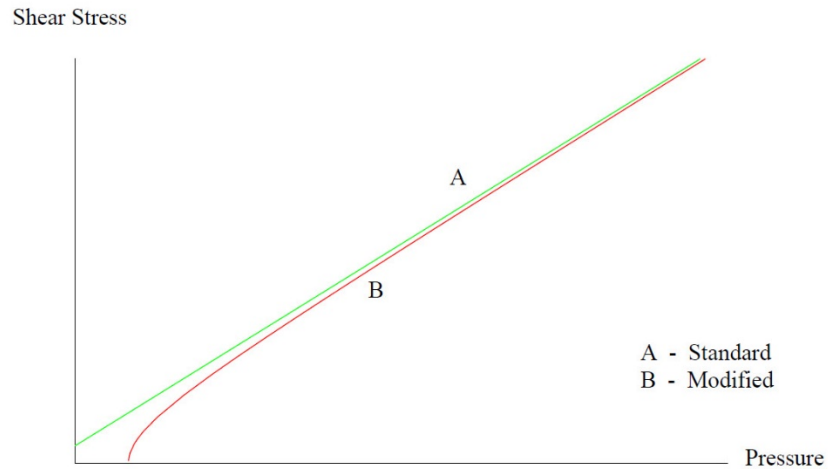


Figure 2.32 Modified Mohr-Coulomb model (96)

Tong et al. (98) developed a Perzyna-based viscoplastic cap model to simulate soil behavior under high strain rate. A viscous flow rule was used to model time-dependent behavior and effects of creep and relaxation were considered. The model was validated against static and dynamic experimental results was shown to simulate high strain rate behavior reasonably well. Figure 2.33 shows an example comparison between the numerical model and experiments. The model was implemented in LS-DYNA for sandy and clayey soils under blast.

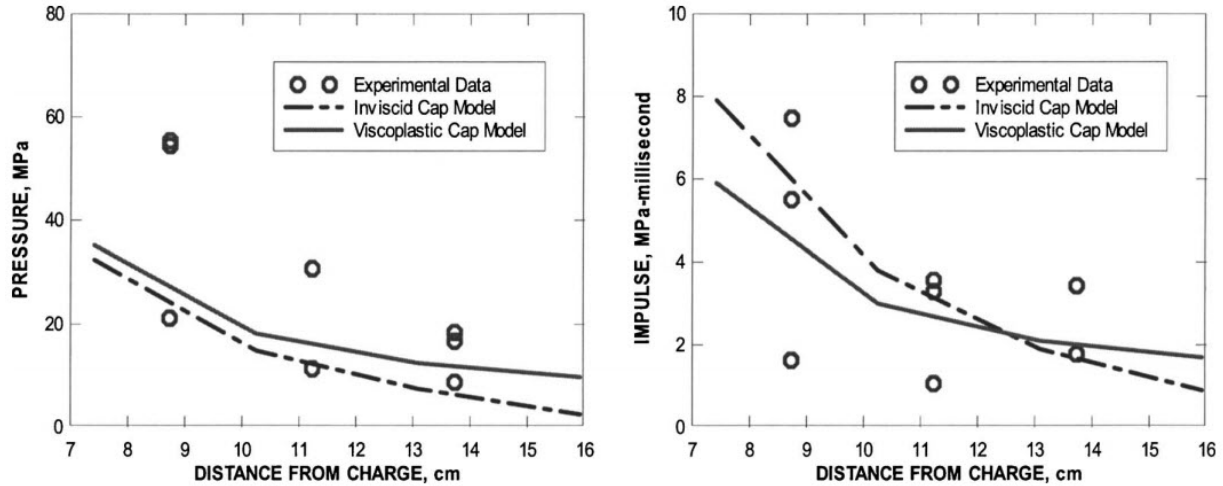


Figure 2.33 Proposed viscoplastic cap model and experimental soil pressure and impulse comparisons (98)

An et al. (99) improved Tong’s viscoplastic cap by: (a) updating soil density and bulk moduli as a function of blast wave propagation; and (b) modeling the soil as a three-phase porous media using a Gruneisen equation for each phase. Figure 2.34 compares predicted and measured soil ejected heights during a blast event. The improved material model was shown to effectively represent soil behavior under blast at different saturation levels, with more noticeable improvement occurring for saturated soils.

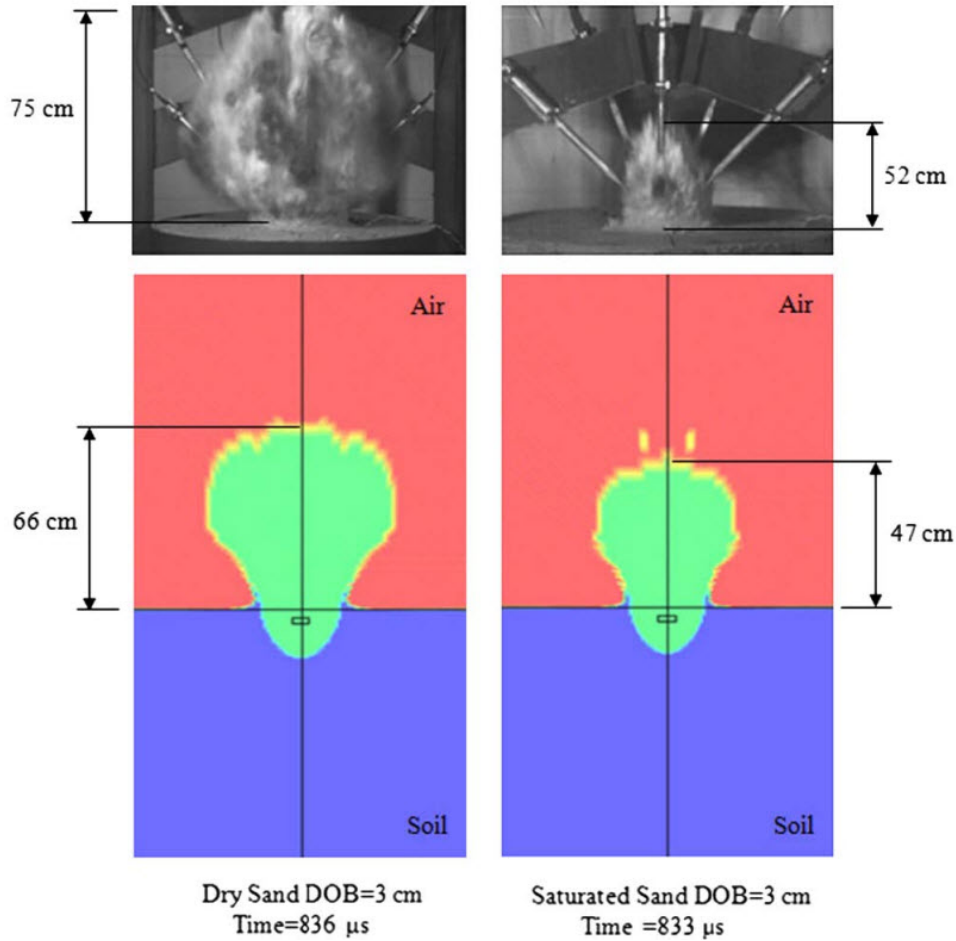


Figure 2.34 Comparison of predicted and measured soil ejected heights, improved viscoplastic cap model (99)

Park et al. (100) studied dry and saturated soils under impact load using LS-DYNA. A fully coupled numerical model was developed to predict underground displacement fields during an impact event. Variation of soil pore pressure was examined during the simulations. Results indicated the numerical model reliably predict depth and degree of soil strength improvement during an impact.

Xie et al. (101) conducted drop hammer tests to investigate behavior of unsaturated soils under impact as a function of drop height and sample depth. Impact depth increased with increase in impact energy and effects decreased as soil depth increased.

2.5 Reliability-based Indices and Equations for RC Bridge Elements

AASHTO-LRFD Bridge Design Specifications were proposed based on a reliability-based calibration considering various combination of dead and live loads (3). The Specifications intend to provide a consistent performance reliability over a 75-year design life over a range of uncertainties. Considered uncertainties address bridge component capacities and intensity and frequency of a demand or combination of demands. Structural risk is represented using a reliability index. Reliability based and stochastic methods have been used to analyze effects of uncertainties on performance, with limited studies examining RC bridge and bridge components under vehicle and blast.

Gardoni et al. (102) constructed probabilistic capacity models for circular, RC columns subjected to cyclic loads based on experimental observations. Bayesian updating was used to consider both aleatory and epistemic uncertainties. Proposed univariate and bivariate probabilistic models for column deformation and shear capacities under dynamic loading are expressed as shown in equation 2.3 a and b.

$$\ln[d(\mathbf{x}, \boldsymbol{\theta}_d, \sigma_d, \rho)] = \ln[\hat{d}(\mathbf{x})] + \gamma_d(\mathbf{x}, \boldsymbol{\theta}_d) + \sigma_d \varepsilon_d \quad (2.3 \text{ a})$$

$$\ln[v(\mathbf{x}, \boldsymbol{\theta}_v, \sigma_v, \rho)] = \ln[\hat{v}(\mathbf{x})] + \gamma_v(\mathbf{x}, \boldsymbol{\theta}_v) + \sigma_v \varepsilon_v \quad (2.3 \text{ b})$$

Corresponding fragilities are shown in Figure 2.35.

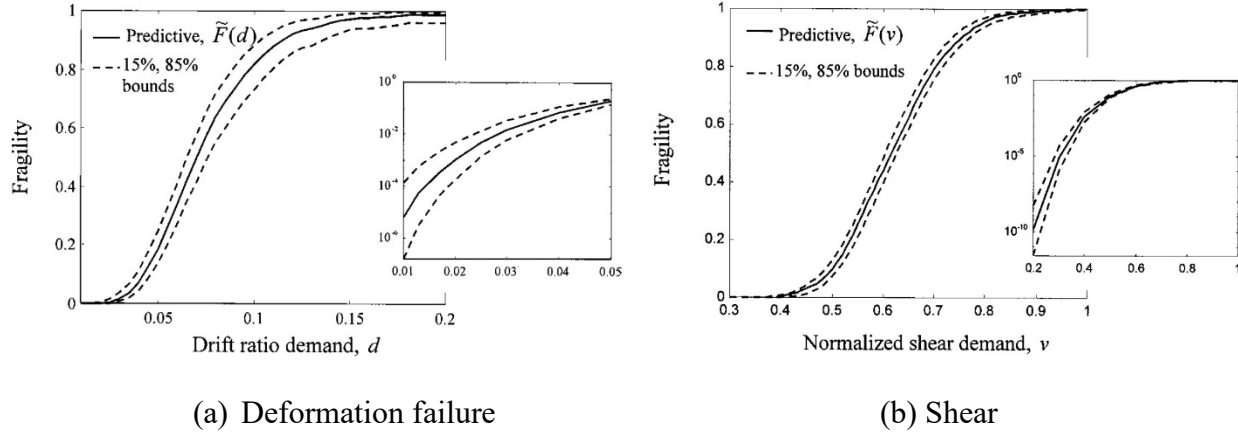


Figure 2.35 Fragility estimates for a RC column (102)

Sharma et al. (20, 21) proposed a probabilistic model to estimate dynamic shear force demand for RC bridge columns under vehicle impact. A performance-based framework was developed to estimate column fragility and results showed that these estimates could effectively evaluate performance during a given impact scenario. A predictive fragility equation was developed as shown in equation 2.4. Figure 2.36 depicts an example fragility estimate contour plot for performance level P3 for given values of impact velocity and mass.

$$\tilde{F}(v_0, m_v) = P[g_{pi} \leq 0 | (v_0, m_v)] \quad (2.4)$$

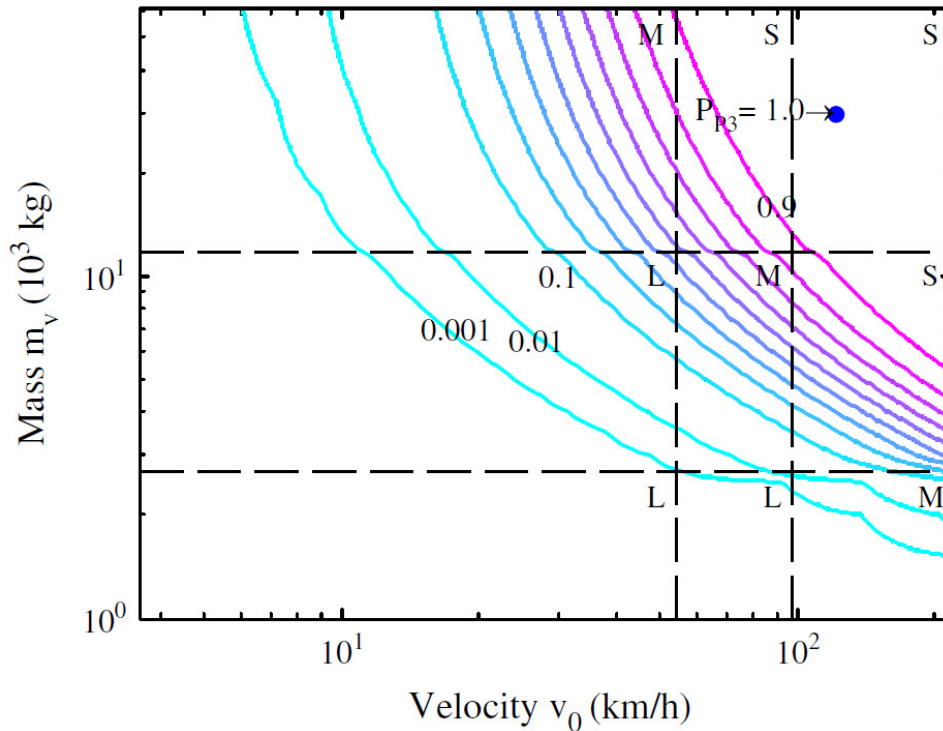


Figure 2.36 RC column fragility contours, performance level P3 (20, 21)

Shi et al. (103) completed a spatial reliability analysis on RC columns subjected to blast loading to predict damage. Material properties and geometric property variations under various blast loads were modelled using stationary and non-stationary random fields. Reliability curves were derived using Monte Carlo simulations and numerical models. Figure 2.37 shows representative reliability curves for RC columns under blast. Results indicated a spatial model could accurately predict damage and safety risks for RC columns subjected to blast loading.

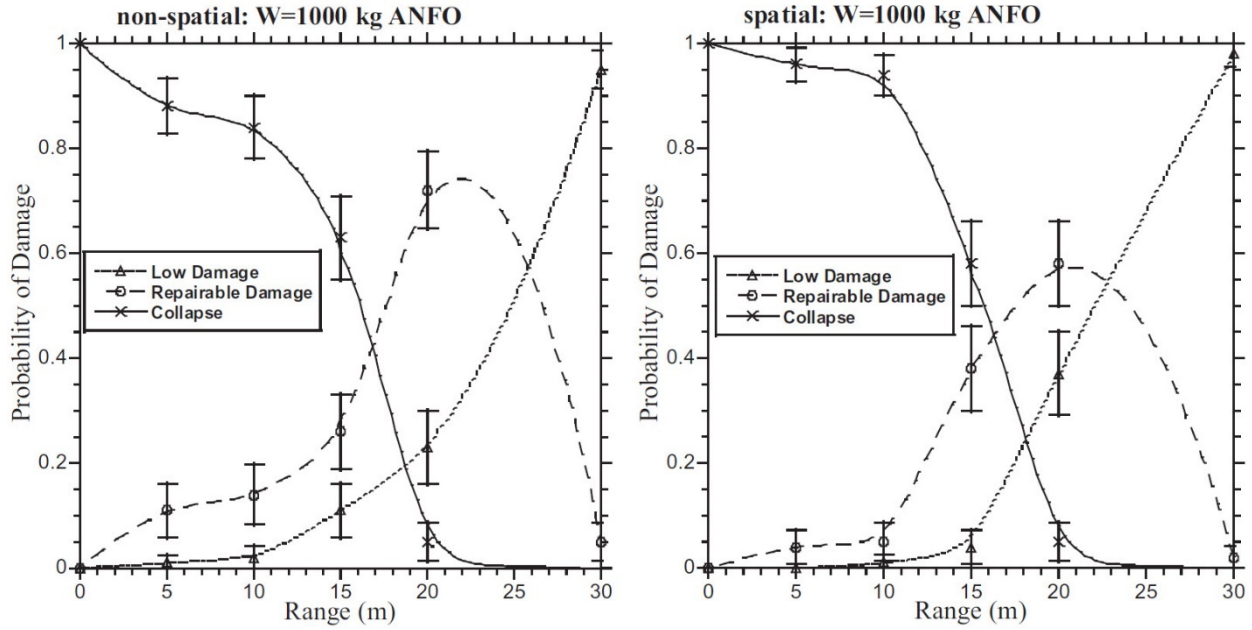


Figure 2.37 Reliability curves for RC columns under blast (103)

Ramanathan et al. (104) developed analytical fragility curves for seismically and non-seismically designed multi-span continuous steel girder bridges using OpenSees models. An equation for the predictive fragility using a standard normal cumulative distribution function was developed and is expressed in equation 2.5.

$$P[D > C/IM] = \Phi \left[\frac{\ln(S_d/S_c)}{\sqrt{\beta_{d/IM}^2 + \beta_c^2}} \right] \quad (2.5)$$

Figure 2.38 shows an example of fragility curves for the studied bridge. Results identified that the column capacity could be improved using seismic detailing.

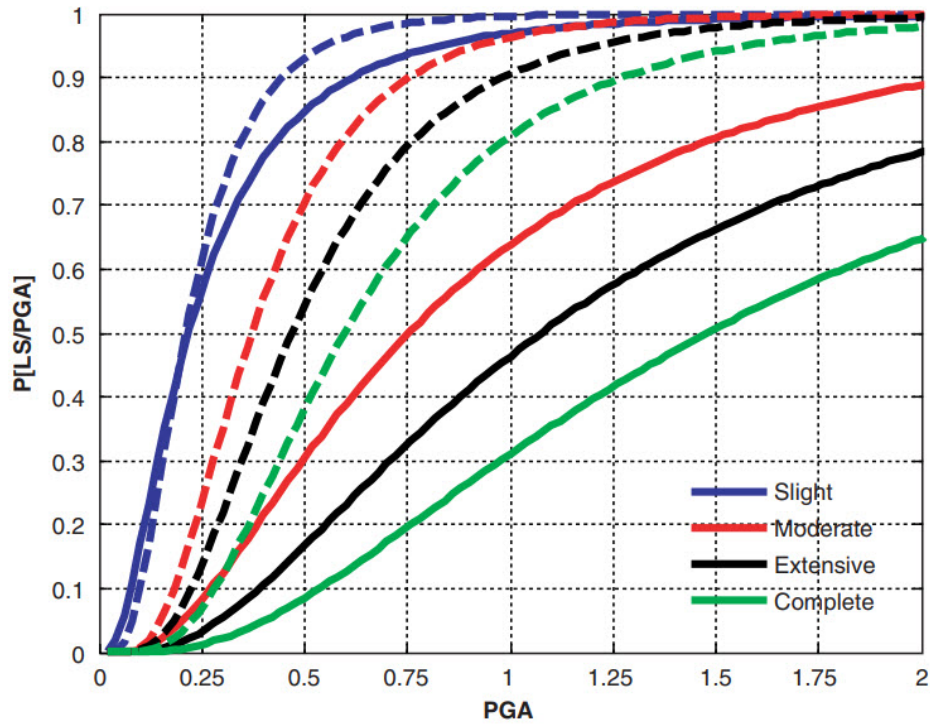


Figure 2.38 Fragility curves for bridge under blast (104)

Hao et al. (105) completed reliability analyses of three RC columns under blast load using LS-DYNA. Failure probabilities based on P-I curves were developed for blast loads at different scaled distances. Results identified that the proposed approach could estimate failure probabilities for RC columns and progressive collapse probabilities for RC buildings. Figure 2.39 shows an example collapse probability curve for a column given values for various scaled distances.

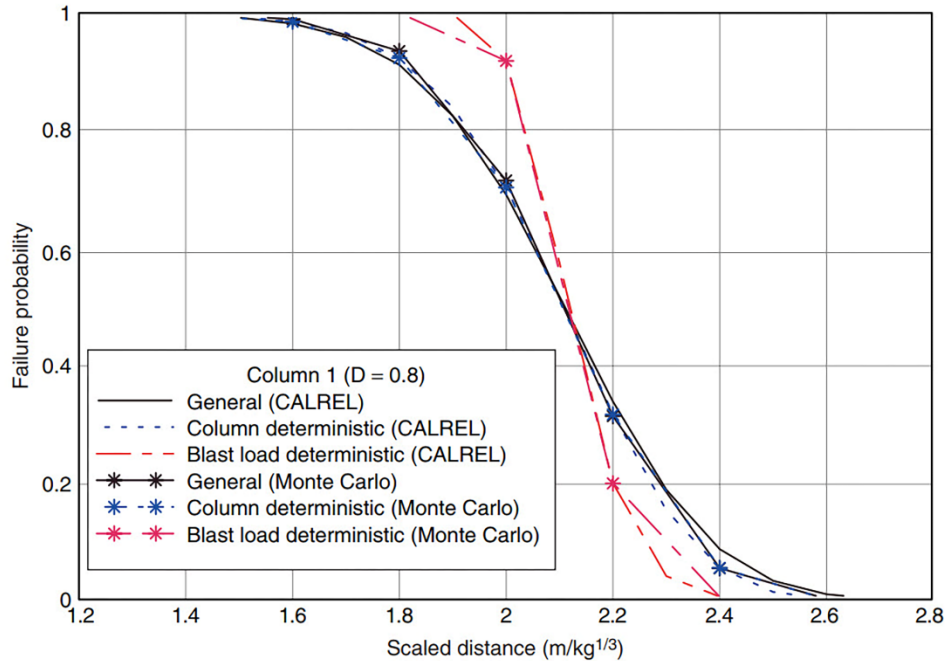


Figure 2.39 RC column collapse probability curves (105)

2.6 Conclusions

This chapter summarizes the current research knowledge base in areas relevant to bridge column performance under blast and impact loads and helped inform the research plan. The review includes the following areas:

1. Studies that investigated response of RC bridge components under vehicle impact, blast, and fire, with an emphasis on bridge piers;
2. Schemes to design and retrofit RC bridge components to resist extreme loads;
3. Studies of innovative retrofit materials, including FRP, UHMWP, and polyurea, for improvement in bridge components performance; and
4. Reliability of RC components under extreme loads.

Chapter 3 Finite Element Model Development

3.1 Introduction

The research project was conducted based on finite element modeling using LS-DYNA. This chapter describes techniques utilized to develop the models of highway bridge columns, its foundation system, and surrounding soil and air volumes. A representative multi-column bridge pier was selected from a FHWA design example as the basis for all analytical work. Reasonable constitutive models for the concrete, reinforcement, soil, explosive, and air were selected for initial models using information gleaned from the literature search. Once the developed numerical models were deemed acceptable, FE modeling techniques were validated as discussed in the following chapter and then used to examine column response to vehicle collision and air blast.

3.2 Prototype Pier Column

A single column from a multi-column highway bridge pier and its supporting foundation and a surrounding soil volume were selected for modeling using LS-DYNA as shown in figure 3.1. The pier and column were obtained from a FHWA design example (106), with the bridge designed following AASHTO's-LRFD (3). Figure 3.2 details the finite element model. The column was a circular cross section with a height of 18 ft. (5400 mm) above the foundation and was supported by a spread footing that is 12 ft. (3600 mm) wide, 12 ft. (3600 mm) long, and 3 ft. (900 mm) thick. The footing was, in turn, supported by eight rectangular reinforced concrete piles that were 1.5 ft. (450 mm) wide and 20 ft. (6000 mm) deep, with the strong axis of the piles parallel to the long axis of the bridge. To ensure the accurate response and avoid unrealistic dynamic disturbances during an impact and blast event, a soil volume that was modeled was

10000 mm (33 ft.) deep, 10000 mm (33 ft.) long, and 10000 mm (33 ft.) wide as shown in figure 3.4 [88, 89].

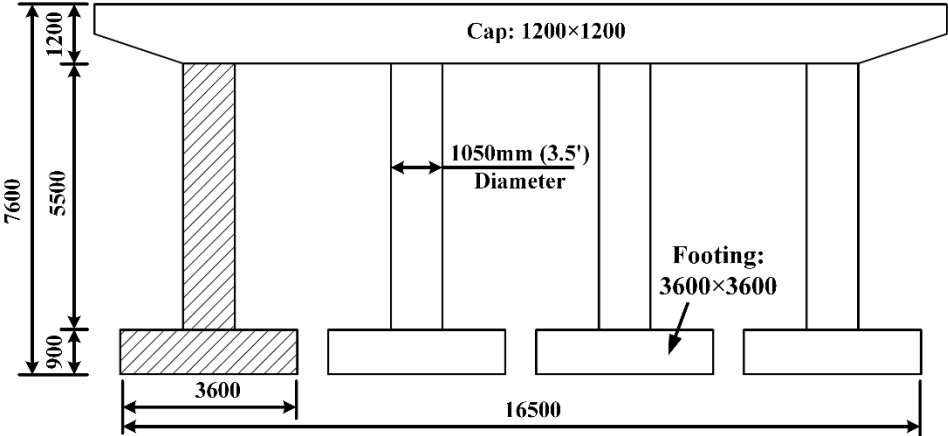


Figure 3.1 Prototype pier and column

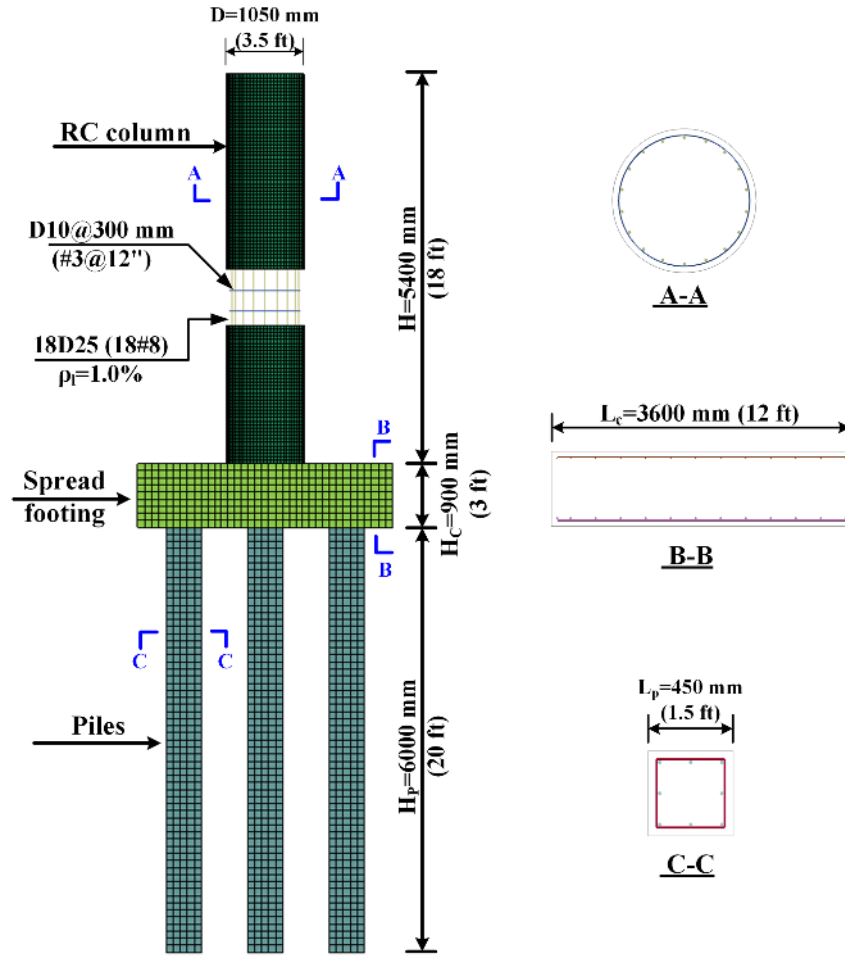


Figure 3.2 Finite element model of column and foundation

Column diameters of 2.5 ft. (750 mm), 3.5 ft. (1050 mm), and 4.5 ft. (1350 mm) were considered assuming a 1% longitudinal reinforcement ratio. The bridge column was reinforced with #8 (No.25) longitudinal bars (31, 106). AASHTOs-LRFD criteria was used to determine shear reinforcement, with #3 (No.10) bars spaced at either 2 in. (50 mm), 6 in. (150 mm), or 12 in. (300 mm).

3.3 Impact and Blast Modeling

3.3.1 Vehicle model

The vehicle model utilized in this study was a Ford F800 Single-Unit Truck (SUT) model developed by the National Crash Analysis Center (NCAC) (107). The SUT is one of the most commonly used trucks to carry materials and goods in various areas (108). According to the study from the Fatality Analysis Reporting System (FARS) and General Estimates System (GES) (109), crashes involving the SUT produced 3% of the fatal accidents, 1.7% of accidents causing injuries, and 2% of accidents causing property damage in 2011.

The SUT model was validated against a series of experimental tests by a number of researchers, with some improving the model to better simulate material strain-rate sensitivity of materials and implement an enhanced suspension system. These evaluations and modifications to the SUT model were completed by Battelle Memorial Institute (BMI), Oak Ridge National Laboratory (ORNL), and University of Tennessee (110).

Highway speed limits can typically range between 15 mph (24 km/h) in urban areas to 75 mph (120 km/h) in rural locations, with a minimum highway speed commonly set at 40 mph (65 km/h). Therefore, SUT impact speeds of 40 mph (65 km/h), 60 mph (95 km/h), and 75 mph (120 km/h) were arbitrarily selected for the current studies.

3.3.2 Simulation of blast load

The Multi-Material Arbitrary Lagrangian Eulerian (MM-ALE) formulation and fluid-structure interaction (FSI) algorithms in LS-DYNA (111) were employed to simulate detonation of a high explosive adjacent to the column in association with the impact. The MM-ALE formulation avoids severe mesh distortion and subsequent computational instabilities by decoupling mesh and fluid deformations over time. Many researchers have effectively modeled

air blast effects on structural components and systems using MM-ALE. For the current study, the air-blast model involved three stages: denotation; blast wave propagation; and interaction between the blast wave, bridge column and soil volume. Lagrangian meshes were used to model the bridge column and pile foundation system. ALE meshes were used for the air, soil volume, and explosive. The explosive, air and soil were defined as ALE material groupings using LS-DYNA *ALE Multi-Material Group*. The Lagrangian and ALE meshes were coupled together using penalty-based coupling algorithms, with contact between the blast wave and bridge column simulated using LS-DYNA *Constrained Lagrange In Solid* command.

Blast load intensity is primarily dependent on explosive weight and standoff distance between the explosive and target structure. Scaled distance (Z) is used to represent blast intensity as a function of these two variables. NCHRP Report 645 (31) recommends that bridge column blast performance be investigated for $Z \leq 1.5 \text{ ft/lbs}^{1/3}$ ($0.6 \text{ m/kg}^{1/3}$). Current research considered a blast 8.2 ft. (2500 mm) away from the column. The equivalent TNT weight was determined from Federal Highway Administration (FHWA) estimated weights for structures subjected to terrorist attack (112). Resulting scaled distances that were examined were $0.5 \text{ ft/lbs}^{1/3}$ ($0.20 \text{ m/kg}^{1/3}$), $0.6 \text{ ft/lbs}^{1/3}$ ($0.25 \text{ m/kg}^{1/3}$), and $0.8 \text{ ft/lbs}^{1/3}$ ($0.30 \text{ m/kg}^{1/3}$).

3.4 Material Models

3.4.1 Concrete

A nonlinear material model, *Mat CSCM Concrete* in LS-DYNA, was used to model the column, footing, and piles. The CSCM model (*Mat_159*) was developed by FHWA to predict dynamic impact response of concrete for roadside safety applications (113, 114). The CSCM model has been shown by multiple researchers (5, 14, 113, 115) to accurately reproduce experimental results and model performance of RC structural components under impact or blast.

A parameter initialization function, which is based on the concrete compressive strength and maximum aggregate size, is used to define concrete properties when detailed information is not available. For the current study, the concrete compressive strength was set at 4 ksi (28 MPa), and the maximum aggregate size was set at 0.75 in. (19 mm). Table 3.1 lists the concrete properties.

Table 3.1 Material properties of concrete and steel reinforcement

Material	Parameters	Values
Concrete	Mass density	0.086 lbs/in. ³ (2380 kg/m ³)
	Compressive strength	4 ksi (28 MPa)
	Aggregate size	0.75 in. (19 mm)
Steel	Mass density	0.28 lbs/in. ³ (7850 kg/m ³)
	Elasticity modulus	2.9×10 ³ ksi (2×10 ⁵ MPa)
	Poisson's ratio	0.3
	Yield stress	69 ksi (475 MPa)
	Ultimate strain	0.12

The CSCM model utilizes an erosion algorithm to delete highly strained elements. Element erosion is activated by defining an erosion coefficient to prevent computational instabilities due to mesh tangling (114). The erosion coefficient depends on the maximum principle strain in the concrete. Based on previous research recommendations and several simulation trials, the erosion coefficient was conservatively selected as 1.10 (113, 116), which equated to a maximum principle strain of 10%.

The concrete used for the column, footing, and piles was represented using a constant-stress hexahedral solid element with hourglass control to minimize nonphysical modes of deformation and inhibit hourglass modes. Flanagan-Belytschko stiffness-based hourglass control (Type_5) was selected with an hourglass coefficient set to 0.1 (111, 113).

3.4.2 Steel

Both longitudinal and hoop reinforcement was modeled using a two-node, Hughes-Liu tubular beam element that utilizes quadrature through the cross section. LS-DYNA's *Mat Piecewise Linear Plasticity* material model (*Mat_24*) accounts for the increase in capacity due to strain rate effect and was used to represent reinforcing steel. *Mat_24* uses Cowper and Symonds material model strain rate parameters (113), which were defined as 40 (C_s) and 5 (p_s) (113, 116). Ultimate strain set to 12%, after which elements will be removed from the model (116, 117). Steel material properties are also provided in table 3.1 Material properties of concrete and steel reinforcement.

3.4.3 Soil

The soil volume was modeled using LS-DYNA's *Mat FHWA Soil* material (*Mat_147*), which was developed by the FHWA to analyze the impact response for roadside safety applications (96). It is a second order model with a smooth hyperbolic yield surface taken from a first order Mohr-Coulomb model as shown in figure 3.3. The model considers kinematic hardening, strain softening behavior, strain rate strengthening, and unconfined soil stability. Soil failure is determined when the coupled shear and effective normal stress exceed the failure envelope. Soil parameters were determined using LS-DYNA recommended values and previous research (96, 97, 118, 119). The friction angle was defined as 35 degrees and the cohesion was set at 7.25×10^{-7} ksi (5×10^{-6} MPa). Soil material parameters are tabulated in table 3.2. The soil element was modeled using a solid element with a multi-material ALE formulation (ELFORM=11).

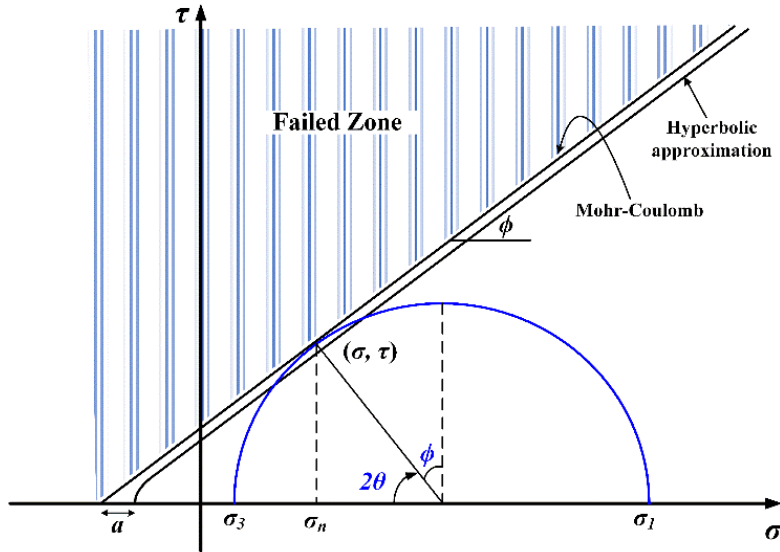


Figure 3.3 FHWA soil model failure surface (96)

Table 3.2 Soil material parameters

Material	Parameters	Values
Soil	Mass density	0.058 lbs/in. ³ (1600 kg/m ³)
	Specific gravity	2.65
	Bulk modulus	21.2 ksi (146 MPa)
	Shear modulus	8.0 ksi (56 MPa)
	Friction angle	35°
	Cohesion coefficient	7.25×10 ⁻⁷ ksi (5×10 ⁻⁶ MPa)

3.4.4 Explosive and air

The explosive was modeled using LS-DYNA's *Mat High Explosive Burn* model, with the Jones-Wilkins-Lee (JWL) equation of state (111). The JWL equation-of-state defines denotation pressure as a function of relative volume of the denotation product and initial internal energy as expressed in equation 3.1:

$$p_{eos} = A \left(1 - \frac{\omega}{R_1 V} \right) e^{-R_1 V} + B \left(1 - \frac{\omega}{R_2 V} \right) e^{-R_2 V} + \frac{\omega E_{0,e}}{V} \quad (3.1)$$

where p_{eos} is the pressure of the denotation product. V is the relative specific volume of the denotation product. A , B , R_1 , R_2 , and ω are specified constants unique to the type of explosive being represented.

Table 3.3 lists the material and EOS parameters for the selected TNT explosive (29). A spherical explosive was used. In order to reduce the modeling efforts, the explosive was contained in the air mesh by defining an initial fraction of the air that was occupied by the explosive using *Initial Volume Fraction Geometry* command. In this command, the air mesh was the background mesh, and the explosive was filled in the background mesh using necessary explosive geometric parameters (its shape, volume, and center location).

Table 3.3 TNT material and EOS parameters

Material	Parameters	Values
TNT	Mass density	0.059 lbs/in. ³ (1.63×10 ⁻⁶ kg/mm ³)
	Detonation velocity	1.55×10 ⁴ mph (6930 m/s)
	Chapman-Jouget pressure	3046 ksi (21 GPa)
	A	5.384×10 ⁴ ksi (371.2 GPa)
	B	468.5 ksi (3.23 GPa)
	R_1	4.15
	R_2	0.95
	ω	0.3
	Detonation energy per unit volume	1015 ksi (7.0 GPa)
	Initial relative volume	1

Air was represented as an ideal gas using LS-DYNA's null material model (*MAT_NULL*) using a linear polynomial EOS as expressed in equation 3.2 (III):

$$p_{air} = C_0 + C_1\mu + C_2\mu^2 + C_3\mu^3 + (C_4 + C_5\mu + C_6\mu^2)E_{0,air} \quad (3.2)$$

where $C_0, C_1, C_2, C_3, C_4, C_5,$ and C_6 are equation constants; $E_{0,air}$ is the internal energy per unit reference volume; $\mu = \frac{\rho_{air}}{\rho_{airo}} - 1$ and $\frac{\rho_{air}}{\rho_{airo}}$ are the ratios of current to reference density; and ρ_{air} is the nominal or reference density.

Air mass density and constants were chosen based on previous research (29, 119). The air was modeled using a solid element having a multi-material ALE formulation (ELFORM=11). Standard viscous hourglass control was selected for the air domain with a reduced hourglass coefficient of 1×10^{-6} to mitigate the effects of inaccurate hourglass forces (120). Table 3.4 lists air material and EOS parameters (29, 31).

Table 3.4 Air material and EOS parameters

Material	Parameters	Values
Air	Mass density	46.7 lbs/in. ³ (1.293×10^{-3} kg/mm ³)
	C_0	0
	C_1	0
	C_2	0
	C_3	0
	C_4	0.4
	C_5	0.4
	C_6	0
	$E_{0,air}$	0.0363 ksi (0.25 MPa)

3.5 Model Coupling and Boundary Conditions

Concrete and steel reinforcement models were created separately. As a result, a constraint was required to model interaction between steel reinforcement and surrounding concrete. The

Constrained Lagrange In Solid command in LS-DYNA was utilized to couple the reinforcement to surrounding concrete.

A segment-based, penalty-type contact formulation was used to model contact between the bridge columns and the vehicle using the *Contact Automatic Surface to Surface* command. Both static and dynamic coefficients of friction were set to 0.3. A penalty-based coupling algorithm was also defined between the air domain and bridge column and between the soil volume and spread footing and piles using the *Constrained Lagrange In Solid* command. Interface air and soil nodes were slaved to structural component nodes. Based on the soil's critical angle of friction, a friction coefficient of 0.315 was defined between it and the spread footing and piles (121).

To avoid dynamic wave reflection that may adversely influence LS-DYNA simulation results, non-reflecting boundary conditions (BNR) were defined along the top and four sides of the air domain and along the bottom side of the soil volume. The bridge column was conservatively simulated as a propped-cantilever with the top of the bridge column translationally restrained using a roller support (29, 31). Effect of superstructure dead load was addressed using an axial pre-load, which was set at 6% of the nominal axial capacity of the column. A representative column finite element model including the SUT, soil and air volumes is shown in figure 3.4.

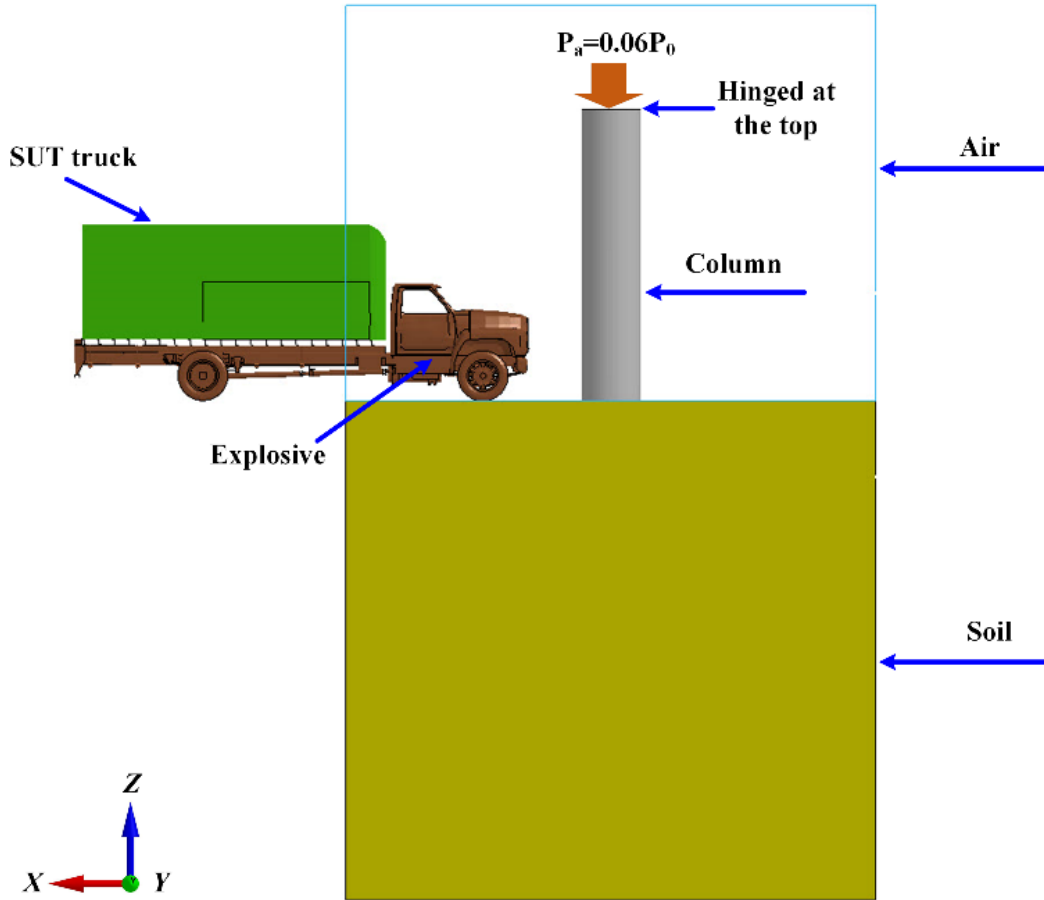


Figure 3.4 Representative column finite element model

3.6 Conclusions

This chapter summarizes the prototype, circular column selected for the current study and provides information on physical and material models used to represent the column, its surrounding soil and air volumes and the impacting vehicle in LS-DYNA. A 3D finite element model of a single RC bridge column and its supporting footing and piles was created with the soil volume restraining its base and the air domain being used to apply load from an air blast. Reasonable constitutive models for the concrete, reinforcement, soil, explosive, and air were selected from the literature. The impacting vehicle was a Ford F800 SUT available in LS-DYNA. The air blast was represented using LS-DYNA's MM-ALE approach.

Chapter 4 Experiments for Material Properties

This chapter summarizes and elaborates upon the experimental efforts undertaken to obtain material properties to be used for numerical model calibration. A literature review was used as the basis for experimental design in which materials and test methods were selected. Since testing is still an ongoing effort, all tests have not yet been concluded.

4.1 Retrofitting Materials Selection:

Among two original candidate retrofitting materials, polyurea (PU) was selected based on its availability and practicality (fig. 4.1). Prior to spraying, the fabricated single-edge notched beam (SENB) cement and cylindrical concrete specimens were cured in a 100% moisture room for 28 days. The geometry of SENB specimens after fabrication is shown in figure 4.2(a). Note the sandwiching of layers between two prismatic samples in the vertical centerline that is composed of a strong glue, retrofitting polymer (i.e., PU) and the cement-polymer interface. The hypothesis of this testing is that the strong glue is stronger than the PU-cement interface and therefore will not fail. As a result, the entirety of the failure will occur exclusively at the interface, which will then be characterized. If the interface is stronger than the glue and does not fail, this will be indicative of a strong adherence between PU-cement. Strong adhesion will minimize the compatibility issue between the retrofitting material and bridge piers that are typically constructed of concrete. In addition, the performance of the retrofitted piers will benefit greatly from the strong adhesion which will help protect against infiltration of water and other malicious agents into the structure.

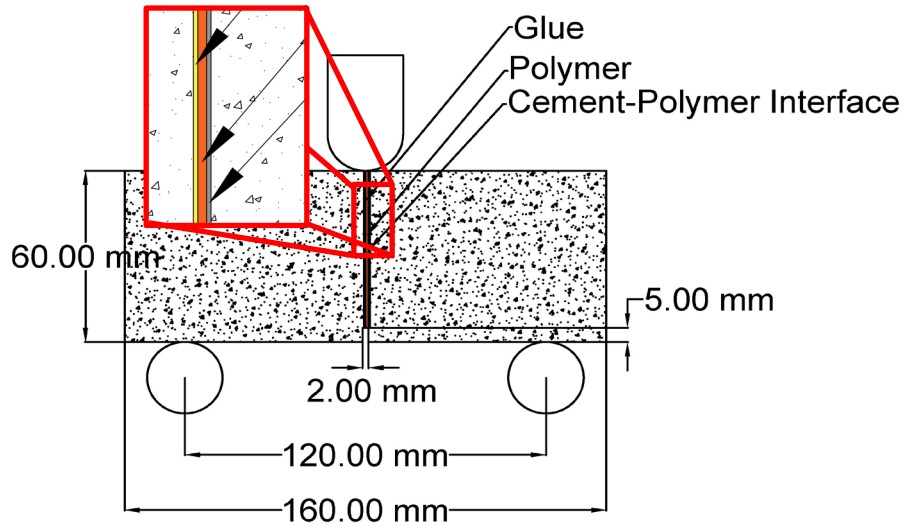


Figure 4.1 Polyurea spraying at a local supplier (VersaFlex®).

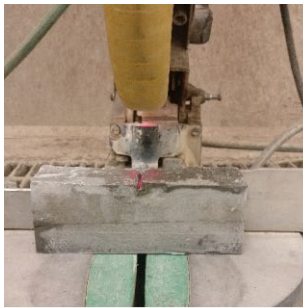
4.2 Sample Preparation and Set-up

4.2.1 Adhesion test

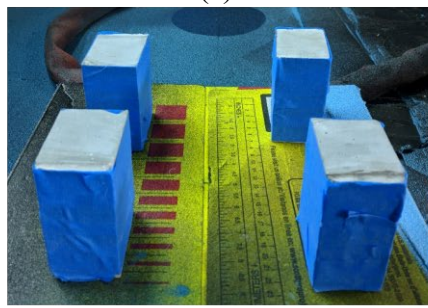
Sample preparation steps are shown in figure 4.2(b). First, a SENB specimen made of cement paste using a water-to-cement ratio of 0.47 is cut in half. One cut side is then sprayed with the PU to make the coating which is then glued to the remaining uncoated prism specimen using a heavy-duty glue. The specimen is then coated with a speckle pattern that is to be used for digital image correlation (DIC) to obtain full-field displacement data.



(a)



Cutting in Half



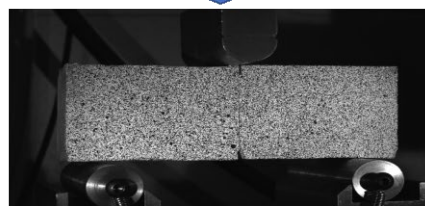
Preparing to Coating



Coating



Gluing



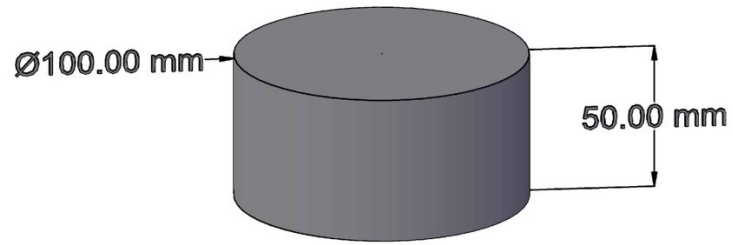
Applying speckle pattern

(b)

Figure 4.2 PU-concrete adhesion test: (a) sample configuration and (b) sample preparation process.

4.2.2 Impact testing

For impact testing, typical cylindrical specimens of 200 mm in height and 100 mm in diameter were prepared, cured for 28 days, and then cut into 50 mm thick disks, as shown in figure 4.3(a). The disks were subsequently prepared for one-sided coating. Finally, the control and coated specimens underwent impact testing by drop tower that had a semi-spherical impactor of 100 mm in diameter and 4 kg in weight, as shown in figure 4.3(b). High-speed DIC cameras were used to record the testing.



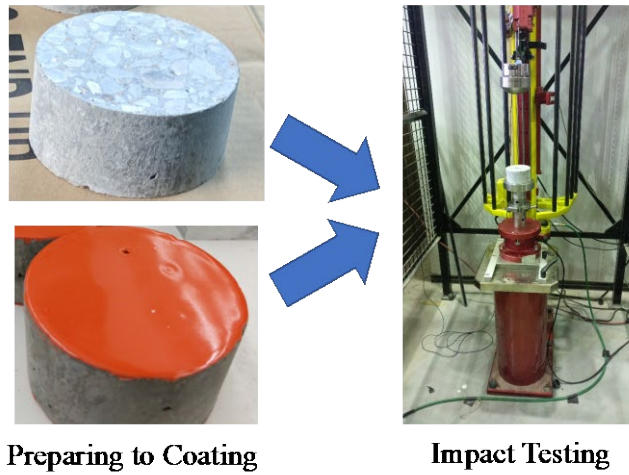
(a)



Cutting

Preparing to Coating

Coating



Preparing to Coating

Impact Testing

(b)

Figure 4.3 Impact testing of PU coated concrete specimens test: (a) sample configuration and (b) sample preparation process.

4.2.3 Blast testing

The blast testing procedure was adopted from *Ha, Yi et al. (89)* and *Tabatabaei, Volz et al. (86)*. Square concrete slabs measuring 1.168 m on one side and 0.14 m thickness are exposed to blasts generated by the TNT explosive. Data will be collected by strain gauges attached to rebars and high-speed DIC cameras. In addition, incident pressure will be recorded by pressure gauges and free-field pressure meters while bottom deflections due to the blast will be recorded by LVDT.

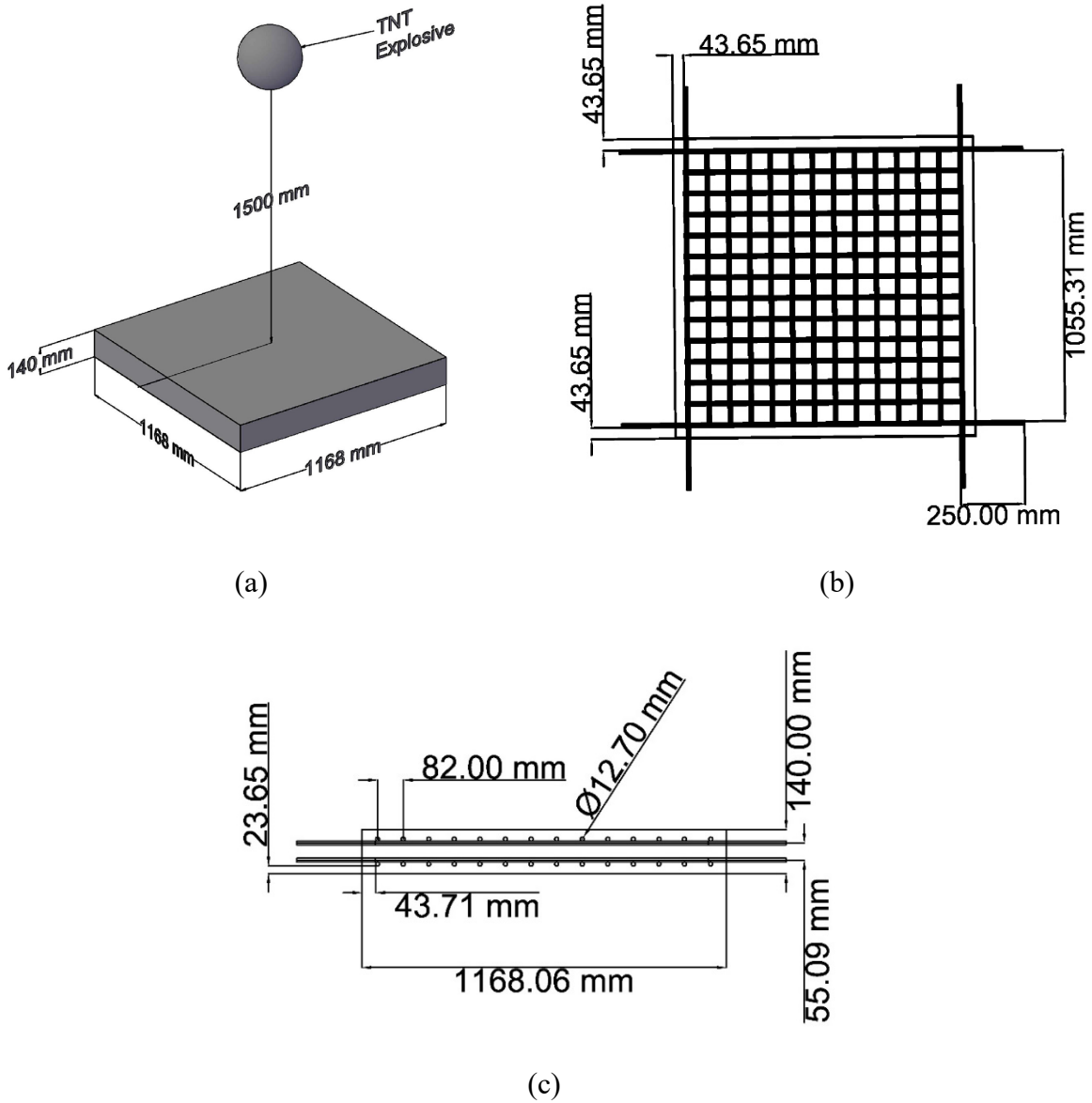


Figure 4.4 Blast experiment set-up: (a) experimental set-up, (b) rebars design top view and (b) rebars design side view.

Due to hazards related to blast testing of the concrete slabs, the Nebraska State Patrol has been contacted for possible assistance. After applying polyurea coating at a local contractor, slab specimens will be transported to a remote testing site where blast testing using TNT explosives

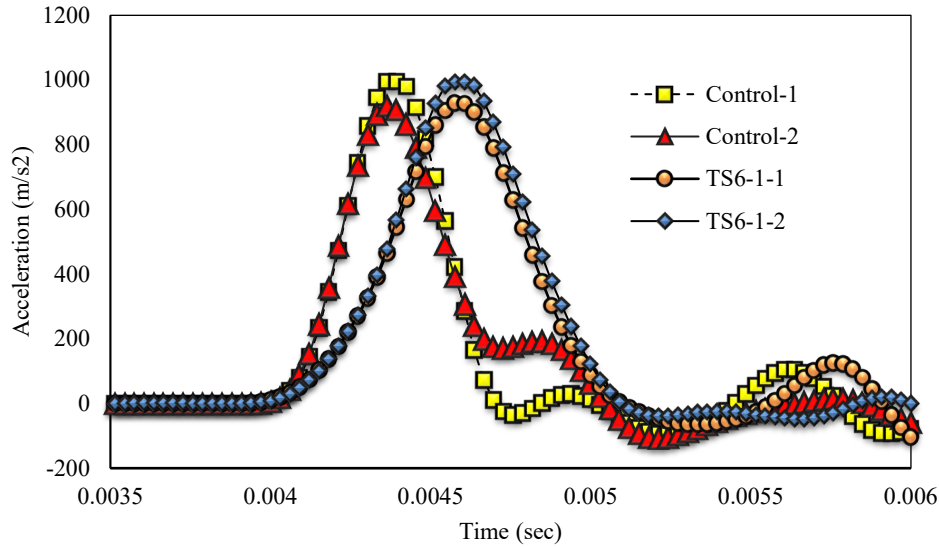
at standoff distance of 1.5 m will be performed (fig. 4.4(a)). In this study, a 15kg TNT equivalent explosive will be used, which is comparable to the amount used by *Ha, Yi et al. (89)*.

4.3 Test results and discussions

4.3.1 Impact testing

Impact testing was conducted using a drop tower with testing parameters determined from preliminary testing. The determined test parameters were the drop height and impactor geometry. During testing, a semi-spherical impactor weighting 4.173 kg was dropped from a height of 60 cm from the top surface of the specimen. The specimen was set in the middle of a circular flat anvil with a diameter of 130 mm. Tests were conducted at room temperature and a data acquisition at a sampling rate of 1650 Hz was used to collect both impact acceleration and time. It should be noted that the impact load was concentrated on a single point in the middle-top of the specimen due to the spherical shape of the impactor.

Figure 4.5(a) shows the results of impact testing for the control (no PU coating) and PU-coated specimens (TS6). It should be noted that the thickness of the coating was 1.5 mm which is equal to four spraying passes. Figure 4.5(b) and (c) show the control and coated specimens after impact testing, respectively. Control specimens showed cracking/damage after the first impact, meaning that two separate specimens were tested (Control-1 and Control-2) which generated test results shown in figure 4.5(a). In contrast, specimens on which PU (TS6-1) was applied showed improved impact resistance and visually remained intact after two consecutive impacts on a single specimen, as shown in figure 4.5(c). Furthermore, the increased impact resilience of the concrete specimen due to PU coating was confirmed by comparing the curves in figure 4.5(a) of the first and second impact (i.e., TS6-1-1 and TS6-1-2) which reveal minimal change in the results.



(a)



(b)



(c)

Figure 4.5 Impact test results: (a) acceleration vs. time at impact, (b) cracks in uncoated specimen (control) and (c) coated specimens after two impact testings.

Further inspection of the impact results shown in figure 4.5(a) reveals that the PU coating improved the dampening characteristics of the concrete by distributing the impact load over a wider time as compared to control specimens. These results imply that the polymeric coating reduced the change in acceleration (i.e., pre- and post-peak slopes), which allowed the concrete to better distribute the impact energy over a wider area, resulting in less damage as compared to control specimens.

4.3.2 Adhesion testing

As mentioned previously, adhesion testing was conducted with SENB specimens containing cement-PU-glue layers in the middle (fig. 2.29). The load was applied in displacement-controlled mode at a rate of 0.5 mm/sec and the reaction force was recorded. After testing, the dimensions of PU coating were measured, and the failure side recorded (table 4.1). In order to investigate the effect of surface treatment on the adhesion performance of PU to the cement, a group composed of sand-blasted treated surfaces was tested. The sand treatment was done to increase the roughness of the cement surface and to increase the interface area of cement-PU, which thus increase the adhesion strength. It should be noted that the treated surface met the International Concrete Repair Institute's concrete surface profiles 4 (ICRI's CSP 4).

Table 4.1 Specimen Information and Failure Characteristics of Adhesion Test Specimens

Sample Name	Thickness Measurements (mm)			Average	Failure Side	Surface Type
	1	2	3			
Beam-1	-	-	-		Cement	
Beam-7	0.97	0.93	0.92	0.94	Glue	Non-treated Surface
Beam-4	1.44	1.32	1.27	1.34	Glue	
Beam-2	1.62	2.04	1.58	1.75	Interface	
Beam-6	2.2	2.19	2.13	2.17	Glue	
Beam-8	1.78	1.25	1.62	1.55	Glue	Treated Surface
Beam-9	2.77	2.72	2.9	2.80	Glue	
Beam-5	3.57	3.57	3.67	3.60	Glue	
Beam-3	-	-	-	-	Cement	

Failure characteristics shown in table 4.1 indicate that the cement-PU interface rarely failed during the testing, while glue-cement failed. These results imply the existence of strong adhesion between retrofitting material (i.e., PU) and the cement. However, it should be noted

that in case of untreated surfaces, failure at the interface was possible, in contrast to treated surfaces. Figure 4.6 presents the load-time curves for both treated (fig. 4.6 (a)) and untreated surfaces (fig. 4.6(b)). Specimens with untreated surfaces generally required a longer time and a higher load to fail, in contrast to specimen with treated surfaces. This may first appear to contradict expectations, since treated surfaces are expected to perform better than untreated specimens. However, since none of the specimens with treated surfaces failed at the interface, the results in figure 4.6(b) can be interpreted as being those of the glue used instead of the interface.

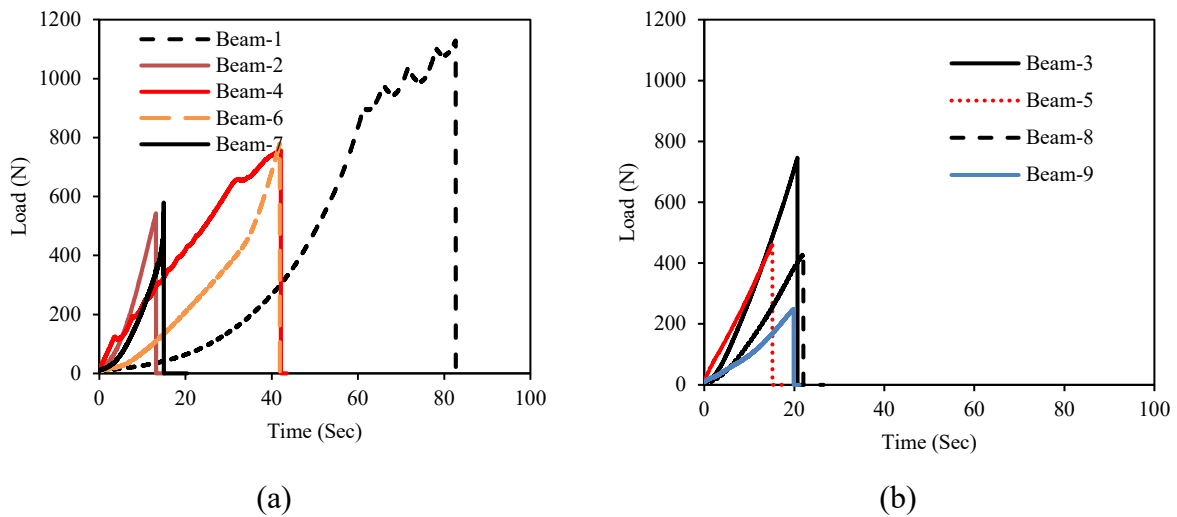


Figure 4.6 Load vs. time results from adhesion testing: (a) for untreated surface and (b) for treated surface.

Based on the results of treated surfaces shown in figure 4.6(a), it appears that increasing the PU coat thickness (i.e., Beam-2 and -6 vs. Beam-7) increased the time to failure while minimally affecting the failure load. These observations imply an increased deformation inside the PU coat during the testing, which in turn delayed failure. In the case of cement failure (i.e., Beam-1 and Beam-3 for untreated and treated, respectively) the load was reasonably higher than

other cases due to the higher strength of cement compared to the interfaces (cement-PU and PU-glue).

Beam-2 was the only instance where failure occurred at the cement-PU interface and had the maximum load of 520 N at 12.75 seconds. Thus experimentally, the interfacial bond strength (T_C) can be approximated from the maximum load (P_{max}) and ligament area ($A_{ligament}$) by:

$$T_C = \frac{P_{max}}{A_{ligament}} = \frac{520 \text{ N}}{40 \text{ mm} \times 55 \text{ mm}} \approx 0.236 \text{ MPa}$$

Figure 4.7 shows the failure surfaces after testing where it can be seen that cement-cement failure (Figure 4.7(a)) produced a larger ligament area, which resulted in a higher maximum load, as shown in figure 4.6. In addition, figure 4.7 shows the interface of PU-glue (fig. 4-7(b)) and cement-PU (fig. 4.7(c)) where clean de-adhesion was observed for both cases after testing.

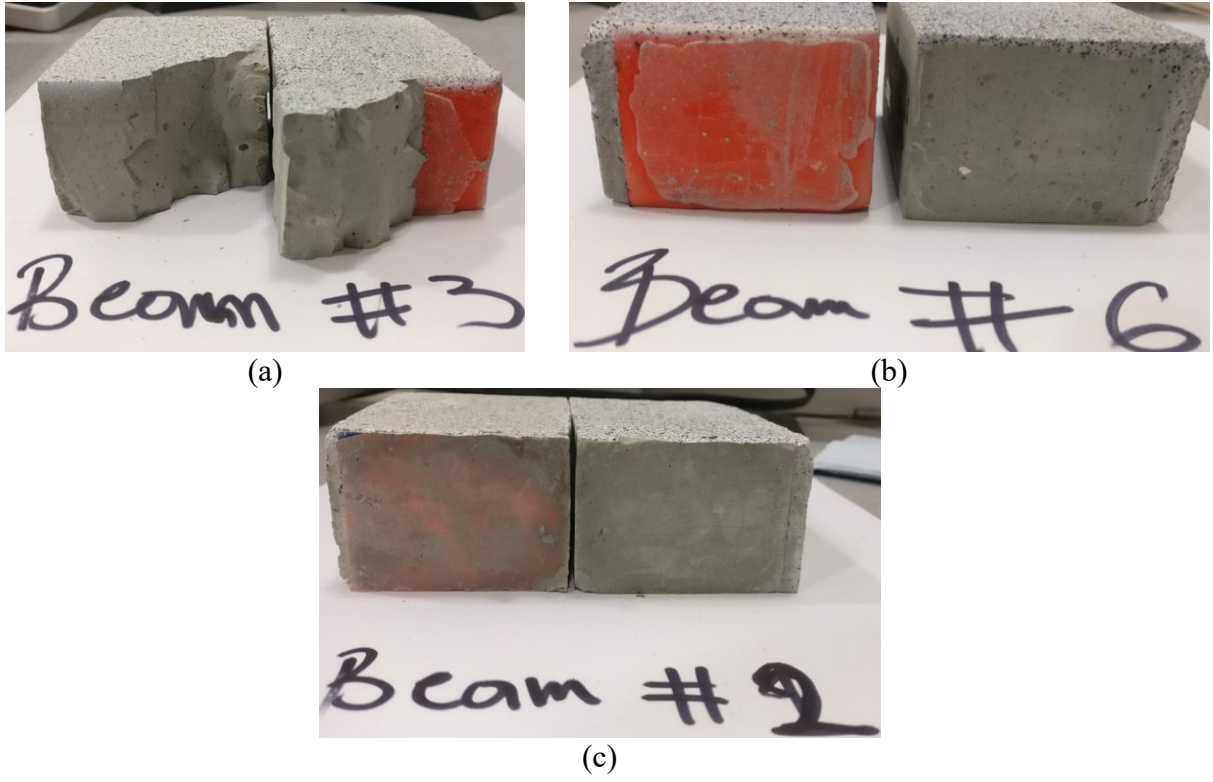


Figure 4.7 Failure surfaces: (a) cement-cement, (b) PU-glue and (c) cement-PU interface.

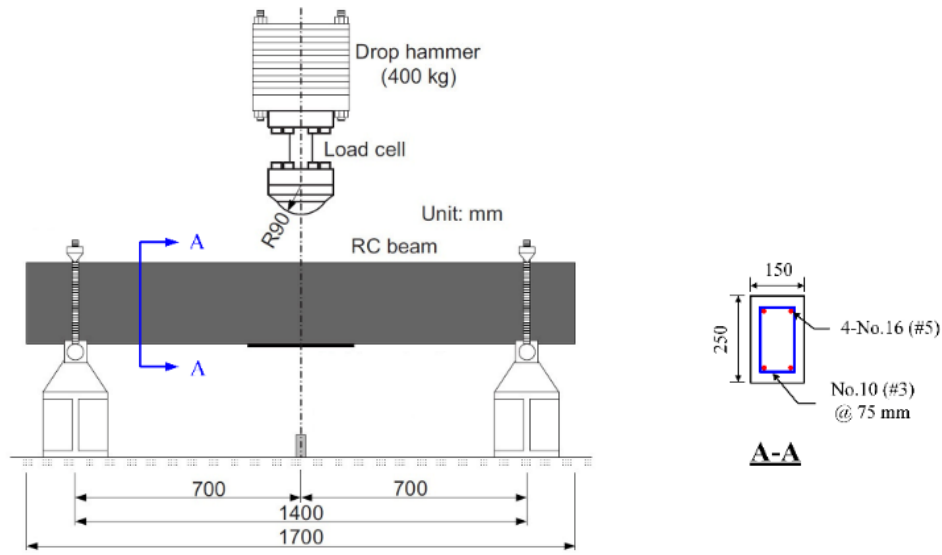
Chapter 5 Validation Study

5.1 Introduction

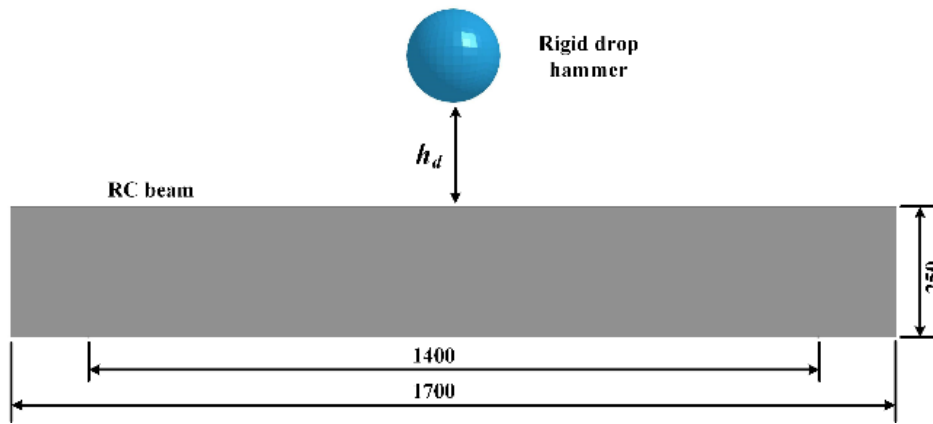
This chapter discusses the validation process that helped evaluate the feasibility of FE modeling approaches utilized in the research. Accuracy of the FE modeling approach was examined by comparing numerical simulation results against published impact and blast tests. The authors could not locate an experimental study in the open literature examining the behavior of RC bridge column subjected to combined impact and blast. As a result, two experimental programs reported in the literature were utilized to validate the modeling approach; one being from impact tests on RC beams (*I22*) and the second being a reduced scale blast test of a RC column in a building frame (*I23*).

5.2 RC beams under impact load

Fujikake et al. (*I22*) performed tests on several RC beams using a drop hammer having a mass of 882 lbs (400 kg) that impacted their top surface at mid span as shown in figure 5.1. Beams had cross-sectional dimensions of 10 in. (250 mm) in depth, 6 in. (150 mm) in width, and were 67 in. (1700 mm) long. They were reinforced using 4 #5 (No. 16) longitudinal bars and #3 (No. 10) hoops spaced at 3 in. (75 mm). The compressive strength of the concrete was 6 ksi (42 MPa), and the yield strength of reinforcement was 62 ksi (426 MPa). Additional details about the testing program are provided in Fujikake et al. (*I22*). Numerical models of the impact tests were developed using LS-DYNA following procedures discussed in the previous chapter. Impact force and mid-span displacement time-histories for drop heights (h_d) of 23.5 in. (600 mm) and 47 in. (1200 mm) were selected for validation.



(a) Experimental configuration



(b) Numerical model

Figure 5.1 Drop-hammer impact test setup and numerical model (mm) (122)

The drop hammer was modeled as a rigid sphere using the *Mat Rigid* command in LS-DYNA. Segment-based contact was defined between the beam and drop hammer using the LS-DYNA *Contact Automatic Surface To Surface* command. Qualitative comparisons between damage and failure modes predicted by the LS-DYNA models and those obtained from the tests are shown in figure 5.2. Predicted damage and failure patterns were in good agreement with test

results. Concrete cracking was observed along the bottom side of the beam and concrete spalling along their top faces.

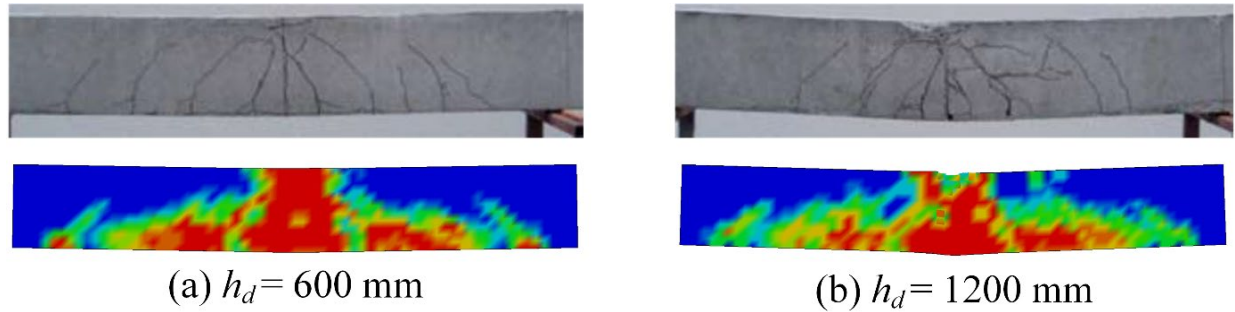


Figure 5.2 Comparison between experimental and simulated damage for: (a) $h_d = 600$ mm; (b) $h_d = 1200$ mm (122)

Force and mid-span displacement time-histories comparisons showed good agreements as indicated in figs. 4.3 and 4.4, with simulated displacements being 10 percent lower than measured values. Peak impact forces were also in good agreement, but predicted post-peak forces were higher than those observed from the tests. Differences were attributed to testing boundary conditions and minor shortcomings of the concrete material model with respect to simulating strength degradation under transient loads. Given that impact studies generally are concerned with initial peak forces, these results were deemed conservative but quite acceptable.

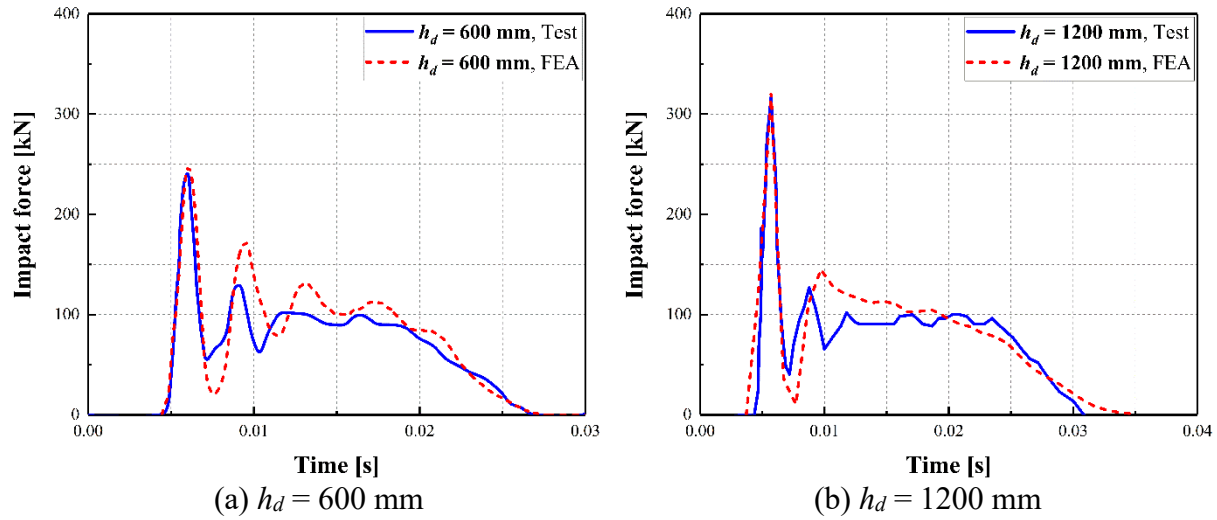


Figure 5.3 RC beam experimental and modeled impact force time histories (122)

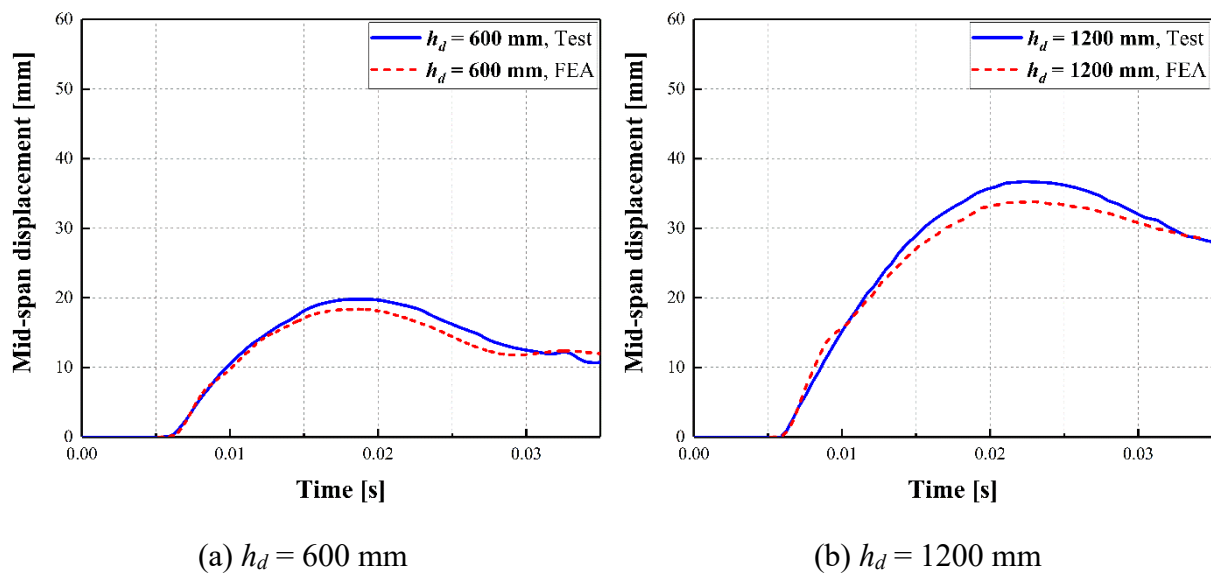


Figure 5.4 RC beam experimental and modeled midspan displacement time histories (122)

5.3 RC column under blast load

A blast test on a quarter scale RC frame that focused on response of the central column was conducted by Baylot et al. (123), as shown in figure 5.5. The blast load was generated using a 17.64 lbs (8 kg) TNT-equivalent high explosive at a standoff distance of 3.5 ft. (1070 mm).

Cross-sectional dimensions of the RC column were 3.5 in. (89 mm) in depth, 3.5 in. (89 mm) in width and 35.5 in. (900 mm) in height. The column was reinforced with eight 0.63-in. (1.6-mm) diameter longitudinal steel bars and 0.63-in. (1.6-mm) diameter hoops spaced at 4 in. (100 mm) along its height. The compressive strength of the concrete was 6 ksi (42 MPa), and the reinforcement yield strength was 65 ksi (450 MPa). Additional details of the test are provided by Baylot et al. (123, 124).

A FE model of the center column was developed in LS-DYNA following procedures in the previous chapter and subject to simulated blast loads. An axial pressure of 0.3 ksi (2.1 MPa) was applied at the top surface of the column before applying the blast load to represent the building dead load. To represent boundary conditions at each floor level, a part of the slab was incorporated into the model and horizontal translations were constrained.

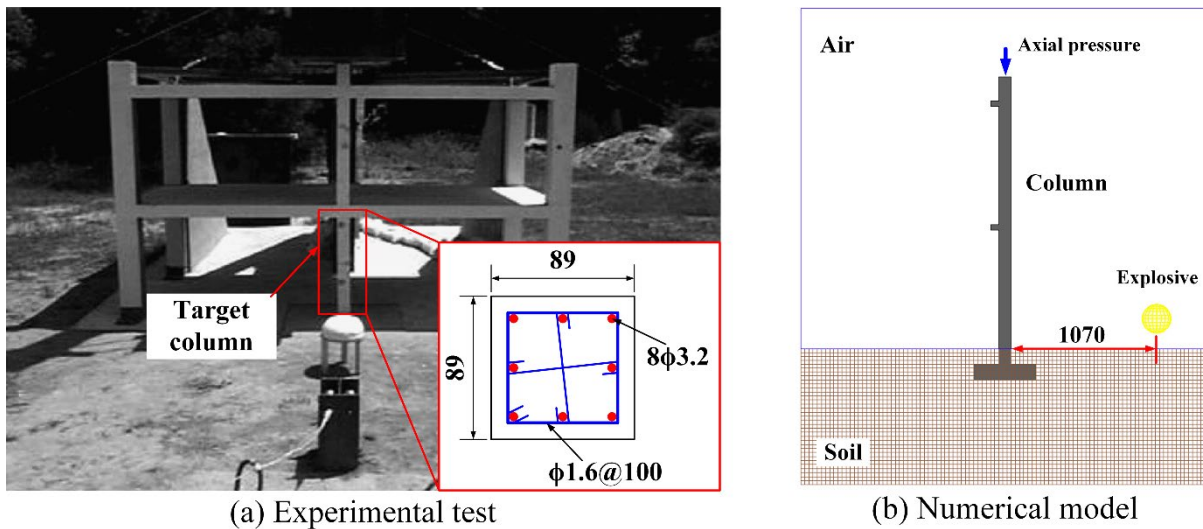
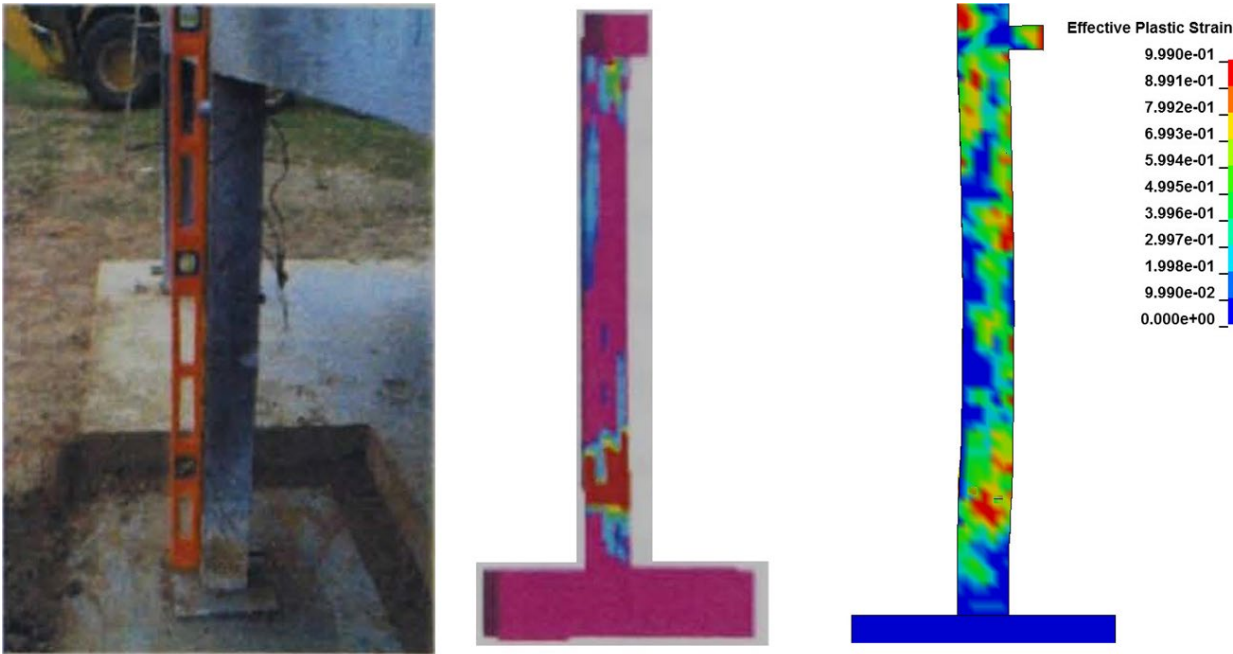


Figure 5.5 Experimental configuration and FE model (mm)

A comparison between predicted and actual damage patterns is shown in figure 5.6, with numerical predictions taken from the present study and from analytical studies conducted by

Baylot et al. (123). Predicted damage and failure patterns agreed reasonably well with measured values. Figure 5.7 compares mid-height displacements for the blast test, the present study and results from Baylot et al. (124) and Shi et al. (125). Simulated mid-height displacement time-histories matched well with measured values, especially for the first peak, and predicted actual behavior better than Baylot et al. or Shi et al.



(a) Tested column (b) Numerical result by Baylot (124) (c) Current study

Figure 5.6 Damage patterns comparisons

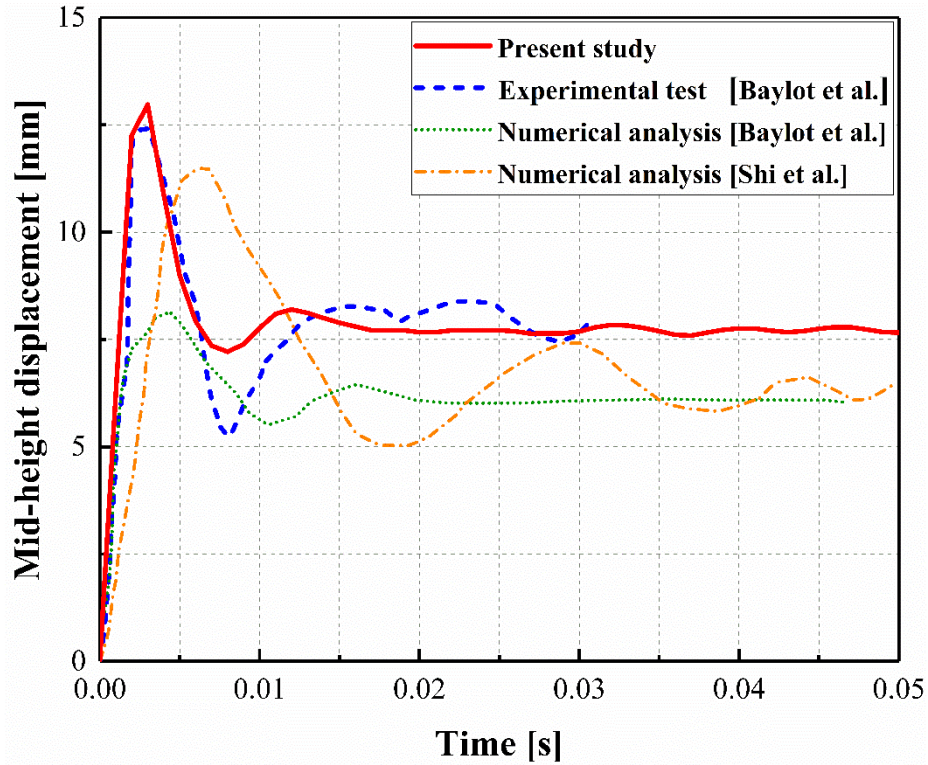


Figure 5.7 Mid-height displacement time histories

5.4 Conclusions

In the chapter, the proposed bridge column numerical model was validated by comparing simulated results against the experimental data using two separate test programs reported in the open literature: (1) drop-weight tests on RC beams; and (2) a reduced-scale blast test of a RC building frame column. Selected modeling approaches were successfully validated against test results and supported using modeling approaches to predict the response of RC members subjected to impact and blast loading.

Chapter 6 Conclusions

6.1 Summary

The ultimate objective of the on-going research project is to improve resilience and robustness of a RC bridge piers in the event of vehicle collision coupled with an additional event, e.g. air blast, or fire. Summarized herein are tasks completed during the first year of the multi-year research project. Research that was completed during year 1 included: (1) literature review of studies that (i) examined the behavior and analysis of materials and structures subjected to vehicle impact and blast, with emphasis on research related to reinforced concrete (RC) and its constituent materials, (ii) reviewed current design specifications as they relate to bridge piers, with a focus on pier columns, (iii) explored and conducted experiments to obtain material properties where impact and/or blast are associated with concrete which is improved by retrofitting materials (such as polymeric costing) to absorb energy, and (iv) the design and detailing of RC bridge elements; and (2) the development and validation of a RC bridge pier column 3D finite element model subjected to simulated vehicle collision and an air blast using LS-DYNA. Future project tasks include: (1) parameterizing bridge pier column behavior over a range of collision and blast demands using the validated numerical model; (2) exploring, developing and recommending viable retrofitting techniques; and (3) developing and recommending viable analysis and design procedures.

6.2 Ongoing Research

To achieve project goals, the following tasks need to be completed:

- Perform parametric analysis that will investigate the effects of column diameter, axial load ratio, column height, transverse reinforcement ratio, longitudinal reinforcement

ratio, vehicle impact velocity, and scaled standoff distance on the performance of bridge columns to provide recommendations for design and detailing of column;

- Examine blast and impact load equivalent static forces using different approaches to evaluate the standard AASHTO-LRFD design impact load;
- Evaluate the effectiveness of various retrofit and design techniques for bridge columns under impact and blast loading and develop design and detailing methodologies;
- Develop recommendations and specifications for design and detailing of bridge columns under vehicle collision and blast loading.
- Blast testing will be carried out using TNT explosives on reinforced concrete slabs and data acquisition will be achieved by a combination of strain gauges, LVDTs and high-speed cameras. Plans for the blast testing program were discussed and currently waiting assistance from the Nebraska State Patrol for the testing.
- More tests on adhesion between concrete and PU coating to induce a strong interface bonding.
- More tests on impact to increase the PU coating's capability of damping so that the impact load can be effectively distributed to a larger area and for a longer time.
- Test results from materials will then be used for numerical structural simulations.

Research project activities and findings have been presented at multiple venues and technical papers are being prepared for submission to peer-reviewed, archival journals. These include an oral presentation at 2018 Structures Congress in Denver, Colorado (126); a poster presentation at 2017 Spring Research Fair in Lincoln, Nebraska (127); and two ready-to-submit manuscripts.

References

1. Tennessean News. *Tennessean News Archive*. 2014 [cited 2012 August 15th]; Available from: <https://www.tennessean.com/story/news/local/williamson/2014/08/15/franklin-tanker-explosion-65/14097717/>.
2. Harold, M. *Pier protection*. in *Final Design Workshop 2017*. 2017. St. Paul, Minnesota: Minnesota Department of Transportation,.
3. American Association of State and Highway Officials AASHTOs, *AASHTO LRFD bridge design specifications, eighth edition*. 2017: Washington, DC.
4. Abdelkarim, O.I. and M.A. ElGawady, *Performance of bridge piers under vehicle collision*. *Engineering Structures*, 2017. **140**: p. 337-352.
5. AuYeung, S. and A. Alipour, *Evaluation of AASHTO Suggested Design Values for Reinforced Concrete Bridge Piers Under Vehicle Collisions*. *Transportation Research Record: Journal of the Transportation Research Board*, 2016(2592): p. 1-8.
6. Buth, E.C., W.F. Williams, M.S. Brackin, D. Lord, S.R. Geedipally, and A.Y. Abu-Odeh, *Analysis of large truck collisions with bridge piers: phase 1. Report of guidelines for designing bridge piers and abutments for vehicle collisions*. Texas: Texas Transportation Institute, 2010.
7. Buth, E.C., M.S. Brackin, W.F. Williams, and G.T. Fry, *Collision loads on bridge piers: phase 2, report of guidelines for designing bridge piers and abutments for vehicle collisions*. 2011, Texas Transportation Institute.
8. Tedesco, J., W. McDougal, and C. Ross, *Structural dynamics: Theory and approach*. 1999, Addison Wesley Longman, Menlo Park, CA.
9. Department of Defense, *Structures to resist the effects of accidental explosions*. 2008: Washington, DC: Unified Facilities Criteria.
10. Malvar, J.L. and J.E. Crawford, *Dynamic increase factors for concrete*. 1998, Naval Facilities Engineering Service Center Port huene me CA.
11. Malvar, J.L. and J.E. Crawford. *Dynamic increase factors for steel reinforcing bars*. in *28th DDESB Seminar. Orlando, USA*. 1998.
12. Wehbe, N.I., X. Qin, B. Tigges, Z. Shen, and A. Boudaqa, *Evaluation and mitigation of vehicle impact hazards for overpasses, MPC-397*. 2017, North Dakota State University - Upper Great Plains Transportation Institute, Fargo: Mountain-Plains Consortium.
13. Maghiar, M., M. Jackson, and G. Maldonado, *Warning systems evaluation for overhead clearance detection*. 2017, Georgia Southern University.
14. Sharma, H., S. Hurlebaus, and P. Gardoni, *Performance-based response evaluation of reinforced concrete columns subject to vehicle impact*. *International Journal of Impact Engineering*, 2012. **43**: p. 52-62.
15. Gomez, N.L., *Performance of circular reinforced concrete bridge piers subjected to vehicular collisions*. 2014.
16. AP News. *AP News Archive*. 2003 [cited 2003 December 10]; Available from: <http://www.apnewsarchive.com/2003/Fatal-Crash-Causes-I-80-Bridge-Collapse/id-241431bd969779343b699abfeb8e6156>.
17. American Association of State Highway and Transportation Officials AASHTOs, *AASHTO LRFD bridge design specifications, first edition*. 1994: Washington, D.C.
18. American Association of State Highway and Transportation Officials AASHTOs, *Manual for Assessing Safety Hardware*. 1993: Washington, D.C.

19. American Association of State Highway and Transportation Officials AASHTOs, *AASHTO LRFD bridge design specifications, sixth edition*. 2012: Washington, D.C.
20. Sharma, H., P. Gardoni, and S. Hurllebaus, *Probabilistic demand model and performance-based fragility estimates for RC column subject to vehicle collision*. Engineering Structures, 2014. **74**: p. 86-95.
21. Sharma, H., P. Gardoni, and S. Hurllebaus, *Performance-based probabilistic capacity models and fragility estimates for RC columns subject to vehicle collision*. Computer-Aided Civil and Infrastructure Engineering, 2015. **30**(7): p. 555-569.
22. El-Tawil, S., E. Severino, and P. Fonseca, *Vehicle collision with bridge piers*. Journal of Bridge Engineering, 2005. **10**(3): p. 345-353.
23. National Crash Analysis Center, *Chevrolet Silverado finite element model validation coarse mesh*. 2012, The George Washington University, Virginia Campus: Ashburn, VA.
24. Agrawal, A.K., G.Y. Liu, and S. Alampalli. *Effects of truck impacts on bridge piers*. in *Advanced Materials Research*. 2013. Trans Tech Publ.
25. Gomez, N. and A. Alipour. *Study of circular reinforced concrete bridge piers subjected to vehicular collisions*. in *Structures Congress 2014*. 2014.
26. Thilakarathna, H.M.I., D. Thambiratnam, M. Dhanasekar, and N. Perera, *Numerical simulation of axially loaded concrete columns under transverse impact and vulnerability assessment*. International Journal of Impact Engineering, 2010. **37**(11): p. 1100-1112.
27. Eurocode-1, *Eurocode 1: actions on structures. Part 1-1. general actions; densities, self-weight, imposed loads for buildings*. 2002: British Standards Institution.
28. Crowl, W., *Structures to resist the effects of accidental explosions, technical manual TM 5-1300*. US Army, Navy and Air Force, US Government Printing Office, Washington DC, 1969.
29. Williams, G.D., *Analysis and response mechanisms of blast-loaded reinforced concrete columns*. 2009.
30. Bulson, P.S., *Explosive loading of engineering structures*. 2002: CRC Press.
31. Williamson, E.B., *Blast-resistant highway bridges: design and detailing guidelines*. Vol. 645. 2010: Transportation Research Board.
32. Winget, D.G., *Design of critical bridges for security against terrorist attacks*. 2003, University of Texas at Austin.
33. Bounds, W.L., *Design of blast-resistant buildings in petrochemical facilities*. 2010: ASCE Publications.
34. Department of Defense, *Design and analysis of hardened structures to conventional weapons effects*. 2002: Washington, DC: Unified Facilities Criteria.
35. Williamson, E.B. and D.G. Winget, *Risk management and design of critical bridges for terrorist attacks*. Journal of Bridge Engineering, 2005. **10**(1): p. 96-106.
36. Matthews, D.S., *Blast effects on prestressed concrete bridges*. 2008, Citeseer.
37. Yi, Z., A. Agrawal, M. Ettouney, and S. Alampalli, *Blast load effects on highway bridges. I: Modeling and blast load effects*. Journal of Bridge Engineering, 2013. **19**(4): p. 04013023.
38. Yi, Z., A. Agrawal, M. Ettouney, and S. Alampalli, *Blast load effects on highway bridges. II: Failure modes and multihazard correlations*. Journal of Bridge Engineering, 2013. **19**(4): p. 04013024.
39. Magnusson, J. and M. Hallgren, *Reinforced high strength concrete beams subjected to air blast loading*. WIT Transactions on The Built Environment, 2004. **73**.

40. Fujikura, S. and M. Bruneau, *Experimental investigation of seismically resistant bridge piers under blast loading*. Journal of Bridge Engineering, 2010. **16**(1): p. 63-71.
41. Fujikura, S., M. Bruneau, and D. Lopez-Garcia, *Experimental investigation of multihazard resistant bridge piers having concrete-filled steel tube under blast loading*. Journal of Bridge Engineering, 2008. **13**(6): p. 586-594.
42. Hao, H. and E.K. Tang, *Numerical simulation of a cable-stayed bridge response to blast loads, Part II: Damage prediction and FRP strengthening*. Engineering Structures, 2010. **32**(10): p. 3193-3205.
43. Tang, E.K. and H. Hao, *Numerical simulation of a cable-stayed bridge response to blast loads, Part I: Model development and response calculations*. Engineering Structures, 2010. **32**(10): p. 3180-3192.
44. Tokal-Ahmed, Y.M., *Response of bridge structures subjected to blast loads and protection techniques to mitigate the effect of blast hazards on bridges*. 2009: Rutgers The State University of New Jersey-New Brunswick.
45. New York State Department of Transportation, *Bridge fire incidents in New York State*. 2008, New York State Department of Transportation.
46. Astaneh-Asl, A., C. Noble, J. Son, A. Wemhoff, M. Thomas, and L. McMichael, *Fire protection of steel bridges and the case of the MacArthur maze fire collapse*, in *TCLÉE 2009: Lifeline Earthquake Engineering in a Multihazard Environment*. 2009. p. 1-12.
47. National Transportation Safety Board, *Fire Damage to Bridge and Subsequent Collapse, Atlanta, Georgia*. 2017: Washington, DC 2.
48. Mendes, P.A., J.C. Valente, and F.A. Branco, *Simulation of ship fire under Vasco da Gama Bridge*. ACI structural journal, 2000. **97**(2): p. 285-290.
49. Nigro, E., G. Manfredi, E. Cosenza, and M. Zappoli. *Effects of high temperature on the performances of RC bridge decks strengthened with externally bonded FRP reinforcement*. in *Proceedings of 2nd International fib Conference, Naples, Italy*. 2006.
50. Nahid, M.N., *Computational study of highway bridges structural response exposed to a large fire exposure*. 2015, Virginia Tech.
51. Payá-Zaforteza, I. and M. Garlock. *A 3D numerical analysis of a typical steel highway overpass bridge under a hydrocarbon fire*. in *Structures in Fire: Proceedings of the Sixth International Conference*. 2010. DEStech Publications, Inc.
52. Drive News. *The Drive News Archive*. 2014 [cited 2018 August 6th]; Available from: <http://www.thedrive.com/news/22668/three-dead-60-injured-after-tanker-truck-explosion-collapses-elevated-highway-in-italy>.
53. Bank, L.C., *Composites for construction: structural design with FRP materials*. 2006: John Wiley & Sons.
54. Teng, J., J.F. Chen, S.T. Smith, and L. Lam, *FRP: strengthened RC structures*. Frontiers in Physics, 2002: p. 266.
55. Baylot, J.T., B. Bullock, T.R. Slawson, and S.C. Woodson, *Blast response of lightly attached concrete masonry unit walls*. Journal of Structural Engineering, 2005. **131**(8): p. 1186-1193.
56. Ross, A.C., M. Purcell, and E.L. Jerome. *Blast response of concrete beams and slabs externally reinforced with fiber reinforced plastics (FRP)*. in *Building to Last*. 1997. ASCE.

57. Muszynski, L.C. and M.R. Purcell, *Use of composite reinforcement to strengthen concrete and air-entrained concrete masonry walls against air blast*. Journal of Composites for Construction, 2003. **7**(2): p. 98-108.
58. Erki, M. and U. Meier, *Impact loading of concrete beams externally strengthened with CFRP laminates*. Journal of Composites for Construction, 1999. **3**(3): p. 117-124.
59. Firmo, J., J. Correia, D. Pitta, C. Tiago, and M. Arruda, *Experimental characterization of the bond between externally bonded reinforcement (EBR) CFRP strips and concrete at elevated temperatures*. Cement and Concrete Composites, 2015. **60**: p. 44-54.
60. Firmo, J.P., J.R. Correia, and L.A. Bisby, *Fire behaviour of FRP-strengthened reinforced concrete structural elements: a state-of-the-art review*. Composites Part B: Engineering, 2015. **80**: p. 198-216.
61. Bisby, L., V. Kodur, and M. Green, *Fire endurance of fiber-reinforced polymer-confined concrete*. ACI Structural Journal, 2005. **102**(6): p. 883-891.
62. Bisby, L.A., M.F. Green, and V.K. Kodur, *Response to fire of concrete structures that incorporate FRP*. Progress in Structural Engineering and Materials, 2005. **7**(3): p. 136-149.
63. Kelly, J.M., *Ultra-high molecular weight polyethylene*. Journal of Macromolecular Science, Part C: Polymer Reviews, 2002. **42**(3): p. 355-371.
64. Sherazi, T.A., *Ultrahigh molecular weight polyethylene*. Encyclopedia of Membranes, 2015: p. 1-2.
65. Zhang, T.G., S.S. Satapathy, L.R. Vargas-Gonzalez, and S.M. Walsh, *Ballistic impact response of ultra-high-molecular-weight polyethylene (UHMWPE)*. Composite structures, 2015. **133**: p. 191-201.
66. Lässig, T., F. Bagusat, M. May, and S. Hiermaier, *Analysis of the shock response of UHMWPE composites using the inverse planar plate impact test and the shock reverberation technique*. International Journal of Impact Engineering, 2015. **86**: p. 240-248.
67. O'Masta, M., B. Compton, E. Gamble, F. Zok, V. Deshpande, and H. Wadley, *Ballistic impact response of an UHMWPE fiber reinforced laminate encasing of an aluminum-alumina hybrid panel*. International Journal of Impact Engineering, 2015. **86**: p. 131-144.
68. Lee, S.Y., G.D. Kim, S.J. Kim, and C.H. Chang, *High-energy impact behaviors of hybrid composite plates strengthened with 3D-UHMWPE composites*. Shock and Vibration, 2018. **2018**.
69. Knox, K.J., M.I. Hammons, T.T. Lewis, and J.R. Porter, *Polymer materials for structural retrofit*. Force Protection Branch, Air Expeditionary Forces Technology Division, Air Force Research Laboratory, Tyndall AFB, Florida, 2000.
70. Delucchi, M., A. Barbucci, and G. Cerisola, *Crack-bridging ability and liquid water permeability of protective coatings for concrete*. Progress in Organic Coatings, 1998. **33**(1): p. 76-82.
71. Zur, E. *Polyurea—the new generation of lining and coating*. in *Advanced Materials Research*. 2010. Trans Tech Publ.
72. Toutanji, H., H. Choi, D. Wong, J. Gilbert, and D. Alldredge, *Applying a polyurea coating to high-performance organic cementitious materials*. Construction and Building Materials, 2013. **38**: p. 1170-1179.
73. Chen, C.-C., *A study of blast effects on polyurea coated steel components*. 2009.

74. Chen, C.-C. and D.G. Linzell, *Numerical Simulations of Dynamic Behavior of Polyurea Toughened Steel Plates under Impact Loading*. Journal of Computational Engineering, 2014. **2014**.
75. Iqbal, N., P. Sharma, D. Kumar, and P. Roy, *Protective polyurea coatings for enhanced blast survivability of concrete*. Construction and Building Materials, 2018. **175**: p. 682-690.
76. Raman, S., T. Pham, P. Mendis, and T. Ngo, *Experimental investigation on the behavior of RC panels retrofitted with polymer coatings under blast effects*. 2013.
77. Raman, S.N., T. Ngo, P. Mendis, and T. Pham, *Elastomeric polymers for retrofitting of reinforced concrete structures against the explosive effects of blast*. Advances in Materials Science and Engineering, 2012. **2012**.
78. Fallon, C. and G. McShane. *Experimental and Numerical Investigation on the Impact Response of Elastomer-Coated Concrete*. in *Multidisciplinary Digital Publishing Institute Proceedings*. 2018.
79. Carey, N.L., J.J. Myers, D. Asprone, and C. Menna, *Polyurea Coated and Plane Reinforced Concrete Panel Behavior under Blast Loading: Numerical Simulation to Experimental Results*. Trends In Civil Engineering And Its Architecture, 2018. **1**(4): p. 87-98.
80. Ettouney, M.M., S. Alampalli, and A.K. Agrawal, *Theory of multihazards for bridge structures*. Bridge Structures, 2005. **1**(3): p. 281-291.
81. Bridge, R.Q., *Concrete filled steel tubular columns*. 1976.
82. Narayanan, R. and I.L. Lee. *Double skin composite construction for submerged tube tunnels*. in *Constructional steel design. World developments. Proceedings of the first world conference on constructional steel design, Acapulco, Mexico*. 1992.
83. Fouche, P.P., *Blast and seismic resistant concrete-filled double skin tubes and modified steel jacketed bridge columns*. 2014: State University of New York at Buffalo.
84. Fouché, P., M. Bruneau, V. Chiarito, and J. Minor. *Blast and earthquake resistant bridge pier concept: retrofit and alternative design options*. in *Structures Congress 2013: Bridging Your Passion with Your Profession*. 2013.
85. Keller, D. and M. Bruneau, *Multi-hazard resistant steel plate shear wall bridge pier concept*. Behavior of Steel Structures in Seismic Areas, STESSA 2009, 2009.
86. Tabatabaei, Z.S., J.S. Volz, J. Baird, B.P. Gliha, and D.I. Keener, *Experimental and numerical analyses of long carbon fiber reinforced concrete panels exposed to blast loading*. International Journal of Impact Engineering, 2013. **57**: p. 70-80.
87. Castedo, R., P. Segarra, A. Alañon, L. Lopez, A. Santos, and J. Sanchidrian, *Air blast resistance of full-scale slabs with different compositions: Numerical modeling and field validation*. International Journal of Impact Engineering, 2015. **86**: p. 145-156.
88. Wu, C., D. Oehlers, M. Rebstrost, J. Leach, and A. Whittaker, *Blast testing of ultra-high performance fibre and FRP-retrofitted concrete slabs*. Engineering structures, 2009. **31**(9): p. 2060-2069.
89. Ha, J.-H., N.-H. Yi, J.-K. Choi, and J.-H.J. Kim, *Experimental study on hybrid CFRP-PU strengthening effect on RC panels under blast loading*. Composite Structures, 2011. **93**(8): p. 2070-2082.
90. Kong, X., X. Qi, Y. Gu, I.A. Lawan, and Y. Qu, *Numerical evaluation of blast resistance of RC slab strengthened with AFRP*. Construction and Building Materials, 2018. **178**: p. 244-253.

91. Maazoun, A., B. Belkassem, B. Reymen, S. Matthys, J. Vantomme, and D. Lecompte, *Blast response of RC slabs with externally bonded reinforcement: Experimental and analytical verification*. Composite Structures, 2018. **200**: p. 246-257.
92. Khalil, E., M. Abd-Elmohsen, and A.M. Anwar, *Impact resistance of rubberized self-compacting concrete*. Water Science, 2015. **29**(1): p. 45-53.
93. Huo, J., J. Liu, X. Dai, J. Yang, Y. Lu, Y. Xiao, and G. Monti, *Experimental study on dynamic behavior of CFRP-to-concrete interface*. Journal of Composites for Construction, 2016. **20**(5): p. 04016026.
94. Khedmati, M., H. Alanazi, Y.-R. Kim, G. Nsengiyumva, and S. Moussavi, *Effects of Na₂O/SiO₂ molar ratio on properties of aggregate-paste interphase in fly ash-based geopolymer mixtures through multiscale measurements*. Construction and Building Materials, 2018. **191**: p. 564-574.
95. Omidvar, M., M. Iskander, and S. Bless, *Stress-strain behavior of sand at high strain rates*. International journal of impact engineering, 2012. **49**: p. 192-213.
96. Lewis, B.A., *Manual for LS-DYNA soil material model 147*. 2004.
97. Reid, J., B. Coon, B. Lewis, S. Sutherland, and Y. Murray, *Evaluation of LS-DYNA soil material model 147*. 2004.
98. Tong, X. and C.Y. Tuan, *Viscoplastic cap model for soils under high strain rate loading*. Journal of Geotechnical and Geoenvironmental Engineering, 2007. **133**(2): p. 206-214.
99. An, J., C.Y. Tuan, B. Cheeseman, and G. Gazonas, *Simulation of soil behavior under blast loading*. International Journal of Geomechanics, 2011. **11**(4): p. 323-334.
100. Pak, A., H. Shahir, and A. Ghassemi. *Behavior of dry and saturated soils under impact load during dynamic compaction*. in *Proceedings of the International Conference on Soil Mechanics and Geotechnical Engineering*. 2005. AA Balkema Publishers.
101. Xie, X., Y. Yao, J. Liu, P. Li, and G. Yang, *Mechanical behavior of unsaturated soils subjected to impact loading*. Shock and Vibration, 2016. **2016**.
102. Gardoni, P., A. Der Kiureghian, and K.M. Mosalam, *Probabilistic capacity models and fragility estimates for reinforced concrete columns based on experimental observations*. Journal of Engineering Mechanics, 2002. **128**(10): p. 1024-1038.
103. Shi, Y. and M.G. Stewart, *Spatial reliability analysis of explosive blast load damage to reinforced concrete columns*. Structural Safety, 2015. **53**: p. 13-25.
104. Ramanathan, K., R. DesRoches, and J. Padgett, *Analytical fragility curves for multispan continuous steel girder bridges in moderate seismic zones*. Transportation Research Record: Journal of the Transportation Research Board, 2010(2202): p. 173-182.
105. Hao, H., M.G. Stewart, Z.-X. Li, and Y. Shi, *RC column failure probabilities to blast loads*. International Journal of Protective Structures, 2010. **1**(4): p. 571-591.
106. Wassef, W., C. Smith, C. Clancy, and M. Smith, *Comprehensive design example for prestressed concrete (PSC) girder superstructure bridge with commentary*. Federal Highway Administration report no. FHWA NHI-04-043, grant no. DTFH61-02-D-63006. Washington, DC: US Government Printing Office, 2003.
107. Mohan, P., D. Marzougui, and C.D.S. Kan, *Validation of a single unit truck model for roadside hardware impact*. International Journal of Vehicle Systems Modelling and Testing, 2007. **2**(1): p. 1-15.
108. Carrigan, C.E. and M.H. Ray, *Assessment of the MASH Heavy Vehicle Weights for Field Relevancy*. 2017.

109. U.S. Department of Transportation, *Single-Unit Straight Trucks in Traffic Crashes*. 2013, NHTSA's National Center for Statistics and Analysis: Washington, DC.
110. Miele, C., C. Plaxico, J. Kennedy, S. Simunovic, and N. Zisi, *Heavy vehicle infrastructure asset interaction and collision*. National Transportation Research Center, Knoxville, TN, 2005.
111. Hallquist, J., *LS-DYNA keyword user's manual, version 971*, in Livermore Software Technology Corporation. 2007: Livermore, CA.
112. Brown, M.D. and A. Loewe, *Reference manual to mitigate potential terrorist attacks against buildings*. USA, FEMA, 2003: p. 4-19.
113. Murray, Y.D., A.Y. Abu-Odeh, and R.P. Bligh, *Evaluation of LS-DYNA concrete material model 159*. 2007, U.S. Department of Transportation: McLean, VA.
114. Murray, Y.D., *Users manual for LS-DYNA concrete material model 159*. 2007, U.S. Department of Transportation: McLean, VA.
115. Coughlin, A., E. Musselman, A. Schokker, and D. Linzell, *Behavior of portable fiber reinforced concrete vehicle barriers subject to blasts from contact charges*. International Journal of Impact Engineering, 2010. **37**(5): p. 521-529.
116. O'Hare, E.V., *Computational Assessment of Steel-Jacketed Bridge Pier Column Performance Under Blast Loads*. 2011.
117. Malvar, L.J., *Review of static and dynamic properties of steel reinforcing bars*. Materials Journal, 1998. **95**(5): p. 609-616.
118. Jayasinghe, L.B., D.P. Thambiratnam, N. Perera, and J. Jayasooriya, *Computer simulation of underground blast response of pile in saturated soil*. Computers & Structures, 2013. **120**: p. 86-95.
119. Koneshwaran, S., D.P. Thambiratnam, and C. Gallage. *Blast response of segmented bored tunnel using coupled SPH-FE method*. in *Structures*. 2015. Elsevier.
120. Group, L.-D.A.W., *Modeling Guidelines Document Version 13-1*. 2013.
121. Reese, L., T. Qiu, D. Linzell, E. O'hare, and Z. Rado, *Field tests and numerical modeling of vehicle impacts on a boulder embedded in compacted fill*. International Journal of Protective Structures, 2014. **5**(4): p. 435-451.
122. Fujikake, K., B. Li, and S. Soeun, *Impact response of reinforced concrete beam and its analytical evaluation*. Journal of structural engineering, 2009. **135**(8): p. 938-950.
123. Baylot, J.T. and T.L. Bevins, *Effect of responding and failing structural components on the airblast pressures and loads on and inside of the structure*. Computers & structures, 2007. **85**(11-14): p. 891-910.
124. Woodson, S.C. and J.T. Baylot, *Structural collapse: quarter-scale model experiments*. 1999, Army Engineer Waterways Experiment Station Vicksburg MS Structures Lab.
125. Shi, Y., H. Hao, and Z.-X. Li, *Numerical derivation of pressure-impulse diagrams for prediction of RC column damage to blast loads*. International Journal of Impact Engineering, 2008. **35**(11): p. 1213-1227.
126. Fang, C. and D. Linzell. *Numerical simulation of reinforced concrete bridge columns under combined vehicle impact and blast*. in *2018 Structures Congress*. 2018. Denver, Colorado.
127. Fang, C. and D. Linzell, *Impact-resistant Behavior of Reinforced Concrete Bridge Columns*, in *2017 Spring UNL Research Fair*. 2017: Lincoln, Nebraska.